Non-Linear Hall Effect: From Theory to Experiment

Helena Dias da Silva
Master in Physics
Department of Physics and Astronomy
Faculty of Sciences of the University of Porto
2024

Non-Linear Hall Effect: From Theory to Experiment

Helena Dias da Silva
Dissertation carried out as part of the Master in Physics
Department of Physics and Astronomy
2024

Supervisor
Eduardo Filipe Vieira de Castro, Associate Professor, Faculty of Sciences of the University of Porto

Co-supervisor
André Miguel Trindade Pereira, Assistant Professor, Faculty of Sciences of the University of Porto

To my beloved godfather

Acknowledgements

This thesis would not have been possible without the support and guidance of several people, to whom I am immensely grateful.

Working with my supervisor, Professor Eduardo Castro, has been an extremely rewarding experience. Our meetings resembled actual classes, with every conversation delving deeply into scientific research - an ideal experience for any student. Your consistent guidance, wise counsel, and endurance throughout this entire process have been extremely helpful. I have gained a great deal from your knowledge and skills, which have played a vital role in molding my work and motivating me to push beyond my limits.

To my co-supervisor, Professor André Pereira, with whom I have been working with for several years, thank you for always allowing your students to discover their true vocation within projects, for never suppressing creativity and individuality, and for never hesitating to provide the resources necessary for a successful path. Your guidance and support have been invaluable to my journey.

I would also like to extend my gratitude to the IFIMUP team, especially Bruno Fernandes and Ana Pires. The experimental work would not have been possible without your guidance and support. Thank you for your patience, and dedication, and for always making time to ensure everything ran smoothly, even when faced with challenges.

On a personal note, I am profoundly grateful to my parents for always prioritizing my academic path. Their unconditional love, belief in my potential and their generosity in providing both financial and emotional support have been indispensable to my success.

To my godfather that taught me what life is truly about, showing me how to find strength in the face of challenges and live with a sense of freedom. His lessons and his example have left a lasting impact on me, and I carry his wisdom with me every day.

Last but certainly not least, I want to thank Diogo Pinheiro, the best friend this journey has given me. Your presence through both academic and personal moments has been a true blessing. We always feel relaxed and safe with each other, sharing endless laughter and spontaneous inside jokes and movie references that feel like our own secret language. Your companionship has been a constant source of joy and support, and I will cherish it forever.

Abstract

The Non-Linear Hall Effect (NLHE) represents a novel class of Hall-like phenomena that emerge without the need for time-reversal symmetry breaking, distinguishing it from conventional Hall effects. It consists of a transverse electric response which has a second-order contribution on the applied longitudinal current. This transverse response arises from both intrinsic and extrinsic contributions. The intrinsic contribution is connected to the dipole moment of the Berry curvature in momentum space, the later producing an anomalous velocity in current-carrying states. Contrary to the intrinsic contribution, which may be finite even in the disorder-free limit, the extrinsic contribution arises from the scattering sources in the system and may become the dominant contribution, in particular when the Berry curvature dipole vanishes. This thesis aims to explore how this second-order response manifests in time-reversal invariant and inversion-breaking materials when subjected to an external electric field. Both the theoretical approach to the effect and its experimental implementation are addressed. On the theory side, using semiclassical Boltzmann transport theory within the framework of the tilted 2D massive Dirac model, this thesis investigates the influence of three scattering mechanisms: impurity scattering described by both a delta function potential for short-range impurities and a screened coulomb potential for long-range interactions, as well as electron-phonon scattering as given by the lattice deformation potential, allowing us to study the effect of temperature variation. On the experimental side, a modified conventional Hall setup with an AC current and lock-in amplifiers is employed to study Bi_2Te_3 samples. This quantum material is a 3D topological insulators where the only contribution to the NLHE is expected to come from the topological surface states, which are well described by the 2D Dirac model. This study opens new pathways for investigating the topological and symmetry properties of emergent quantum materials.

Resumo

O Efeito de Hall Não-Linear (NLHE) representa uma nova classe de fenómenos do tipo Hall que surge sem a necessidade de quebrar a simetria de inversão temporal, distinguindo-se dos efeitos de Hall convencionais. O efeito consiste numa resposta elétrica transversal que tem uma contribuição de segunda ordem relativamente à corrente longitudinal aplicada. Esta resposta transversal surge de contribuições tanto intrínsecas como extrínsecas. A contribuição intrínseca está ligada ao momento dipolar da curvatura de Berry, no espaço de momentos, que gera uma velocidade anómala nos estados transportadores de corrente. Ao contrário da contribuição intrínseca, que pode ser finita mesmo no limite sem desordem, a contribuição extrínseca resulta das fontes de dispersão no sistema e pode tornar-se dominante, especialmente quando o dipolo da curvatura de Berry é nulo. Esta tese tem como objetivo explorar como essa resposta de segunda ordem se manifesta em materiais que preservam a simetria de inversão temporal mas quebram a simetria de inversão espacial, quando sujeitos a um campo elétrico externo. Tanto a perspetiva teórica do efeito quanto a sua implementação experimental são abordadas. No lado teórico, utilizando a teoria semiclássica do transporte de Boltzmann, no âmbito do modelo tilted 2D massive Dirac, esta tese investiga a influência de três mecanismos de scattering: scattering por impurezas, descrita por um potencial de função delta para impurezas de curto alcance e por um potencial de screened Coulomb para interações de longo alcance, assim como o scattering de eletrão-fonão, dado pelo potencial de deformação da rede, permitindo estudar o efeito da variação de temperatura. No lado experimental é utilizado uma montagem de Hall convencional modificada com uma corrente alternada (AC) e amplificadores lock-in, para estudar amostras de Bi_2Te_3. Este material quântico é um isolante topológico tridimensional, onde se espera que a única contribuição para o NLHE provenha dos estados de superfície topológicos, que são bem descritos pelo modelo de Dirac bidimensional. Este estudo abre novas vias para investigar as propriedades topológicas e de simetria de materiais quânticos emergentes.

List of Figures

Contents

Chapter 1

Introduction

Within the field of condensed matter physics, transport measurements have become the guiding compass for comprehending the intricate nature of materials. By providing valuable insights into the behavior and movement of charge carriers, it allows scientists to understand the fundamental principles behind conductivity, magnetism, non-trivial topological matter, and other phenomena. These insights are crucial to the development of innovative technologies and materials.

As the simplest form of transport measurement, the temperature dependence of resistivity (ρ) enables a straightforward distinction between metals ($d\rho/dT > 0$) and insulators or intrinsic semiconducting materials ($d\rho/dT < 0$). Meanwhile, mobility measurements offer a deeper layer of analysis, allowing the assessment of the quality of new materials, as exemplified in the study of graphene [1].

One of the oldest but most vital transport measurements are the Hall effects, continuing till this day to inspire new findings such as quantum Hall effects and topological phases of matter. In the domain of two-dimensional electron systems, such as the inversion layer of a metal-oxide-semiconductor field-effect transistor (MOSFET) [2] or in 2D materials [3], the quantized Hall conductivity emerges as a powerful probe. Expressed in multiples of the conductance quantum, $\sigma_{xy} = ne^2/h$, with $n = 0, \pm 1, \pm 2, \ldots$, this quantization grants direct access to fundamental constants of nature, such as the elementary charge (e) and Planck's constant (h). Furthermore, the advent of the quantum Hall effect has significantly influenced the trajectory of modern physics, leading to the recognition of the field of topological matter with a Nobel Prize in 2016 [4].

Recent advances introduced the Non-Linear Hall Effect (NLHE) as a novel addition to the family of Hall effects. Beyond conventional linear responses, this effect offers a unique view into intrinsic material properties, unraveling features like the Berry curvature dipole [5], without requiring time-reversal symmetry breaking. This effect is deeply connected to symmetry and topology, which expands its potential for uncovering new properties in emerging quantum materials and phases of matter [6]. Thus, it stands out as a valuable technique for any quantum materials research lab, where a theoretical understanding can unlock a wide range of material properties. The aim of this thesis is to take an initial step in both areas: developing the theoretical framework and implementing the experimental approach.

1.1 The Non-Linear Hall Effect

The Hall effect, discovered by Edwin Hall in 1879, has played a crucial role in understanding the behavior of charge carriers in conductive materials, under the influence of a magnetic field, giving access to the carrier concentration and mobility. Traditionally, the Hall effect is observed when a longitudinal direct current, I_x, is applied to a conduc-

tive material in the presence of a perpendicular magnetic field, B_z, resulting in a voltage transverse to both the direction of the current and the magnetic field, V_y, known as the Hall voltage. The magnitude of the Hall voltage can be measured and the Hall resistance, R_{yx}, can be obtained from the ratio V_y/I_x. In agreement with Drude theory, the Hall resistance is proportional to the strength of the magnetic field and inversely proportional to the number of charge carriers in the material,

$$V_y = R_{yx} I_x = \frac{B_z}{net} I_x, \tag{1.1}$$

this proportionality is defined by the Hall coefficient, $R_H = \frac{1}{ne}$, which is characteristic of the material, and t is the linear size of the material sample cross-section, assumed squared for simplicity.

But what happens if the current is alternating instead of direct? This question leads us to the concept of the Non-Linear Hall Effect. By applying an AC longitudinal current, $I_x^\omega = I_0 \sin(\omega t)$, the transverse electric response has a second-order contribution, $V_y^{2\omega}$, which depends quadratically on I_x^ω, in the absence of an external magnetic field,

$$V_y^{2\omega} = R_{yxx} (I_x^\omega)^2. \tag{1.2}$$

Experimentally, the direct measurement of $V_y^{2\omega}$ and I_x^ω, as shown in Fig.1.1, gives access to R_{yxx} which is proportional to the non-linear conductivity tensor χ_{yxx} that, on the other hand, may be theoretically derived, allowing a direct comparison between theory and experiment.

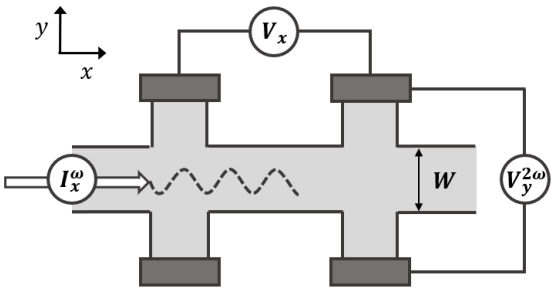

Figure 1.1: Representation of non-linear transport measurement by the second harmonic method in a Hall bar device.

The current density J_y and the electric field E_x can be related to the experimentally relevant parameters $V_y^{2\omega}$ and I_x^ω through the Hall bar width W (see Figure 1.1) and the longitudinal conductivity of the material σ, assuming the system to be two-dimensional or a thin film. We may then obtain the relation between the theoretically derived tensor and the experimentally measured R_{yxx} (see Equation 1.2):

$$\chi_{yxx} = W \sigma^3 R_{yxx}. \tag{1.3}$$

1.1.1 A few pros of the NLHE

One might also ask why would anyone be interested in the non-linear counterpart of the Hall effect. From the point of view of experiments, the NLHE provides a unique opportunity as the same setup used for conventional Hall measurements can be used, once adapted with an oscillating current source and lock-in amplifiers to suppress noise, since these responses are typically smaller than linear responses, requiring either higher intensities or clever strategies to extract the signals.

Most Hall effects arise from broken time-reversal symmetry, which can be induced either by applying an external magnetic field or due to the intrinsic magnetic ordering in the material, as imposed by Onsager's reciprocal relations (see Box 1 in [5] for details).

However, these constraints are limited to the linear response regime and do not prevent the occurrence of Hall effects in the non-linear response regime. This is advantageous as it simplifies the experimental setup by eliminating the need for a magnetic field, while also broadening the range of materials that may exhibit the effect. However, it should be noted that despite the theoretical and experimental results supporting the fact that time reversal symmetry breaking is not required for a finite NLHE to show up, the exact role of time-reversal symmetry in constraining non-linear response functions remains unknown [5].

While not constrained by time-reversal symmetry, it requires the breaking of inversion symmetry regardless of whether the mechanism is intrinsic or extrinsic [6, 7]. Therefore, one of the key interests in the NLHE is its ability to probe topological surface states (TSS) of materials with bulk inversion symmetry, as is the case of the 3D topological insulators of the A_2B_3 family, with A=Bi,Sb and B=Se,Te [7].

As will be discussed below and further shown in section 2.3, the NLHE has an intrinsic contribution that is proportional to the Berry curvature dipole, which has a quantum origin precisely as the quantum Hall effect and the intrinsic anomalous Hall effect. This characteristic makes the NLHE a unique toolbox to probe the geometric properties of electronic wavefunctions in time-reversal invariant materials. From an applications perspective, the observation of electrical second-harmonic generation, which can be extended to the GHz and THz range, is a particularly promising result [7].

1.1.2 Theoretical description of transport

The Non-Linear Hall effect has a quantum origin, as it is intrinsically linked to the Berry curvature. Although a quantum theoretical method could be employed to describe the transport, such an approach is often too complex and involves approximations that are challenging to manage or control. Historically, the Drude model has been important in understanding electron transport, but it is insufficient when applied to crystalline solids, especially from the perspective of modern quantum mechanics. Its primary limitation is that it treats electrons as classical particles undergoing random collisions. In a crystal lattice, electron behavior is more accurately described by Bloch's theorem, which states that the energy eigenfunctions are plane waves modulated by a periodic function. This gives rise to the concept of electrons propagating as Bloch waves, with their wavefunctions extending across the entire crystal, due to coherent quantum interference [8].

An alternative approach for describing the transport is the semiclassical Boltzmann transport theory. To maintain the particle-like behavior of the electrons, the Boltzmann theory describes the electrons as wavepackets of Bloch states. To ensure the robustness of the wavepacket concept even when translational invariance is slightly broken, the corresponding spatial variations have to occur on length scales much larger than the wavepacket size. In order to not violate the Heisenberg uncertainty principle, a wavepacket with a wave vector that is well defined on the scale of the Brillouin zone ($\Delta k \ll 1/\text{lattice constant}$) must be spread in real space over many primitive cells ($\Delta r \gg$ lattice constant) [9]. Thus a semiclassical wavepacket description of Bloch electrons assumes that there is a hierarchy of three distinct length scales [8]:

$$\text{Lattice constant} \ll \text{wavepacket size} \ll \begin{array}{c}\text{wavelength of the applied} \\ \text{external fields.}\end{array}$$

Similarly, scattering sources that influence transport coefficients can be incorporated into the Boltzmann framework, provided the associated disorder is not so strong as to disrupt

the wavepacket description. Moreover, for this approach to remain valid, not only the external field's wavelength must be large, but its frequency must be sufficiently small, to avoid inducing interband transitions. Under these conditions, the band index can be disregarded, allowing the wavepacket to be constructed from Bloch states of a single band.

The strength of the semiclassical approach lies in its clarity and intuitive appeal. It operates with concepts that have simple classical interpretations, while incorporating key rules that connect these classical ideas to quantum mechanical principles, enabling accurate quantitative results. Besides the Bloch states of the electrons, quantum principles are presented in the Berry curvature which relates the anomalous velocity to Bloch wavefunctions, but also in the scattering mechanisms by the scattering matrix, which has no analog in classical physics [10]. For these reasons, the Boltzmann approach remains widely used, particularly for comparing theoretical predictions with experimental results. It is also the approach we follow here.

1.2 State of the art

The existing literature of the NLHE encompasses both theoretical descriptions and experimental studies. This section presents a comprehensive overview of the field's current status, where it will be explored and build upon both theoretical and experimental insights in the subsequent sections.

1.2.1 Theory

The linear Hall conductivity σ_{ab} can be conceptualized as the zeroth-order moment of the Berry curvature over occupied states,

$$\sigma_{ab} = \epsilon_{abc}\frac{e^2}{\hbar}\int_k f_0\Omega_c, \tag{1.4}$$

where the Berry curvature $\Omega_a \equiv \epsilon_{abc}\partial^b_{\mathbf{k}}A_c$ is given in terms of the Berry connection $A_c = -i\langle u_k|\partial_c u_k\rangle$, and $|u_k\rangle$ is the ket corresponding to the periodic part of the Bloch wave function.

This is a particularly insightful transport coefficient in two-dimensions (2D). For a 2D metal, for example, Eq. (1.4) becomes the momentum space integration of the Berry curvature over the Fermi surface, leading the Hall conductivity to be proportional to the Berry phase for an adiabatic path around the Fermi surface [11]. In the case of a 2D insulator, however, the integration over the full Brillouin zone is proportional to the first Chern number $C \in \mathbb{Z}$, and the celebrated quantum Hall effect is obtained [12],

$$\sigma_{ab} = \frac{e^2}{h}C. \tag{1.5}$$

In contrast, as shown by I. Sodemann and L. Fu [5], the non-linear Hall conductivity tensor assesses a first-order moment of the Berry curvature over occupied states,

$$\chi_{abc} = \epsilon_{adc}\frac{e^3\tau}{2\hbar^2(1+i\omega\tau)}\int_k(\partial^b_{\mathbf{k}}f_0)\Omega_d, \tag{1.6}$$

or its dipolar distribution consequently referred to as the Berry curvature dipole (BCD)[5],

$$D_{ab} = -\int_k(\partial^a_{\mathbf{k}}f_0)\Omega_b = \int_k f_0(\partial^a_{\mathbf{k}}\Omega_b), \tag{1.7}$$

where the last equality is obtained after integration by parts. This expression arises from the Boltzmann theory in the constant relaxation time approximation, working in

the complex plane, and will worked out in this thesis. The BCD shows the importance of the distribution of Berry curvature in k-space to determine the electrical properties of new materials. Experimentally, to obtain the BCD from the signal of the non-linear Hall effect, only τ is further needed, which can be obtained from standard electrical transport measurements [13]. Moreover, from Eq. (1.6) it is seen that a finite response may be present even in the clean limit ($\tau \to \infty$), in which case the conductivity tensor becomes independent of τ. For this reason, this contribution is referred to as *intrinsic*.

As its linear counterpart, the intrinsic contribution to the NLHE has a quantum origin arising from the anomalous velocity of Bloch electrons generated by the Berry curvature. However, while the Hall effect in the linear response regime requires the breaking of time-reversal symmetry by magnetic fields or other means, the NLHE does not need time-reversal symmetry breaking but rather inversion symmetry breaking [14].

Within a time-reversal invariant system, the Berry curvature is odd in momentum space, $\Omega_a(\mathbf{k}) = -\Omega_a(-\mathbf{k})$, causing its integral weighed by the equilibrium Fermi distribution (f_0) to vanish since the states at k and $-k$ are equally occupied, forming Kramers pairs. On the other hand, in the second-order response, the integral of the Berry curvature can be finite because it is weighed by the non-equilibrium distribution, which is not symmetric under $k \to -k$. This leads to a net anomalous velocity and, consequently, a transverse current [5].

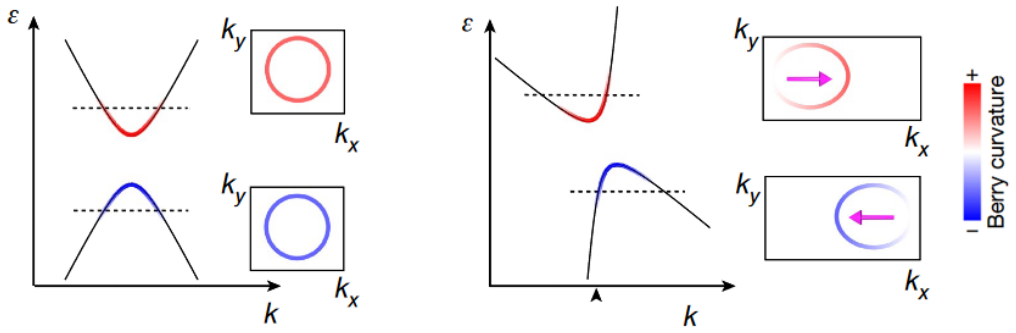

Figure 1.2: Intrinsic BCD mechanism illustrated with the 2D tilted massive Dirac model. Color bar shows the value of the Berry curvatures. Left: Zero tilt case. Right: The tilt leads to a non-zero BCD (purple arrows), which has opposite signs in conduction and valence bands (Adapted from [13]).

Concerning symmetry requirements, a minimal model for the NLHE is the tilted 2D massive Dirac model, whose Hamiltonian can be written as

$$\hat{H} = v(k_y\sigma_x + k_x\sigma_y) + m\sigma_z + tk_x\sigma_0, \tag{1.8}$$

where σ_α, with $\alpha = x, y, z$, are the three Pauli matrices, and σ_0 is the 2×2 identity. In Eq. (1.8), the first term represents a massless Dirac cone characterized by the Fermi velocity v, while m in the second term opens a gap, allowing for a sizeable Berry curvature around the gap edges, as shown in the left panel of Fig. 1.2. The last term, proportional to the parameter t, breaks the inversion symmetry along the x direction by tilting the Dirac cone [6]. The tilt leads to imbalanced Berry curvature and group velocity, and their product gives a non-zero BCD,

$$D_{ab} = \int_k \partial^a_{\mathbf{k}} \epsilon_k \Omega_b \delta(\epsilon_k - \epsilon_F), \tag{1.9}$$

where ϵ_F is the Fermi level. The obtained BCD is represented by purple arrows in the right panel of Fig. 1.2. Equation (1.9), which derives from Eq. (1.7) at zero temperature,

makes it clear that the BCD contribution to the NLHE stems entirely from the Fermi surface, and that it can be tuned experimentally by adjusting the Fermi level through doping [15]. The contribution from valence and conduction band is the same since the elliptical distortion of the Fermi lines is opposite in the two bands. It may then be shown [16] that the BCD is directly proportional to the tilt parameter t,

$$D_{ab} = \frac{3t}{4\pi}\frac{m}{\epsilon_F^4}\left(\epsilon_F^2 - m^2\right). \tag{1.10}$$

In addition to general symmetry considerations, as the lack of inversion, point group symmetries further constrain the Berry curvature-mediated contribution to the NLHE. For instance, in 2D crystals, a non-vanishing Berry curvature can only appear when there is either a threefold rotation symmetry or all rotation symmetries are broken [16].

Disorder-induced mechanisms

In the disorder-free limit ($\omega\tau \gg 1$) the non-linear conductivity tensor in Eq. (1.6) becomes τ-independent, as previously mentioned, showing that the BCD is an intrinsic contribution to the NLHE. At finite disorder, however, the BCD is not the only contribution in a non-centrosymmetric quantum material and extrinsic mechanisms, such as side-jump and skew-scattering, start to appear. Using either the quantum Boltzmann transport approach [17] or the semiclassical Boltzmann theory beyond the constant relaxation time approximation [14], it was shown that these disorder-mediated contributions may be relevant.

Experimentally, it is important to distinguish the different contributions to the non-linear Hall signal. This can be achieved based on the scaling law of the transverse non-linear Hall signal to the linear longitudinal signal, $V_a^{2\omega}/(V_b^L)^2 = \chi_{abb}\rho_{bb}$, where ρ_{bb} is the total resistivity [14].

The non-linear Hall conductivity corresponding to the double-frequency response can be written as

$$\chi_{abb} = \chi_{abb}^{\text{intrinsic}} + \chi_{abb}^{\text{side-jump}} + \chi_{abb}^{\text{skew-scattering}}, \tag{1.11}$$

where $\chi_{abb}^{\text{side-jump}}$ and $\chi_{abb}^{\text{skew-scattering}}$ are extrinsic, disorder driven contributions. Expressions for each contribution in Eq. (1.11) have been obtained in Ref. [14] and will also be derived in this thesis. While the intrinsic mechanism is linear in τ in the low frequency limit ($\omega\tau \ll 1$, often the relevant case experimentally), the extrinsic mechanisms have higher powers in τ: $\chi_{abb}^{\text{side-jump}} \propto \tau^2$ and $\chi_{abb}^{\text{skew-scattering}} \propto \tau^3$ [7].

Due to the different dependence on τ, differences in the behavior with ϵ_F are expected as these two quantities are related. The various terms of χ_{abb} for the tilted massive Dirac cone model, obtained in Ref. [14] through the Boltzmann formalism in the constant relaxation time approximation, are shown as a function of ϵ_F in Fig. 1.3. At higher ϵ_F, the skew-scattering becomes the dominant contribution, although as $\epsilon_F \to 0$ all contributions vanish.

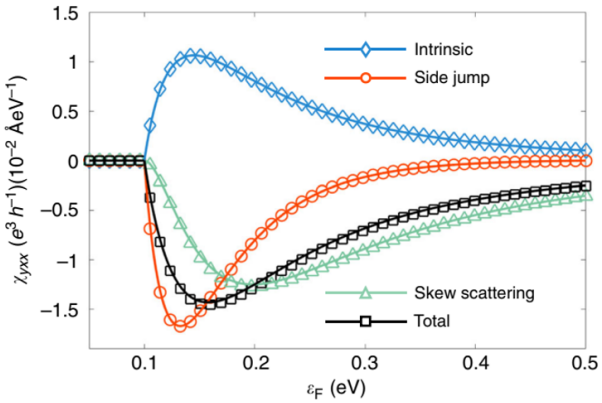

Figure 1.3: The intrinsic, extrinsic and total contributions to χ_{yxx} of the 2D tilted massive Dirac model as a function of ϵ_F at zero temperature with a constant relaxation time τ [14].

Attempts have been made to go beyond the semiclassical Boltzmann equation. A quantum theory based on the Feynman diagram technique has also been constructed, in which multiple new terms have been found [18].

The intrinsic contribution from the quantum theory is identical to the result from the semiclassical theory (Fig.1.4**a**). However, the extrinsic contributions calculated by the quantum theory demonstrate opposite signs, compared to the semiclassical results (Fig.1.4**b**, **c**). As a result, the total non-linear conductivity also shows opposite signs for the different approaches (Fig.1.4**d**). As the intrinsic part is similar, the NLHE can still be well described by the BCD, however a quantum description becomes specially important when disorder effects are relevant, as the extrinsic parts include qualitatively new contributions that go beyond the semiclassical description.

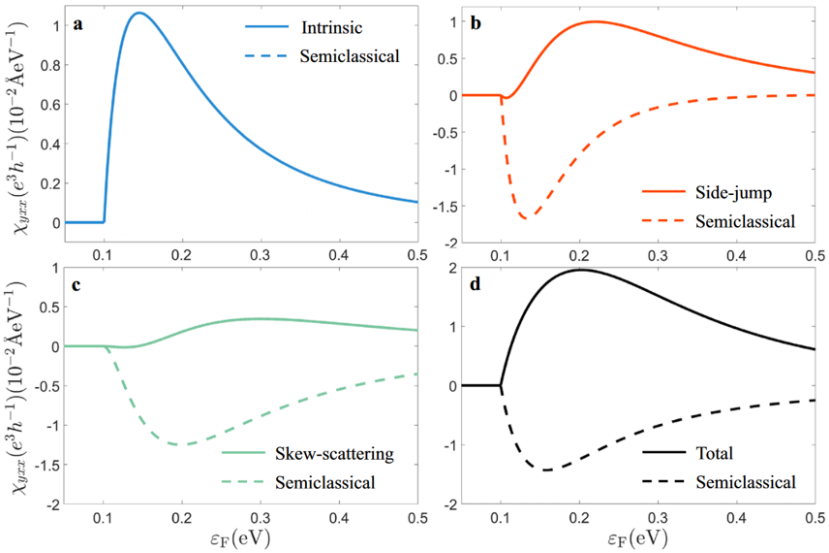

Figure 1.4: The intrinsic and extrinsic contributions to χ_{yxx} of the 2D tilted massive Dirac model as functions of ϵ_F at zero temperature for both quantum and semiclassical approaches [18].

1.2.2 Experiment

In 2019, one of the first experimental observations on the NLHE was reported in bilayers of the non-magnetic quantum material WTe_2 [13]. By applying a longitudinal AC current

I_a^ω, they measured both the longitudinal voltage $V_{aaa}^{2\omega}$, between the electrodes 1 and 3 and the electrodes 1 and 5 (see inset in Fig. 1.5), and the transverse voltage $V_{baa}^{2\omega}$ between the electrodes 3 and 4. In Fig.1.5, $V_{baa}^{2\omega}$ exhibits a clear quadratic dependence on the current, establishing a second-order nature.

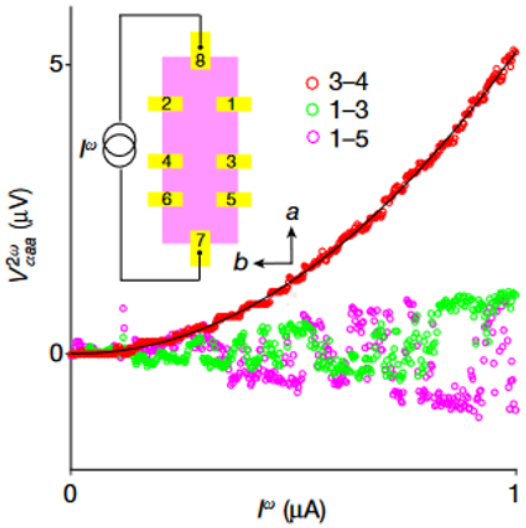

Figure 1.5: By flowing an AC current (I_a^ω; frequency ω=177.77 Hz) between electrodes 7 and 8, non-linear voltages $V_{\alpha aa}^{2\omega}$ are detected along the longitudinal (α=a; green and purple) and transverse (α=b; red) directions [13].

The frequencies used correspond to the $\omega\tau \ll 1$ limit and $\hbar\omega \ll \mu$, E_g, where μ is the chemical potential and E_g is the typical band gap (see Supplementary notes of [13]). Such low-frequency electrical excitations usually induce intraband transitions and are therefore sensitive to electronic states near the Fermi surface. By employing electrical gates, the Fermi level was further tuned, enabling energy sensitivity in this second-order generation measurements. In this way, it is noticeable that the $V_{baa}^{2\omega}$ signal depends strongly on the gate voltage, as shown in Fig. 1.6.

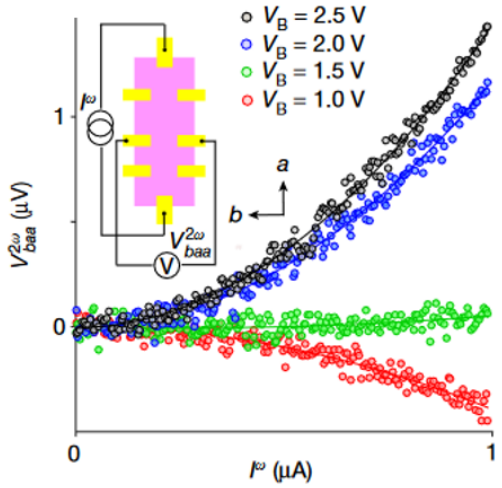

Figure 1.6: The $V_{baa}^{2\omega}$ dependence on I_a^ω by varying the gate voltage V_B [13].

Later, other materials were considered and subsequently, a series of experiments were conducted as shown on Table 1.1. Since the intrinsic contribution to the NLHE requires a non-zero BCD, it is advantageous to choose low-symmetry crystals with tilted Dirac or

Weyl points. Some examples of classes of materials that exhibit these characteristics are topological crystalline insulators, two-dimensional transition metal dichalcogenides, and three-dimensional Weyl semimetals [5].

Table 1.1: Experiments on the non-linear Hall effect [6].

Materials	Dimension	Temperature (K)	Input current frequency (Hz)	Input current maximum (μA)	Output voltage maximum (μV)
Bilayer WTe_2[13]	2	10-100	10-1000	1	200
Few-layer WTe_2[19]		1.8-100	17-137	600	30
Strained monolayer WSe_2[20]		50-140	17.777	5	20
Twisted bilayer WSe_2[21]		1.5-30	4.579	0.04	20000
Corrugated bilayer graphene[22]		1.5-15	77	0.1	2
Bi_2Se_3 surface[7]		2-200	9-263	1500	20
Bulk WTe_2[23]	3	1.4-4.2	110	4000	2
Cd_3As_2[23]		1.4-4.2	110	4000	1
$Ce_3Bi_4Pd_3$[24]		0.4-4	dc	100	-
$TaIrTe_4$[25]		2-300	13.7-213.7	600	120
T_d-$MoTe_2$[26]		2-40	17-277	5000	0.4
α-(BEDT-TTF)$_2I_3$[27]		4.2-40	dc	2000	40

Among the materials tested, P. He reported an electric frequency doubling in the absence of BCD on a surface of the topological insulator Bi_2Se_3, under zero magnetic field [7]. In this experiment, high-quality Bi_2Se_3 films were grown on Al_2O_3 substrates with the molecular beam epitaxy method. The lattice constant of Bi_2Se_3 film relaxes to its bulk value, implying the absence of strain from the substrate. Thus, the induction of BCD via breaking the threefold rotational symmetry of the Fermi surface of the topological surface states does not occur in these films. Therefore, it was found that the NLHE emerges from skew-scattering, which arises from the inherent chirality of the topological surface state and is compatible with symmetry.

However, to overcome the vanishing of the BCD, M. Qin applied uniaxial strain to break the threefold rotational symmetry in monolayer WSe_2 [20]. The uniaxial strain is induced by a piezoelectric field E_P applied onto the single crystal PMN-PT substrate. From the non-linear Hall measurements, the Berry curvature dipole is estimated by the formula (easily derived from Eqs. (1.6), (1.3) and (1.2)):

$$D = \frac{2\hbar^2\sigma^3 W}{e^3\tau}\frac{V_{xy}^{2\omega}}{(I_x^{\omega})^2}, \tag{1.12}$$

where, as before, σ is the longitudinal conductivity and W is the channel width. The scattering time $\tau \approx 1.2 \times 10^{-14} s$ is calculated through $\sigma = ne^2\tau/m^*$ with effective mass $m^* = 5.4m_e$ and the carrier density estimated from conventional Hall measurements. By controlling the strain values, the calculated BCD of WSe_2 is shown in Fig. 1.7, being clear that it is highly tunable by tuning strain and significantly enhanced with increasing E_P.

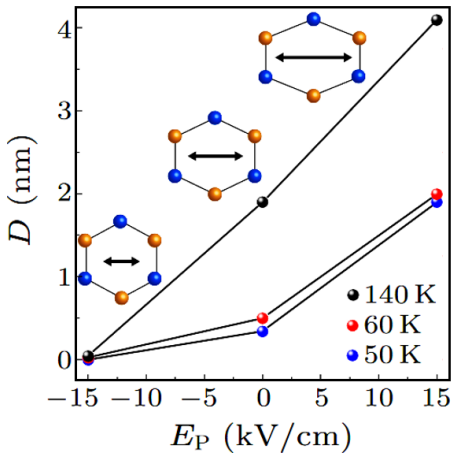

Figure 1.7: The estimated Berry curvature dipole D versus the piezoelectric field E_P at various temperatures [20].

Another observation from the results is the decrease in the BCD value with decreasing temperature. As for the NLHE, the quadratic dependence of $V_{xy}^{2\omega}$ in I_x^{ω} shows a non-monotonic behavior as the temperature decreases from $140K$ to $50K$. This can be understood in terms of the competition between temperature-dependent strain of PMN-PT crystals and thermal fluctuations. From the data of Fig. 1.8, the maximum non-linear Hall signals emerge at the moderate temperature of $\sim 80K$.

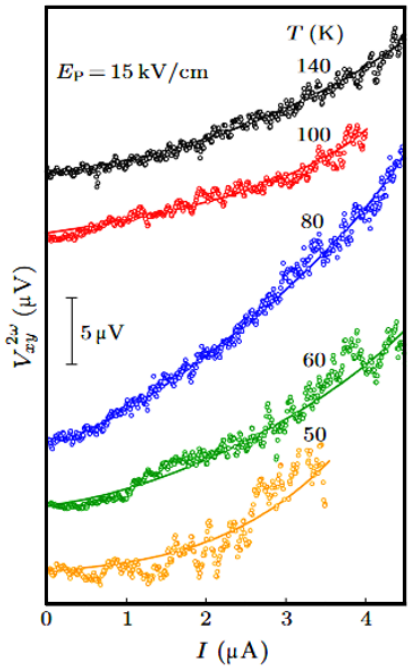

Figure 1.8: The quadratic dependence of $V_{xy}^{2\omega}$ in I_x^{ω} at various temperatures under $E_P = 15kV/cm$. The curves are shifted for clarity [20].

Although the NLHE with time-reversal symmetry finds a natural realization in 2D materials (or 2D surface states), it can also arise in 3D bulk materials, as seen in the lower half of Table 1.1. For example, $TaIrTe_4$, a type-II Weyl semimetal ternary compound, has been recently shown [25] to possess a NLHE surviving even at room temperature.

Chapter 2

Boltzmann Transport Theory

Within the Boltzmann transport theory, the motion of carriers within solids is characterized by wavepackets with well defined Bloch momentum $\mathbf{k}$ and position $\mathbf{r}$, and can be described by a semiclassical distribution function $f_{\mathbf{k}}(\mathbf{r}, t)$. This function encapsulates the phase-space dynamics of the particles within the infinitesimal volume element $d\mathbf{r}d\mathbf{k}$ surrounding the point $(\mathbf{r}, \mathbf{k})$ at a given time t [28].

After some time interval dt, the particles will occupy a new volume element $d\tilde{\mathbf{r}}d\tilde{\mathbf{k}}$, centered around the point $(\tilde{\mathbf{r}}, \tilde{\mathbf{k}})$. In the absence of dissipative effects, the conservation of particle number dictates that

$$f_{\mathbf{k}}(\mathbf{r}, t)\ d\mathbf{r}d\mathbf{k} = f_{\tilde{\mathbf{k}}}(\tilde{\mathbf{r}}, t + dt)\ d\tilde{\mathbf{r}}d\tilde{\mathbf{k}}. \tag{2.1}$$

According to Liouville's theorem, the phase-space volume remains invariant during this evolution, meaning that $d\mathbf{r}d\mathbf{k} = d\tilde{\mathbf{r}}d\tilde{\mathbf{k}}$. As a result, the distribution function remains constant,

$$f_{\mathbf{k}}(\mathbf{r}, t) = f_{\tilde{\mathbf{k}}}(\tilde{\mathbf{r}}, t + dt), \tag{2.2}$$

and the equation of continuity in phase-space is satisfied

$$\frac{df_{\mathbf{k}}(\mathbf{r}, t)}{dt} \equiv \frac{\partial f_{\mathbf{k}}(\mathbf{r}, t)}{\partial t} + \dot{\mathbf{r}} \cdot \frac{\partial f_{\mathbf{k}}(\mathbf{r}, t)}{\partial \mathbf{r}} + \dot{\mathbf{k}} \cdot \frac{\partial f_{\mathbf{k}}(\mathbf{r}, t)}{\partial \mathbf{k}} = 0. \tag{2.3}$$

Under conditions of thermal equilibrium, where the temperature is homogeneous and no external fields are present, the carrier distribution is represented by the Fermi-Dirac distribution function:

$$f_{\mathbf{k}}(\mathbf{r}, t)^{eq} \equiv f^0_{\mathbf{k}} = \frac{1}{e^{(\varepsilon_{\mathbf{k}} - \mu)/k_B T} + 1}. \tag{2.4}$$

However, the presence of scattering events during the infinitesimal interval dt can cause the distribution function to change over time,

$$\frac{df_{\mathbf{k}}(\mathbf{r}, t)}{dt} = \left(\frac{\partial f_{\mathbf{k}}(\mathbf{r}, t)}{\partial t}\right)_{scatt}. \tag{2.5}$$

In this process, some particles are scattered out of the phase-space, from $\mathbf{k}$ to $\mathbf{k}'$, associated with a transition probability rate $W^{\mathbf{k}'}_{\mathbf{k}}$. The scattering mechanism depends on the number of carriers in the initial state, $f_{\mathbf{k}}$, and the number of vacancies available in the final state, $(1 - f_{\mathbf{k}'})$. Conversely, particles can also be scattered into the phase space, from $\mathbf{k}'$ to $\mathbf{k}$ [29],

$$\left(\frac{\partial f_{\mathbf{k}}(\mathbf{r}, t)}{\partial t}\right)_{scatt} = \sum_{\mathbf{k}'} W^{\mathbf{k}}_{\mathbf{k}'} \left[1 - f_{\mathbf{k}}\right] f_{\mathbf{k}'} - \sum_{\mathbf{k}'} W^{\mathbf{k}'}_{\mathbf{k}} \left[1 - f_{\mathbf{k}'}\right] f_{\mathbf{k}}, \tag{2.6}$$

where the summation, $\sum_{\mathbf{k}}$, carries the same meaning as the integration, $\int_{\mathbf{k}}$, introduced before, and the two will be used interchangeably in the next sections. Therefore, the transport equation becomes the so-called Boltzmann equation:

$$\frac{\partial f_{\mathbf{k}}(\mathbf{r},t)}{\partial t} + \dot{\mathbf{r}} \cdot \frac{\partial f_{\mathbf{k}}(\mathbf{r},t)}{\partial \mathbf{r}} + \dot{\mathbf{k}} \cdot \frac{\partial f_{\mathbf{k}}(\mathbf{r},t)}{\partial \mathbf{k}} = \left(\frac{\partial f_{\mathbf{k}}(\mathbf{r},t)}{\partial t}\right)_{scatt}. \tag{2.7}$$

In the following sections, we will address both sides of the equation.

2.1 The Scattering Term

According to quantum mechanics, the decisive quantity for the description of scattering processes is the transition probability rate $W_{\mathbf{k}}^{\mathbf{k}'}$ given by the generalized Fermi's Golden Rule [30]

$$W_{\mathbf{k}}^{\mathbf{k}'} = \frac{2\pi}{\hbar}\left|\mathcal{T}_{\mathbf{k}\mathbf{k}'}\right|^2 \delta(\varepsilon_{\mathbf{k}'} - \varepsilon_{\mathbf{k}}). \tag{2.8}$$

The $\mathcal{T}$-matrix is defined as

$$\mathcal{T}_{\mathbf{k}\mathbf{k}'} = \langle \mathbf{k}|\tilde{\mathcal{H}}|\psi_{\mathbf{k}'}\rangle, \tag{2.9}$$

where $\tilde{\mathcal{H}}$ is the term responsible for scattering in the Hamiltonian, with $|\mathbf{k}\rangle$ being the Bloch state and $|\psi_{\mathbf{k}'}\rangle$ the scattering eigenstate of the total Hamiltonian, $\mathcal{H} = \mathcal{H}_0 + \tilde{\mathcal{H}}$, that satisfies the Lippman-Schwinger equation at the Bloch eigenenergy $\varepsilon_{\mathbf{k}'}$:

$$|\psi_{\mathbf{k}'}\rangle = \left|\mathbf{k}'\right\rangle + \frac{\tilde{\mathcal{H}}}{\varepsilon_{\mathbf{k}'} - \mathcal{H}_0 + i\eta}\left|\psi_{\mathbf{k}'}\right\rangle. \tag{2.10}$$

Note that, from Equation 2.9, $\mathcal{T}_{\mathbf{k}\mathbf{k}'}$ may be different from $\mathcal{T}^*_{\mathbf{k}'\mathbf{k}}$, allowing the scattering transition probability rate to be formally decomposed into the symmetric and antisymmetric part with respect to the interchange of the initial, $\mathbf{k}$, and final, $\mathbf{k}'$, states:

$$W_{\mathbf{k}}^{\mathbf{k}'} = w^{sy}_{\mathbf{k}\mathbf{k}'} + w^{as}_{\mathbf{k}\mathbf{k}'} \tag{2.11a}$$

where

$$w^{sy}_{\mathbf{k}\mathbf{k}'} = w^{sy}_{\mathbf{k}'\mathbf{k}} \qquad\qquad w^{as}_{\mathbf{k}\mathbf{k}'} = -w^{as}_{\mathbf{k}'\mathbf{k}}. \tag{2.11b}$$

As a result, from Equation 2.6 the scattering term in the Boltzmann equation can be rewritten as:

$$\left(\frac{\partial f_{\mathbf{k}}(\mathbf{r},t)}{\partial t}\right)_{scatt} = \sum_{\mathbf{k}'} w^{sy}_{\mathbf{k}\mathbf{k}'}\left[f_{\mathbf{k}'} - f_{\mathbf{k}}\right] - w^{as}_{\mathbf{k}\mathbf{k}'}\left[f_{\mathbf{k}'} + f_{\mathbf{k}} - 2f_{\mathbf{k}'}f_{\mathbf{k}}\right]. \tag{2.12}$$

As seen in subsection 1.1.2, the wavepacket description implies weak disorder. We thus expect that the scattering term in the Hamiltonian can be treated perturbatively. Using the expression of the $\mathcal{T}$-matrix in terms of the Born series in powers of the scattering Hamiltonian matrix elements [10],

$$\mathcal{T}_{\mathbf{k}\mathbf{k}'} \approx \tilde{\mathcal{H}}_{\mathbf{k}\mathbf{k}'} + \sum_{\mathbf{k}''} \frac{\tilde{\mathcal{H}}_{\mathbf{k}\mathbf{k}''}\tilde{\mathcal{H}}_{\mathbf{k}''\mathbf{k}'}}{\varepsilon_{\mathbf{k}'} - \varepsilon_{\mathbf{k}''} + i\eta} + \dots, \tag{2.13}$$

we may keep only the first terms in this series in order to capture the basic microscopic processes. Substituting Equation 2.13 into Equation 2.8 one arrive at the expansion [10]

$$W_{\mathbf{k}}^{\mathbf{k}'} \approx \frac{2\pi}{\hbar}\left[T^{(2)}_{\mathbf{k}\mathbf{k}'} + T^{(3)}_{\mathbf{k}\mathbf{k}'} + T^{(4)}_{\mathbf{k}\mathbf{k}'} + \dots\right]\delta(\varepsilon_{\mathbf{k}'} - \varepsilon_{\mathbf{k}}) \tag{2.14}$$

where

$$T^{(2)}_{\mathbf{k}\mathbf{k}'} = \left|\tilde{\mathcal{H}}_{\mathbf{k}\mathbf{k}'}\right|^2 \tag{2.15a}$$

$$T^{(3)}_{\mathbf{k}\mathbf{k}'} = \sum_{\mathbf{k}''} \frac{\tilde{\mathcal{H}}_{\mathbf{k}'\mathbf{k}}\tilde{\mathcal{H}}_{\mathbf{k}\mathbf{k}''}\tilde{\mathcal{H}}_{\mathbf{k}''\mathbf{k}'}}{\varepsilon_{\mathbf{k}'} - \varepsilon_{\mathbf{k}''} + i\eta} + \text{c.c.} \tag{2.15b}$$

$$\begin{aligned} T^{(4)}_{\mathbf{k}\mathbf{k}'} =& \sum_{\mathbf{k}''}\sum_{\mathbf{k}'''} \frac{\tilde{\mathcal{H}}_{\mathbf{k}\mathbf{k}''}\tilde{\mathcal{H}}_{\mathbf{k}''\mathbf{k}'}\tilde{\mathcal{H}}_{\mathbf{k}'\mathbf{k}'''}\tilde{\mathcal{H}}_{\mathbf{k}'''\mathbf{k}}}{(\varepsilon_{\mathbf{k}'} - \varepsilon_{\mathbf{k}''} + i\eta)(\varepsilon_{\mathbf{k}'} - \varepsilon_{\mathbf{k}'''} - i\eta)} + \\ &+ \sum_{\mathbf{k}''}\sum_{\mathbf{k}'''}\left[\frac{\tilde{\mathcal{H}}_{\mathbf{k}'\mathbf{k}}\tilde{\mathcal{H}}_{\mathbf{k}\mathbf{k}''}\tilde{\mathcal{H}}_{\mathbf{k}''\mathbf{k}'''}\tilde{\mathcal{H}}_{\mathbf{k}'''\mathbf{k}'}}{(\varepsilon_{\mathbf{k}'} - \varepsilon_{\mathbf{k}''} + i\eta)(\varepsilon_{\mathbf{k}'} - \varepsilon_{\mathbf{k}'''} + i\eta)} + \text{c.c.}\right]. \end{aligned} \tag{2.15c}$$

Since $T^{(2)}_{\mathbf{k}\mathbf{k}'}$ is symmetric, the leading contribution to $w^{as}_{\mathbf{k}\mathbf{k}'}$ appears in $T^{(3)}_{\mathbf{k}\mathbf{k}'}$ (non-Gaussian disorder distribution) and $T^{(4)}_{\mathbf{k}\mathbf{k}'}$ (Gaussian disorder distribution)[6].

Another effect which is potentially important is the fact that the center of mass of the wavepacket gets displaced during the scattering event. Taking into account the work done by the electric field, the conservation of energy implies that the change in energy corresponds to this displacement, $\varepsilon_{\mathbf{k}'} - \varepsilon_{\mathbf{k}} = e\mathbf{E}\cdot\delta\mathbf{r}_{\mathbf{k}\mathbf{k}'}$, where $\delta\mathbf{r}_{\mathbf{k}\mathbf{k}'} = \langle u_{\mathbf{k}}|i\partial_{\mathbf{k}}u_{\mathbf{k}}\rangle - \langle u_{\mathbf{k}'}|i\partial_{\mathbf{k}'}u_{\mathbf{k}'}\rangle - (\partial_{\mathbf{k}} + \partial_{\mathbf{k}'})\arg(\tilde{\mathcal{H}}_{\mathbf{k}\mathbf{k}'})$ is the coordinate shift [31]. In the first two terms of the coordinate shift expression, $|u_{\mathbf{k}}\rangle$ corresponds to the periodic part of the $\mathbf{k}$ Bloch state. Thus, in the elastic or quasi-elastic regime, the Fermi Golden Rule can be adapted to:

$$\tilde{W}^{\mathbf{k}'}_{\mathbf{k}} = \frac{2\pi}{\hbar}\left|\mathcal{T}_{\mathbf{k}\mathbf{k}'}\right|^2\delta(\varepsilon_{\mathbf{k}'} - \varepsilon_{\mathbf{k}} - e\mathbf{E}\cdot\delta\mathbf{r}_{\mathbf{k}\mathbf{k}'}). \tag{2.16}$$

Taking into account contributions up to the first order in $\delta\mathbf{r}_{\mathbf{k}\mathbf{k}'}$, we are allowed to approximate the δ-function as:

$$\delta(\varepsilon_{\mathbf{k}'} - \varepsilon_{\mathbf{k}} - e\mathbf{E}\cdot\delta\mathbf{r}_{\mathbf{k}\mathbf{k}'}) \approx \delta\left(\varepsilon_{\mathbf{k}'} - \varepsilon_{\mathbf{k}}\right) - e\mathbf{E}\cdot\delta\mathbf{r}_{\mathbf{k}\mathbf{k}'}\partial_{\varepsilon_{\mathbf{k}'}}\delta\left(\varepsilon_{\mathbf{k}'} - \varepsilon_{\mathbf{k}}\right). \tag{2.17}$$

Therefore, the transition probability rate becomes

$$\tilde{W}^{\mathbf{k}'}_{\mathbf{k}} \approx \frac{2\pi}{\hbar}\left|\mathcal{T}_{\mathbf{k}\mathbf{k}'}\right|^2\delta\left(\varepsilon_{\mathbf{k}'} - \varepsilon_{\mathbf{k}}\right) - \frac{2\pi}{\hbar}\left|\mathcal{T}_{\mathbf{k}\mathbf{k}'}\right|^2 e\mathbf{E}\cdot\delta\mathbf{r}_{\mathbf{k}\mathbf{k}'}\partial_{\varepsilon_{\mathbf{k}'}}\delta\left(\varepsilon_{\mathbf{k}'} - \varepsilon_{\mathbf{k}}\right). \tag{2.18}$$

By implementing the same expansion of the transition probability rate as in Equation 2.14, we obtain

$$\tilde{W}^{\mathbf{k}'}_{\mathbf{k}} \approx \frac{2\pi}{\hbar}\left[T^{(2)}_{\mathbf{k}\mathbf{k}'} + T^{(3)}_{\mathbf{k}\mathbf{k}'} + T^{(4)}_{\mathbf{k}\mathbf{k}'}\right]\delta\left(\varepsilon_{\mathbf{k}'} - \varepsilon_{\mathbf{k}}\right) - \frac{2\pi}{\hbar}\left[T^{(2)}_{\mathbf{k}\mathbf{k}'}\right]e\mathbf{E}\cdot\delta\mathbf{r}_{\mathbf{k}\mathbf{k}'}\partial_{\varepsilon_{\mathbf{k}'}}\delta\left(\varepsilon_{\mathbf{k}'} - \varepsilon_{\mathbf{k}}\right), \tag{2.19}$$

where, in the second term, since it includes the small displacement $\delta\mathbf{r}_{\mathbf{k}\mathbf{k}'}$, we retained only the leading term from the expansion. As before, we can separate the expression into the symmetric and antisymmetric parts, $\tilde{W}^{\mathbf{k}'}_{\mathbf{k}} = \tilde{w}^{sy}_{\mathbf{k}\mathbf{k}'} + \tilde{w}^{as}_{\mathbf{k}\mathbf{k}'}$. The symmetric part may then be written as,

$$\begin{aligned} \tilde{w}^{sy}_{\mathbf{k}\mathbf{k}'} \approx& \frac{2\pi}{\hbar}\left[T^{(2)}_{\mathbf{k}\mathbf{k}'}\right]\delta\left(\varepsilon_{\mathbf{k}'} - \varepsilon_{\mathbf{k}}\right) - \frac{2\pi}{\hbar}\left[T^{(2)}_{\mathbf{k}\mathbf{k}'}\right]e\mathbf{E}\cdot\delta\mathbf{r}_{\mathbf{k}\mathbf{k}'}\partial_{\varepsilon_{\mathbf{k}'}}\delta\left(\varepsilon_{\mathbf{k}'} - \varepsilon_{\mathbf{k}}\right) \\ \equiv& w^{in}_{\mathbf{k}\mathbf{k}'} + w^{sj}_{\mathbf{k}\mathbf{k}'}, \end{aligned} \tag{2.20}$$

keeping only the lowest order contribution in the $\mathcal{T}$-matrix. For the antisymmetric part we obtain,

$$\tilde{w}^{as}_{\mathbf{k}\mathbf{k}'} = \frac{2\pi}{\hbar}\left[T^{(3)as}_{\mathbf{k}\mathbf{k}'} + T^{(4)as}_{\mathbf{k}\mathbf{k}'}\right]\delta\left(\varepsilon_{\mathbf{k}'} - \varepsilon_{\mathbf{k}}\right) \equiv w^{sk}_{\mathbf{k}\mathbf{k}'}, \tag{2.21}$$

where $T^{(3)as}_{\mathbf{k}\mathbf{k}'}$ and $T^{(4)as}_{\mathbf{k}\mathbf{k}'}$ are the antisymmetric components of the third and fourth orders of the $\mathcal{T}$-matrix, respectively. In Eqs. 2.20 and 2.21 we have introduced the conventional notation [10, 14], where the symmetric part of the transition probability rate is associated to the intrinsic and side-jump mechanisms, with rates $w^{in}_{\mathbf{k}\mathbf{k}'}$ and $w^{sj}_{\mathbf{k}\mathbf{k}'}$ respectively, while the antisymmetric part is referred to the skew-scattering mechanism, with transition probability rate $w^{sk}_{\mathbf{k}\mathbf{k}'}$. Consequently, the Boltzmann equation scattering term can be decomposed into the intrinsic, side-jump and skew-scattering parts,

$$\begin{aligned}\left(\frac{\partial f_{\mathbf{k}}(\mathbf{r},t)}{\partial t}\right)_{scatt} &= \mathcal{I}_{in}(f_{\mathbf{k}}) \;+\; \mathcal{I}^{sj}_{ex}(f_{\mathbf{k}}) \;+\; \mathcal{I}^{sk}_{ex}(f_{\mathbf{k}}) \\ &= \sum_{\mathbf{k}'} w^{in}_{\mathbf{k}\mathbf{k}'}\left[f_{\mathbf{k}'} - f_{\mathbf{k}}\right] + \sum_{\mathbf{k}'} w^{sj}_{\mathbf{k}\mathbf{k}'}\left[f_{\mathbf{k}'} - f_{\mathbf{k}}\right] - \sum_{\mathbf{k}'} w^{sk}_{\mathbf{k}\mathbf{k}'}\left[f_{\mathbf{k}'} + f_{\mathbf{k}} - 2f_{\mathbf{k}'}f_{\mathbf{k}}\right].\end{aligned} \tag{2.22}$$

Both the side-jump and skew-scattering contributions, known as the extrinsic terms, are small compared to the intrinsic term. The side-jump term is small due to the coordinate shift, while the skew-scattering term is small because the antisymmetric contribution only appears in the third and fourth orders. Therefore, it is expected that the inequality $\mathcal{I}_{in}(f_{\mathbf{k}}) \gg \mathcal{I}^{sj}_{ex}(f_{\mathbf{k}}), \mathcal{I}^{sk}_{ex}(f_{\mathbf{k}})$ holds. Such inequality will be important in the next section.

2.2 Tailoring the Boltzmann Equation

In the absence of external magnetic field, as will be the case of the NLHE, the canonical momentum changes in time in response to the external electric field, according to the semiclassical equation of motion, $\dot{\mathbf{k}} = -\frac{e}{\hbar}\mathbf{E}$. The idea that an electron remains confined to a single energy band corresponds to an adiabatic evolution of the electron state as $\mathbf{k}$ changes over time. This adiabatic behavior persists as long as $\dot{\mathbf{k}}$ is sufficiently slow, which is characteristic of a weak field regime [8, 32]. Furthermore, on scales much larger than the distance between scatterers, the system is spatially uniform. Under these conditions, the semiclassical Boltzmann equation from Equation 2.7 takes the following form:

$$\left[\frac{\partial}{\partial t} - \frac{e}{\hbar}\mathbf{E}\cdot\frac{\partial}{\partial \mathbf{k}}\right] f_{\mathbf{k}} = \mathcal{I}_{in}(f_{\mathbf{k}}) \;+\; \mathcal{I}_{ex}(f_{\mathbf{k}}), \tag{2.23}$$

where $\mathcal{I}_{ex}(f_{\mathbf{k}}) \equiv \mathcal{I}^{sj}_{ex}(f_{\mathbf{k}}) + \mathcal{I}^{sk}_{ex}(f_{\mathbf{k}})$.

In the weak field regime, the steady-state distribution should not depart very far from equilibrium, $f_{\mathbf{k}} = f^0_{\mathbf{k}} + \delta f_{\mathbf{k}}$ [29], such that $\delta f_{\mathbf{k}}$ can be expanded in the applied field. As seen in section 2.1, in the right-hand side of the Boltzmann equation 2.23, the intrinsic term is bigger than the extrinsic one, $\mathcal{I}_{in}(f_{\mathbf{k}}) \gg \mathcal{I}^{sj}_{ex}(f_{\mathbf{k}}), \mathcal{I}^{sk}_{ex}(f_{\mathbf{k}})$. To achieve the same inequality on the left-hand side of the equation, let us write $\delta f_{\mathbf{k}} = \delta f^{in}_{\mathbf{k}} + \delta f^{ex}_{\mathbf{k}}$ where $\delta f^{in}_{\mathbf{k}} \gg \delta f^{ex}_{\mathbf{k}}$. For simplicity, we define the linear operator $\hat{B}_E \equiv \frac{\partial}{\partial t} - \frac{e}{\hbar}\mathbf{E}\cdot\frac{\partial}{\partial \mathbf{k}}$ and $f^{in}_{\mathbf{k}} = f^0_{\mathbf{k}} + \delta f^{in}_{\mathbf{k}}$, and rewrite the Boltzmann equation as,

$$\begin{aligned}\hat{B}_E\Big[f^{in}_{\mathbf{k}} + \delta f^{ex}_{\mathbf{k}}\Big] &= \mathcal{I}_{in}(f^{in}_{\mathbf{k}} + \delta f^{ex}_{\mathbf{k}}) + \mathcal{I}_{ex}(f^{in}_{\mathbf{k}} + \delta f^{ex}_{\mathbf{k}}) \\ &\approx \mathcal{I}_{in}(f^{in}_{\mathbf{k}}) + \mathcal{I}_{in}(\delta f^{ex}_{\mathbf{k}}) + \mathcal{I}_{ex}(f^{in}_{\mathbf{k}}),\end{aligned} \tag{2.24}$$

where we discarded the smaller term $\mathcal{I}_{ex}(f^{ex}_{\mathbf{k}})$. Since $\hat{B}_E\ f^{in}_{\mathbf{k}} \gg \hat{B}_E\ \delta f^{ex}_{\mathbf{k}}$ and $\mathcal{I}_{in}(f^{in}_{\mathbf{k}}) \gg \mathcal{I}_{in}(\delta f^{ex}_{\mathbf{k}}) + \mathcal{I}_{ex}(f^{in}_{\mathbf{k}})$, we can follow the usual procedure in perturbation theory and separate the Boltzmann equation into intrinsic and extrinsic parts,

$$\begin{aligned}\text{Intrinsic: } &\left[\frac{\partial}{\partial t} - \frac{e}{\hbar}\mathbf{E}\cdot\frac{\partial}{\partial \mathbf{k}}\right] f^{in}_{\mathbf{k}} = \mathcal{I}_{in}(f^{in}_{\mathbf{k}}) \\ \text{Extrinsic: } &\left[\frac{\partial}{\partial t} - \frac{e}{\hbar}\mathbf{E}\cdot\frac{\partial}{\partial \mathbf{k}}\right] \delta f^{ex}_{\mathbf{k}} = \mathcal{I}_{in}(\delta f^{ex}_{\mathbf{k}}) + \mathcal{I}_{ex}(f^{in}_{\mathbf{k}}).\end{aligned} \tag{2.25}$$

The next step involves finding solutions for both components of Eq. (2.25). The Intrinsic equation can be solved in the relaxation time approximation, a widely used approach, such that

$$\mathcal{I}_{in}(f_{\mathbf{k}}) = \mathcal{I}_{in}(\delta f_{\mathbf{k}}) = -\frac{\delta f_{\mathbf{k}}}{\tau_{\mathbf{k}}}, \tag{2.26}$$

where the relaxation time is given by (see Appendix A)

$$\frac{1}{\tau_{\mathbf{k}}} = \sum_{\mathbf{k}'} w^{in}_{\mathbf{k}\mathbf{k}'}\Big[1 - \cos\theta_{\mathbf{k}\mathbf{k}'}\Big], \tag{2.27}$$

with $\theta_{\mathbf{k}\mathbf{k}'}$ being the angle between the momenta $\mathbf{k}'$ and $\mathbf{k}$. With this approximation for the term $\mathcal{I}_{in}(\delta f_{\mathbf{k}})$ and the solution for the intrinsic distribution function, $f^{in}_{\mathbf{k}}$, the extrinsic component in Eq. (2.25) is easily solved.

To capture the different contributions clearly, we rewrite the Boltzmann equation and separate the extrinsic terms into side-jump and skew-scattering components, $\delta f^{ex}_{\mathbf{k}} = \delta f^{sj}_{\mathbf{k}} + \delta f^{sk}_{\mathbf{k}}$, as these mechanisms are independent of each other. This leads to the final Boltzmann equation that will be used in the further sections:

$$\begin{aligned}\text{Intrinsic: } &\left[\frac{\partial}{\partial t} - \frac{e}{\hbar}\mathbf{E}\cdot\frac{\partial}{\partial \mathbf{k}}\right] f^{in}_{\mathbf{k}} = -\frac{\delta f^{in}_{\mathbf{k}}}{\tau_{\mathbf{k}}} \\ \text{Side-jump: } &\left[\frac{\partial}{\partial t} - \frac{e}{\hbar}\mathbf{E}\cdot\frac{\partial}{\partial \mathbf{k}}\right] \delta f^{sj}_{\mathbf{k}} = -\frac{\delta f^{sj}_{\mathbf{k}}}{\tau_{\mathbf{k}}} + \mathcal{I}^{sj}_{ex}(f^{in}_{\mathbf{k}}) \\ \text{Skew-scattering: } &\left[\frac{\partial}{\partial t} - \frac{e}{\hbar}\mathbf{E}\cdot\frac{\partial}{\partial \mathbf{k}}\right] \delta f^{sk}_{\mathbf{k}} = -\frac{\delta f^{sk}_{\mathbf{k}}}{\tau_{\mathbf{k}}} + \mathcal{I}^{sk}_{ex}(f^{in}_{\mathbf{k}})\end{aligned} \tag{2.28}$$

By isolating the intrinsic, side-jump, and skew-scattering contributions, this approach not only simplifies the mathematical treatment but also provides a clearer understanding of the physical origins of the non-linear response. Each term can now be analyzed

independently, facilitating the computation of transport coefficients and a more detailed characterization of the NLHE. The approach we have adopted here follows closely that of Ref. [14]. An equation similar to Eq. (2.28) can be found in Supplementary Note 1 of that reference.

With the distribution function $f_{\mathbf{k}} = f^0_{\mathbf{k}} + \delta f^{in}_{\mathbf{k}} + \delta f^{sj}_{\mathbf{k}} + \delta f^{sk}_{\mathbf{k}}$, obtained by solving Eq. (2.28), we may compute the current and both linear and non-linear response coefficients. In the next section we focus on the non-linear conductivity tensor.

2.3 Non-Linear Conductivity Tensor

An applied electric field induces an electric current. The corresponding electric current density in the a-direction, j_a, is given by the integral of the physical velocity of the electrons, v_a, weighed by their distribution function:

$$j_a = -e \int f_{\mathbf{k}} v_a \, \frac{d\mathbf{k}}{(2\pi)^2}, \tag{2.29}$$

where $-e$ is the electron charge. The velocity in Eq. (2.29) contains three contributions, namely, the group velocity of the wavepacket of Bloch electrons, the anomalous velocity arising from the Berry curvature and the side-jump velocity associated to the coordinate shift [5],

$$v_a = \frac{1}{\hbar}\partial^a_{\mathbf{k}}\varepsilon_{\mathbf{k}} + \epsilon_{abc}\Omega_b \frac{e}{\hbar}E_c + v^{sj}_a, \tag{2.30}$$

with the Berry curvature given by $\Omega_a = \epsilon_{abc}\partial^b_{\mathbf{k}}\mathcal{A}_c = i\epsilon_{abc}\partial^b_{\mathbf{k}}\langle u_{\mathbf{k}}|\partial_c|u_{\mathbf{k}}\rangle$ and the side-jump velocity [31],

$$v^{sj}_a = \sum_{\mathbf{k}'} w^{in}_{\mathbf{k}\mathbf{k}'}\delta\mathbf{r}^a_{\mathbf{k}\mathbf{k}'}. \tag{2.31}$$

The current density, j_a, can be formally expressed as a power series in electric field. Here we are interested in the non-linear response. Up to second order, we may write

$$j_a = \sigma_{ab}E_b + \chi_{abc}E_bE_c, \tag{2.32}$$

where $a,\ b,\ c \in (x,\ y,\ z)$, σ_{ab} $(a \neq b)$ is the linear Hall conductivity, and the leading second-order term is characterized by the non-linear conductivity tensor χ_{abc}. In order to extract from Eq. (2.29) the transport coefficients defined in Eq. (2.32), we must expand the distribution function, $f_{\mathbf{k}}$, in powers of the electric field. By expanding up to second-order, $f_{\mathbf{k}} \approx f^0_{\mathbf{k}} + \delta^1 f_{\mathbf{k}} + \delta^2 f_{\mathbf{k}}$, where the term $\delta^n f_{\mathbf{k}}$ is understood to vanish as powers of the electric field E^n, we obtain

$$j_a = -e\int_k \Big(f^0_{\mathbf{k}} + \delta^1 f_{\mathbf{k}} + \delta^2 f_{\mathbf{k}}\Big)\Big(\frac{1}{\hbar}\partial^a_{\mathbf{k}}\varepsilon_{\mathbf{k}} + \epsilon_{abc}\Omega_b\frac{e}{\hbar}E_c + v^{sj}_a\Big). \tag{2.33}$$

Assuming the AC driving electric field written as $E_a(t) = \mathfrak{Re}\Big(\mathcal{E}_a e^{i\omega t}\Big)$, with $\mathcal{E} \in \mathbb{C}$, the distribution function can be expressed similarly, $\delta^n f_{\mathbf{k}} = \mathfrak{Re}\Big(\delta^n \tilde{f}_{\mathbf{k}} e^{in\omega t}\Big)$. Focusing on the second order contribution to the current, $j^{2\omega}_a = \mathfrak{Re}\Big(\tilde{j}^0_a + \tilde{j}^{2\omega}_a e^{i2\omega t}\Big)$, the current density at twice the frequency can be written as (see Appendix B)

$$\tilde{j}^{2\omega}_a = -e\int_k \delta^1\tilde{f}_{\mathbf{k}}\epsilon_{abc}\Omega_b\frac{e}{2\hbar}\mathcal{E}_c + \delta^2\tilde{f}_{\mathbf{k}}\Big(\frac{1}{\hbar}\partial^a_{\mathbf{k}}\varepsilon_{\mathbf{k}} + v^{sj}_a\Big) = \tilde{\chi}_{abc}\mathcal{E}_b\mathcal{E}_c. \tag{2.34}$$

Equation (2.34) can be further decomposed into the intrinsic and extrinsic mechanisms,

$$\begin{aligned}
\text{Intrinsic:} \quad \left[\tilde{j}_a^{2\omega}\right]_{in} &= -e\int_k \delta^1\tilde{f}_{\mathbf{k}}^{in}\epsilon_{abc}\Omega_b\frac{e}{2\hbar}\mathcal{E}_c + \delta^2\tilde{f}_{\mathbf{k}}^{in}\frac{1}{\hbar}\partial_{\mathbf{k}}^a\varepsilon_{\mathbf{k}} \\
\text{Side-jump:} \quad \left[\tilde{j}_a^{2\omega}\right]_{sj} &= -e\int_k \delta^1\tilde{f}_{\mathbf{k}}^{sj}\epsilon_{abc}\Omega_b\frac{e}{2\hbar}\mathcal{E}_c + \delta^2\tilde{f}_{\mathbf{k}}^{sj}\frac{1}{\hbar}\partial_{\mathbf{k}}^a\varepsilon_{\mathbf{k}} + \delta^2\tilde{f}_{\mathbf{k}}^{in}v_a^{sj} \\
\text{Skew-scattering:} \quad \left[\tilde{j}_a^{2\omega}\right]_{sk} &= -e\int_k \delta^1\tilde{f}_{\mathbf{k}}^{sk}\epsilon_{abc}\Omega_b\frac{e}{2\hbar}\mathcal{E}_c + \delta^2\tilde{f}_{\mathbf{k}}^{sk}\frac{1}{\hbar}\partial_{\mathbf{k}}^a\varepsilon_{\mathbf{k}}
\end{aligned} \tag{2.35}$$

where we discarded the term $\delta^2\tilde{f}_{\mathbf{k}}^{sj}v_a^{sj}$ as it is a second order contribution in the coordinate shift. To determine the non-linear conductivity tensor, we only need to solve the Boltzmann equation given by Eq. (2.28), in order to obtain the various distribution function terms.

In the following subsections, we write expressions for the intrinsic, side-jump, and skew-scattering contributions to the conductivity tensor. For each contribution we also write the respective distribution function, from which the conductivity tensor follows. A detailed derivation of these results can be found in Appendix B. We note that, even though the distribution functions are derived for a generic k-dependent relaxation time, the conductivity tensor is obtained within the constant relaxation time approximation (see Appendix A).

2.3.1 Intrinsic Term

By using the intrinsic part from Eq. (2.28), the solutions for the distribution functions, expressed in terms of the equilibrium distribution function $f_{\mathbf{k}}^0$, are given as follows (see Appendix B.1.1):

$$\delta^1\tilde{f}_{\mathbf{k}}^{in} = \frac{e}{\hbar}\frac{\tau\partial_{\mathbf{k}}^a f_{\mathbf{k}}^0}{(1+i\omega\tau)}\mathcal{E}_a, \tag{2.36}$$

$$\delta^2\tilde{f}_{\mathbf{k}}^{in} = \frac{e^2}{\hbar^2}\frac{\tau}{(1+i2\omega\tau)}\partial_{\mathbf{k}}^a\left(\frac{\tau\partial_{\mathbf{k}}^b f_{\mathbf{k}}^0}{1+i\omega\tau}\right)\mathcal{E}_a\mathcal{E}_b. \tag{2.37}$$

The intrinsic contribution to the non-linear conductivity tensor (see Appendix B.1.2), for a constant relaxation time, is:

$$\tilde{\chi}_{abc}^{in} = -\frac{e^3}{\hbar^2}\frac{\tau}{1+i\omega\tau}\left[\frac{1}{2}\int_k \partial_{\mathbf{k}}^b f_{\mathbf{k}}^0\epsilon_{adc}\Omega_d + \frac{1}{\hbar}\frac{\tau}{1+i2\omega\tau}\int_k \partial_{\mathbf{k}}^b\partial_{\mathbf{k}}^c f_{\mathbf{k}}^0\partial_{\mathbf{k}}^a\varepsilon_{\mathbf{k}}\right]. \tag{2.38}$$

2.3.2 Side-Jump Term

By using the side-jump part from Eq. (2.28), the solutions for the distribution functions, expressed in terms of the equilibrium distribution function $f_{\mathbf{k}}^0$, are given as follows (see Appendix B.2.1):

$$\delta^1\tilde{f}_{\mathbf{k}}^{sj} = \frac{-e\tau\mathcal{E}_a}{1+i\omega\tau}\partial_{\mathbf{k}}^a\sum_{\mathbf{k}'}S_{\mathbf{k}\mathbf{k}'}^a\left[f_{\mathbf{k}'}^0 - f_{\mathbf{k}}^0\right], \tag{2.39}$$

$$\delta^2\tilde{f}_{\mathbf{k}}^{sj} = \frac{e\tau\mathcal{E}_a}{1+i2\omega\tau}\left[\frac{\partial_{\mathbf{k}}^a\delta^1\tilde{f}_{\mathbf{k}}^{sj}}{\hbar} - \sum_{\mathbf{k}'}S_{\mathbf{k}\mathbf{k}'}^a\left[\delta^1\tilde{f}_{\mathbf{k}'}^{in} - \delta^1\tilde{f}_{\mathbf{k}}^{in}\right]\right], \tag{2.40}$$

where we defined $w^{sj}_{\mathbf{k}\mathbf{k}'} \equiv -e\mathbf{E}\cdot\mathbf{S}_{\mathbf{k}\mathbf{k}'}$, with $\mathbf{S}_{\mathbf{k}\mathbf{k}'} = \frac{2\pi}{\hbar}\left[T^{(2)}_{\mathbf{k}\mathbf{k}'}\right]\delta\mathbf{r}_{\mathbf{k}\mathbf{k}'}\partial_{\varepsilon_{\mathbf{k}'}}\delta\left(\varepsilon_{\mathbf{k}'}-\varepsilon_{\mathbf{k}}\right)$, in order to explicitly have the dependence of the electric field in the Boltzmann equation.

The side-jump contribution to the non-linear conductivity tensor (see Appendix B.2.2), for a constant relaxation time, is:

$$\tilde{\chi}^{sj}_{abc} = \frac{e^3}{\hbar}\frac{\tau}{1+i\omega\tau}\left[\frac{1}{2}\int_k\left[\partial^b_{\mathbf{k}}\sum_{\mathbf{k}'}S^b_{\mathbf{k}\mathbf{k}'}\left[f^0_{\mathbf{k}'}-f^0_{\mathbf{k}}\right]\right]\epsilon_{adc}\Omega_d + \frac{1}{\hbar}\frac{\tau}{1+i2\omega\tau}\int_k\partial^b_{\mathbf{k}}f^0_{\mathbf{k}}\partial_c v^{sj}_a + \right.$$
$$\left. + \frac{1}{\hbar}\frac{\tau}{1+i2\omega\tau}\int_k\left[\partial^b_{\mathbf{k}}\partial_c\sum_{\mathbf{k}'}S^c_{\mathbf{k}\mathbf{k}'}\left[f^0_{\mathbf{k}'}-f^0_{\mathbf{k}}\right]-\sum_{\mathbf{k}'}S^b_{\mathbf{k}\mathbf{k}'}\left[\partial^c_{\mathbf{k}'}f^0_{\mathbf{k}'}-\partial_c f^0_{\mathbf{k}}\right]\right]\partial^a_{\mathbf{k}}\varepsilon_{\mathbf{k}}\right]. \tag{2.41}$$

2.3.3 Skew-Scattering Term

By using the skew-scattering part from Equation 2.28, the solutions for the distribution functions, expressed in terms of the equilibrium distribution function f_0, are given as follows (see Appendix B.3.1):

$$\delta^1\tilde{f}^{sk}_{\mathbf{k}} = -\frac{e}{\hbar}\frac{\tau^2}{(1+i\omega\tau)^2}\sum_{\mathbf{k}'}w^{sk}_{\mathbf{k}\mathbf{k}'}\left[\mathcal{E}_{a'}\partial^a_{\mathbf{k}'}f^0_{\mathbf{k}}+\mathcal{E}_a\partial^a_{\mathbf{k}}f^0_{\mathbf{k}}\right], \tag{2.42}$$

$$\delta^2\tilde{f}^{sk}_{\mathbf{k}} = \frac{\tau}{1+i2\omega\tau}\left[\frac{e}{\hbar}\mathcal{E}_a\partial^a_{\mathbf{k}}\delta^1\tilde{f}^{sk}_{\mathbf{k}}-\sum_{\mathbf{k}'}w^{sk}_{\mathbf{k}\mathbf{k}'}\left[\delta^2\tilde{f}^{in}_{\mathbf{k}'}+\delta^2\tilde{f}^{in}_{\mathbf{k}}-2\delta^1\tilde{f}^{in}_{\mathbf{k}'}\delta^1\tilde{f}^{in}_{\mathbf{k}}\right]\right]. \tag{2.43}$$

The skew-scattering contribution to the non-linear conductivity tensor (see Appendix B.3.2), for a constant relaxation time, is:

$$\tilde{\chi}^{sk}_{abc} = \frac{e^3}{\hbar^2}\frac{\tau^2}{1+i\omega\tau}\left[\frac{1}{2}\int_k\frac{1}{1+i\omega\tau}\sum_{\mathbf{k}'}w^{sk}_{\mathbf{k}\mathbf{k}'}\left[\partial^b_{\mathbf{k}'}f^0_{\mathbf{k}}+\partial^b_{\mathbf{k}}f^0_{\mathbf{k}}\right]\epsilon_{adc}\Omega_d + \right.$$
$$+\frac{1}{\hbar}\frac{\tau}{1+i2\omega\tau}\int_k\frac{1}{1+i\omega\tau}\partial^b_{\mathbf{k}}\sum_{\mathbf{k}'}w^{sk}_{\mathbf{k}\mathbf{k}'}\left[\partial^c_{\mathbf{k}'}f^0_{\mathbf{k}'}+\partial^c_{\mathbf{k}}f^0_{\mathbf{k}}\right]\partial^a_{\mathbf{k}}\varepsilon_{\mathbf{k}} +$$
$$\left.+\frac{1}{\hbar}\frac{\tau}{1+i2\omega\tau}\int_k\sum_{\mathbf{k}'}w^{sk}_{\mathbf{k}\mathbf{k}'}\left[\frac{1}{1+i2\omega\tau}\left[\partial^b_{\mathbf{k}'}\partial^c_{\mathbf{k}'}f^0_{\mathbf{k}'}+\partial^b_{\mathbf{k}}\partial^c_{\mathbf{k}}f^0_{\mathbf{k}}\right]-\frac{2}{1+i\omega\tau}\partial^b_{\mathbf{k}'}f^0_{\mathbf{k}'}\partial^b_{\mathbf{k}}f^0_{\mathbf{k}}\right]\partial^a_{\mathbf{k}}\varepsilon_{\mathbf{k}}\right]. \tag{2.44}$$

2.4 Conclusion

In this chapter, we have established a theoretical framework for understanding the NLHE within the semiclassical Boltzmann transport theory. By carefully deriving and analyzing the Boltzmann equation, we identified the three primary disorder contributions: the intrinsic, side-jump, and skew-scattering mechanisms. These contributions arise from distinct physical origins and are captured through the corresponding distribution functions, which were systematically separated and solved under appropriate approximations.

Having established the general structure of the non-linear conductivity tensor, the next step is to apply this formalism to a specific physical model. Additionally, incorporating scattering mechanisms, such as impurity or lattice scattering, allows us to determine the $\mathcal{T}$-matrix elements and the relaxation time parameter, which are crucial for quantifying the contributions.

Chapter 3

Tilted 2D Dirac Model

To study the NLHE, we consider the tilted 2D massive Dirac model, which captures the low-energy properties of various Dirac materials, such as the surface states of 3D topological insulators and strained transition metal dichalcogenides [16]. We will apply the Boltzmann formalism developed in the previous chapter to compute the non-linear conductivity tensor for this model. A significant advantage of this model is its analytical treatment, which allows us to obtain closed-form expressions for the conductivity tensor. This facilitates better physical insight and easier comparison with experimental results.

3.1 The clean limit

The Hamiltonian can be written as

$$\mathcal{H} = \hbar v(k_x\sigma_x + k_y\sigma_y) + m\sigma_z + tk_x\sigma_0, \tag{3.1}$$

where σ_α, with $\alpha = x, y, z$, are the three Pauli matrices, and σ_0 is the 2×2 identity. The first term represents a massless Dirac cone characterized by the Fermi velocity v, while m in the second term opens a gap, allowing for a sizeable Berry curvature around the gap edges. The last term, proportional to the parameter t, breaks the inversion symmetry by tilting the Dirac cone. Without loss of generality, we tilt the cone in the x direction [6].

The dispersion relation is found to be:

$$\varepsilon^{\pm}_{\mathbf{k}} = tk_x \pm \sqrt{\hbar^2 v^2 k^2 + m^2} \tag{3.2}$$

where $\varepsilon^{\pm}_{\mathbf{k}}$ represents the energy of the conduction $(+)$ and valence $(-)$ bands. A representation of the two bands, both without (grey) and with tilt (color) can be found in Figure 3.1.

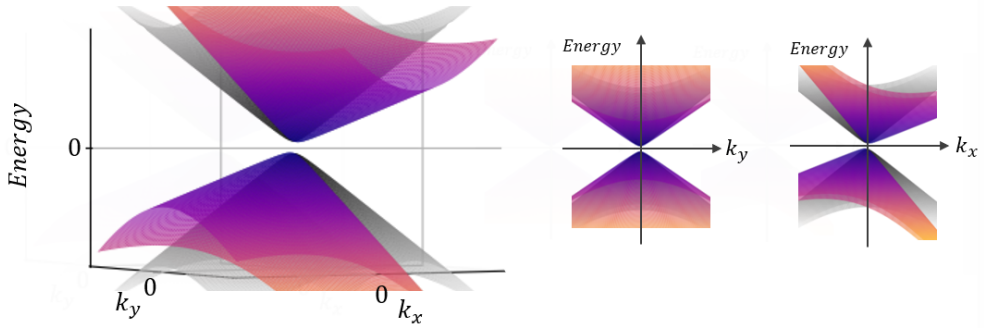

Figure 3.1: Energy dispersion of the tilted 2D massive Dirac cone with isotropic Fermi velocity ($v_x = v_y = v$). The greyscale Dirac cones illustrate the energy dispersion for the case with zero tilt. In contrast, the colored cones represent the tilted Dirac cones with a tilt parameter $t = 0.5$. The parameters used for the plots are $\hbar = m = v = 1$.

In the following we will assume that the system is electron doped, with the Fermi level in the conduction band. The corresponding eigenstates of the Hamiltonian, for states in the conduction band, are described by Bloch states, $|\psi_{\mathbf{k}}\rangle$, given by

$$|\psi_{\mathbf{k}}\rangle = \frac{e^{i\mathbf{k}\cdot\mathbf{r}}}{\sqrt{\nu}}|u_{\mathbf{k}}\rangle = \frac{e^{i\mathbf{k}\cdot\mathbf{r}}}{\sqrt{\nu}}\begin{pmatrix}\cos\frac{\phi_{\mathbf{k}}}{2}\\ \sin\frac{\phi_{\mathbf{k}}}{2}e^{i\theta_{\mathbf{k}}}\end{pmatrix}, \tag{3.3}$$

where ν is the normalization factor (the area of the system in 2D), $\cos\phi_{\mathbf{k}} = \dfrac{m}{\sqrt{\hbar^2v^2k^2+m^2}}$ and $\tan\theta_{\mathbf{k}} = \dfrac{k_y}{k_x}$. For simplicity, we will use the shorthand notation,

$$\begin{aligned}\phi_{\mathbf{k}} &\equiv \phi \qquad \theta_{\mathbf{k}} \equiv \theta\\ \phi_{\mathbf{k}'} &\equiv \phi' \qquad \theta_{\mathbf{k}'} \equiv \theta'\end{aligned} \qquad \theta_{\mathbf{k}\mathbf{k}'} \equiv \tilde{\theta}' \tag{3.4}$$

in the subsequent sections.

Since the NLHE may be finite when time reversal symmetry is either present of absent, we have the option to either preserve or break time-reversal symmetry in our analysis. The single cone 2D tilted Dirac model breaks time-reversal symmetry due to the mass term and inversion symmetry due to the tilt. However, this model can also be applied to time-reversal invariant systems. In such cases, an even number of Dirac cones must be considered, with pairs of Dirac cones related by time-reversal symmetry [5].

3.2 Conductivity Tensor Preliminaries

Before working out the conductivity tensor for this model, there are two preliminary considerations that should be made at this point. The first has to do with the intrinsic term: Why is it intrinsic and how is it related with the Berry curvature dipole? The second is an important simplification of the coordinate shift $\delta\mathbf{r}_{\mathbf{k}\mathbf{k}'}$ which will be used in subsequent calculations.

3.2.1 Intrinsic Term

The intrinsic term of the non-linear conductivity tensor, derived in section 2.3, is given by Equation 2.38, which we rewrite here for convenience of the reader:

$$\tilde{\chi}^{in}_{abc} = -\frac{e^3}{\hbar^2}\frac{\tau}{1+i\omega\tau}\left[\frac{1}{2}\int_k \partial^b_{\mathbf{k}} f^0_{\mathbf{k}}\epsilon_{adc}\Omega_d + \frac{1}{\hbar}\frac{\tau}{1+i2\omega\tau}\int_k \partial^b_{\mathbf{k}}\partial^c_{\mathbf{k}} f^0_{\mathbf{k}}\partial^a_{\mathbf{k}}\varepsilon_{\mathbf{k}}\right].$$

The first term in this expression depends on the Berry curvature. Contrary to the linear response Hall conductivity given by Equation 1.4, where the integral is over the full Brillouin zone, implying a zero response whenever time reversal symmetry is present, now the integral is over the Fermi surface (as long as $\mu \gg k_BT$, characteristic of a metal) and may be non-zero even if the system is time reversal invariant. For this model, the second term, related to the group velocity, vanishes due to the angular integral (see Appendix C.1.1). Therefore, in our analysis, the intrinsic contribution reduces to the first term, which requires the determination of the Berry curvature for the tilted 2D Dirac model.

To derive the Berry curvature, we first need to determine the Berry connection:

$$\vec{\mathcal{A}}_{\mathbf{k}} = i\langle u_{\mathbf{k}}|\vec{\nabla}_{\mathbf{k}}|u_{\mathbf{k}}\rangle = i\begin{pmatrix}\cos\frac{\phi}{2} & \sin\frac{\phi}{2}e^{-i\theta}\end{pmatrix}\frac{1}{k}\frac{\partial}{\partial\theta}\begin{pmatrix}\cos\frac{\phi}{2}\\ \sin\frac{\phi}{2}e^{i\theta}\end{pmatrix}\hat{\theta} = \frac{\cos\phi-1}{2k}\,\hat{\theta}. \tag{3.5}$$

Therefore, the Berry curvature for the tilted 2D Dirac model is:

$$\vec{\Omega}_{\mathbf{k}} = \vec{\nabla}_{\mathbf{k}} \times \vec{\mathcal{A}}_{\mathbf{k}} = \frac{1}{k}\frac{\partial}{\partial k}(k\mathcal{A}_\theta)\hat{z} = \frac{-m\hbar^2 v^2}{2(\hbar^2 v^2 k^2 + m^2)^{\frac{3}{2}}}\hat{z}. \tag{3.6}$$

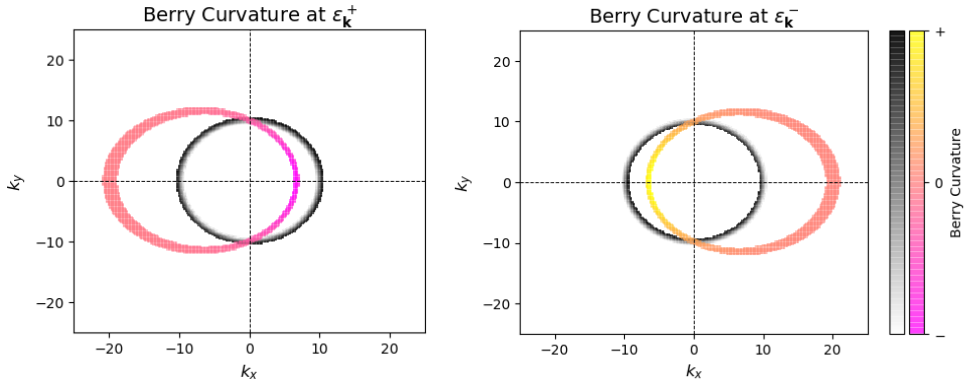

Figure 3.2: Berry Curvature Analysis: The plot compares the Berry curvature at a specific energy for both the conduction and valence bands. The greyscale illustrates the Berry curvature for the untilted massive Dirac cone. In contrast, the colored cones illustrate the Berry curvature for tilted Dirac cones with a tilt parameter $t = 0.5$. The parameters used for the plots are $\hbar = m = v = 1$.

In Fig. 3.2 we plot the Berry curvature on top of the Fermi surface for both the tilted and untilted cones. Note that the Berry curvature in Equation 3.6 does not depend on the tilt, so the expression is valid in the two cases. However, while for the untilted cone k is constant, for the tilted case k changes along the Fermi surface. The left panel of Fig. 3.2 is for the case when the Fermi energy lies on the conduction band, as we have assumed. The right panel is for the valence band, where the sign change is apparent.

Using this result, we can now compute the intrinsic contribution to the conductivity tensor. Taking into account that the second term in Equation 2.38 vanishes, we obtain (see Appendix C.1.2 for details),

$$\tilde{\chi}^{in}_{yxx} = -\frac{e^3}{2\hbar^2}\frac{\tau}{1+i\omega\tau}\int_k \partial_x f_0 \Omega_z = \frac{\tau}{(1+i\omega\tau)}\frac{3e^3}{16\pi}\frac{mt}{\hbar^2}\left[\frac{{\varepsilon_F}^2 - m^2}{{\varepsilon_F}^4}\right], \tag{3.7}$$

where we have assumed $\mu \gg k_B T$, in which case, through the Sommerfeld expansion, the chemical potential becomes $\mu \approx \varepsilon_F + \mathcal{O}(k_B^2 T^2)$, and therefore we can approximate $\partial_{\varepsilon_{\mathbf{k}}} f^0_{\mathbf{k}} \approx \delta(\varepsilon_{\mathbf{k}} - \varepsilon_F)$. From this result and the definition in Equation 1.7, we can extract the expression for the Berry curvature dipole,

$$D_{xz} = \frac{3m}{8\pi}\, t\left[\frac{{\varepsilon_F}^2 - m^2}{{\varepsilon_F}^4}\right], \tag{3.8}$$

which makes it clear that the Berry curvature dipole, D_{xz}, is strongly dependent on the tilt parameter t. If $t = 0$, the dipole vanishes and the non-linear Hall effect does not manifest in the system. The presence of a nonzero tilt breaks inversion symmetry, a condition that is essential for the existence of the non-linear response. Note that in the clean limit, $\tau \to \infty$, the conductivity tensor reduces to

$$\tilde{\chi}^{in}_{yxx} = \frac{1}{i\omega}\frac{3e^3}{16\pi}\frac{mt}{\hbar^2}\left[\frac{{\varepsilon_F}^2 - m^2}{{\varepsilon_F}^4}\right], \tag{3.9}$$

and the NLHE may be non-zero.

3.2.2 Coordinate Shift

In section 3.3 we will derive the remaining terms in the conductivity tensor for the 2D Dirac model – side-jump and skew-scattering. These contributions arise from scattering mechanisms and vanish in the clean limit, contrary to the intrinsic contribution given by Equation 3.9, which may be finite in the absence of scattering. Before working out those terms in the conductivity tensor, we recall that the side-jump contribution is a consequence of the coordinate shift $\delta\mathbf{r}_{\mathbf{k}\mathbf{k}'}$. We take the opportunity to detail a useful simplification in $\delta\mathbf{r}_{\mathbf{k}\mathbf{k}'}$.

As discussed in section 2.1, the coordinate shift, $\delta\mathbf{r}_{\mathbf{k}\mathbf{k}'}$, is given by,

$$\delta\mathbf{r}_{\mathbf{k}\mathbf{k}'} = \langle u_{\mathbf{k}}|i\partial_{\mathbf{k}}u_{\mathbf{k}}\rangle - \langle u_{\mathbf{k}'}|i\partial_{\mathbf{k}'}u_{\mathbf{k}'}\rangle - (\partial_{\mathbf{k}} + \partial_{\mathbf{k}'})\arg(V_{\mathbf{k}\mathbf{k}'}). \tag{3.10}$$

The first two terms are easily calculated from the eigenvectors given in Equation 3.3. The last term is the one we have to worry about since it depends explicitly on the scattering potential through the matrix element $V_{\mathbf{k}\mathbf{k}'}$.

The presence of the Pauli matrices in the 2D Dirac Hamiltonian in Equation 3.1, and the consequent two-component structure of the eigenstates in Equation 3.3, implies that there is an extra degree of freedom in this system with an Hilbert space dimension of two (two orbitals, two sublattices, spin, etc). We will assume that the scattering potential is diagonal in this space for all the cases studied in this thesis. This may be a reasonable assumption, for example, if the scattering is due to a charged impurity which affects equally the two orbitals, or the two sublattices, or is spin independent. In such cases the coordinate shift simplifies considerably since it becomes independent of the impurity potential and can be expressed in terms of initial and final states only [31, 10].

In order to see how $\delta\mathbf{r}_{\mathbf{k}\mathbf{k}'}$ becomes independent of the scattering potential, we consider a central potential, $V(\vec{r}) = v(r)$, and write the matrix element $V_{\mathbf{k}\mathbf{k}'}$ as,

$$V_{\mathbf{k}\mathbf{k}'} = \langle\mathbf{k}|\,\hat{V}\,|\mathbf{k}'\rangle = \frac{1}{\nu}\int d^2r\, v(r)e^{i(\mathbf{k}'-\mathbf{k})\cdot\mathbf{r}}\,\langle u_{\mathbf{k}}|\,\sigma_0\,|u_{\mathbf{k}'}\rangle\,, \tag{3.11}$$

where $\langle u_{\mathbf{k}}|\,\sigma_0\,|u_{\mathbf{k}'}\rangle = \langle u_{\mathbf{k}}|u_{\mathbf{k}'}\rangle$. Since the Fourier transform of the central potential is a real number,

$$\frac{1}{\nu}\int d^2r\, v(r)e^{i(\mathbf{k}'-\mathbf{k})\cdot\mathbf{r}} = \frac{2}{\nu}\int dr\, rv(r)J_0(||\mathbf{k}'-\mathbf{k}||r) \in \mathbb{R}, \tag{3.12}$$

where $J_0(x)$ is the Bessel function, we conclude that

$$\delta\mathbf{r}_{\mathbf{k}\mathbf{k}'} = \langle u_{\mathbf{k}}|i\partial_{\mathbf{k}}u_{\mathbf{k}}\rangle - \langle u_{\mathbf{k}'}|i\partial_{\mathbf{k}'}u_{\mathbf{k}'}\rangle - (\partial_{\mathbf{k}} + \partial_{\mathbf{k}'})\arg\left(\langle u_{\mathbf{k}}|u_{\mathbf{k}'}\rangle\right). \tag{3.13}$$

The derivatives in the last term are computed by noting that,

$$\arg\left(\langle u_{\mathbf{k}}|u_{\mathbf{k}'}\rangle\right) = -i\ln\frac{\langle u_{\mathbf{k}}|u_{\mathbf{k}'}\rangle}{|\langle u_{\mathbf{k}}|u_{\mathbf{k}'}\rangle|}. \tag{3.14}$$

This simplification allows us to compute the coordinate shift regardless of the scattering potential.

Taking into account the eigenket in Equation 3.3 for the conduction band, we obtain (see Appendix C.2),

$$\delta\mathbf{r}^y_{\mathbf{k}\mathbf{k}'} = \frac{1}{4|A|^2}\left(\frac{\sin\phi}{k} + \frac{\sin\phi'}{k'}\right)\Big(\cos\phi\sin\phi'\cos\theta' - \sin\phi\cos\phi'\cos\theta\Big), \tag{3.15}$$

for the y component, while for the x component the result reads,

$$\delta\mathbf{r}^x_{\mathbf{k}\mathbf{k}'} = \frac{1}{4|A|^2}\left(\frac{\sin\phi}{k} + \frac{\sin\phi'}{k'}\right)\Big(\sin\phi\cos\phi'\sin\theta - \cos\phi\sin\phi'\sin\theta'\Big), \tag{3.16}$$

where

$$|A|^2 \equiv |\langle u_{\mathbf{k}}|u_{\mathbf{k}'}\rangle|^2 = \frac{1}{2}\Big[1 + \cos\phi' \cos\phi + \sin\phi' \sin\phi \cos\tilde{\theta}'\Big]. \tag{3.17}$$

3.3 Scattering Mechanisms and Conductivity Tensor

In this section, we derive the three contributions to the conductivity tensor – intrinsic, side-jump, and skew-scattering – for the tilted 2D Dirac model.

In real-world systems, the idealized transport behavior is rarely observed, as charge carriers are often subjected to several scattering events. In solids, these scattering events typically arise from two primary sources: impurity scattering and lattice scattering. Impurity scattering occurs when charge carriers encounter localized disruptions in the lattice caused by impurities or defects and can be modeled mathematically depending on the nature of the interaction. When highly localized, a delta function potential is often used, representing short-range interactions. In contrast, long-range interactions are generally described by a screened Coulomb potential, where the presence of other charges within the material attenuates the interaction.

On the other hand, lattice scattering occurs when electrons interact with the vibrations of the atoms in the crystal lattice, known as phonons. These interactions perturb the periodic potential of the lattice, leading to scattering events that become more pronounced at higher temperatures. The electron-phonon interaction potential is typically used to mathematically represent this type of scattering.

3.3.1 Delta Function Potential

Representing short-range interactions between electrons and impurities, consider a delta function potential described by:

$$U_D = \sum_{j=1}^{N_{imp}} u_0 \delta(\vec{r} - \vec{R}_j), \tag{3.18}$$

where N_{imp} is the number of impurities, $\vec{R}_j$ represents their random positions, and u_0 is the magnitude of the potential centered at $\vec{R}_j$.

As a common quantity for both the intrinsic and extrinsic contributions, we can start by determining the Boltzmann relaxation time derived in section 2.2, and written for a generic transition probability rate in Equation 2.27. Specifying for the intrinsic transition probability rate, we have

$$\frac{1}{\tau_{\mathbf{k}}} = \sum_{k'} w^{in}_{\mathbf{k}\mathbf{k}'} \Big[1 - \cos\tilde{\theta}'\Big]. \tag{3.19}$$

The intrinsic transition probability rate, as seen in chapter 2, is simply given by Fermi's golden rule (see Equation 2.20):

$$w^{in}_{\mathbf{k}\mathbf{k}'} = \frac{2\pi}{\hbar}\Big|\langle \mathbf{k}'|\hat{U}_D|\mathbf{k}\rangle\Big|^2 \delta(\varepsilon_{\mathbf{k}'} - \varepsilon_{\mathbf{k}}). \tag{3.20}$$

The matrix elements are defined as:

$$\begin{aligned}\langle \mathbf{k}'|\hat{U}_D|\mathbf{k}\rangle &= \int d\vec{r}\ \Psi^{\dagger}_{\mathbf{k}'}(\vec{r})\ U_D(\vec{r})\ \Psi_{\mathbf{k}}(\vec{r}) \\ &= \frac{u_0}{\nu}\left(\cos\frac{\phi'}{2}\cos\frac{\phi}{2} + \sin\frac{\phi'}{2}\sin\frac{\phi}{2}e^{-i\tilde{\theta}}\right)\left[\sum_{j=1}^{N_{imp}} e^{i(\mathbf{k}-\mathbf{k}')\cdot\mathbf{R_j}}\right],\end{aligned} \tag{3.21}$$

where $\Psi_{\mathbf{k}}(\vec{r})$ is the electronic spinor wave function. By inserting the matrix element in the Fermi's golden rule and simplifying the modulus squared terms, we obtain:

$$\begin{aligned} w^{in}_{\mathbf{k}\mathbf{k}'} &= \frac{2\pi}{\hbar}\frac{u_0^2}{\nu^2}\left|\cos\frac{\phi'}{2}\cos\frac{\phi}{2}+\sin\frac{\phi'}{2}\sin\frac{\phi}{2}e^{-i\tilde{\theta}'}\right|^2\left|\sum_{j=1}^{N_{imp}}e^{i(\mathbf{k}-\mathbf{k}')\cdot\mathbf{R}_j}\right|^2\delta(\varepsilon_{\mathbf{k}'}-\varepsilon_{\mathbf{k}}) \\ &= \frac{\pi}{\hbar}\frac{u_0^2 n_{imp}}{\nu}\left[1+\cos\phi'\cos\phi+\sin\phi'\sin\phi\cos\tilde{\theta}'\right]\delta(\varepsilon_{\mathbf{k}'}-\varepsilon_{\mathbf{k}}), \end{aligned} \tag{3.22}$$

where we have used the approximation $\left|\sum_{j=1}^{N_{imp}} e^{i(\mathbf{k}-\mathbf{k}')\cdot\mathbf{R}_j}\right|^2 \approx \nu n_{imp}$, since for a large number of randomly distributed impurities we have $\sum_{j,k=1}^{N_{imp}} e^{i(\mathbf{k}-\mathbf{k}')\cdot(\mathbf{R}_j-\mathbf{R}_k)} \approx N_{imp}$ because only the terms with $j=k$ will contribute in the thermodynamic limit [28].

By substituting $w^{in}_{\mathbf{k}\mathbf{k}'}$ in the expression for the relaxation time given by Equation 3.19,

$$\frac{1}{\tau(\vec{k})} = \sum_{k'}\frac{\pi}{\hbar}\frac{u_0^2 n_{imp}}{\nu}\left[1+\cos\phi'\cos\phi+\sin\phi'\sin\phi\cos\tilde{\theta}'\right]\left[1-\cos\tilde{\theta}'\right]\delta(\varepsilon_{\mathbf{k}'}-\varepsilon_{\mathbf{k}}), \tag{3.23}$$

we can solve it by transforming the sum into an integral in polar coordinates, $\frac{\nu}{(2\pi)^2}\int k'dk'd\theta'$, and assuming t small compared to the Fermi velocity, allowing the expansion of the Dirac delta as $\delta(\varepsilon_{\mathbf{k}'}-\varepsilon_{\mathbf{k}}) \approx \delta\left(\varepsilon^0_{\mathbf{k}'}-\varepsilon^0_{\mathbf{k}}\right) + t(k'\cos\theta'-k\cos\theta)\partial_{\varepsilon^0_{\mathbf{k}'}}\delta\left(\varepsilon^0_{\mathbf{k}'}-\varepsilon^0_{\mathbf{k}}\right)$ with $\varepsilon^0_{\mathbf{k}}$ indicating the energy of the untilted massive Dirac cone. Intermediate steps of the calculation can be found in Appendix C.3.1. Here, we just provide the obtained result for Boltzmann relaxation time of the tilted Dirac cone for a delta function potential,

$$\tau_{\mathbf{k}} = \frac{4\hbar^3 v^2}{u_0^2 n_{imp}}\left[\frac{{\varepsilon^0_{\mathbf{k}}}^2+3m^2}{\varepsilon^0_{\mathbf{k}}}+\frac{t\cos\theta}{\hbar v}\frac{{\varepsilon^0_{\mathbf{k}}}^2-3m^2}{\sqrt{{\varepsilon^0_{\mathbf{k}}}^2-m^2}}\right]^{-1}. \tag{3.24}$$

It is obvious from Equation 3.24 that the relaxation time is not isotropic as it depends on the angle θ between the electric field and the wave vector $\mathbf{k}$. We are facing a contradiction here: $\tau_{\mathbf{k}}$ is not isotropic, which stems from the fact that any constant energy surface is not isotropic due to the tilt, but we derived the relaxation time starting from Equation 3.19, which holds for the isotropic case (as discussed in Appendix A). In order to be consistent, we have to drop the term proportional to the tilt t in Equation 3.24. This means that we are working in the approximation $t \ll \hbar v$, in which case the relaxation time becomes isotropic and is given by,

$$\tau_{\mathbf{k}} \simeq \frac{4\hbar^3 v^2}{u_0^2 n_{imp}}\frac{\varepsilon^0_{\mathbf{k}}}{{\varepsilon^0_{\mathbf{k}}}^2+3m^2}. \tag{3.25}$$

The constant relaxation time approximation (see Appendix A) follows easily by replacing $\varepsilon^0_{\mathbf{k}}$ with ε_F in Equation 3.25.

Intrinsic contribution

By incorporating the Boltzmann relaxation time into the intrinsic conductivity tensor from Equation 3.7 for scattering described by a delta-function potential, we obtain

$$\tilde{\chi}^{in}_{yxx} = \frac{e^3}{\hbar}\frac{mt}{u_0^2 n_{imp}}\frac{3\hbar^2 v^2\varepsilon_F}{4\pi({\varepsilon_F}^2+3m^2)}\left[\frac{{\varepsilon_F}^2-m^2}{{\varepsilon_F}^4}\right], \tag{3.26}$$

where we have assumed the low frequency regime $\omega\tau \ll 1$. As we will see in chapter 4, the current source in our case has a maximum frequency in the range of 100 MHz. If we use typical values for the parameters of the tilted Dirac cone model [33], $\hbar v \sim 1\text{eVÅ}$, $m \sim 0.1\text{eV}$ and $t \sim 0.1\text{eVÅ}$, and choose Delta impurities characterized by $n_{imp}u_0^2 = 100\text{eV}^2\text{Å}^2$, we obtain $\tau \sim 10^{-16}\text{s}$, which is not unrealistic given that for a good metal we expect $\tau \sim 10^{-14}\text{s}$ [9] and the surface of a topological insulator, though conducting, is expected to conduct less than good metal. For these values of frequency and relaxation time we are well within the regime $\omega\tau \ll 1$, and we will always approximate $1 + i\omega\tau \approx 1$ whenever this appears in the conductivity tensor.

In Figure 3.3 we show how the intrinsic conductivity tensor as a function of Fermi energy for different values of the tilt parameter. The non-monotonous behavior comes essentially from the BCD, which is given by Equation 3.8. The non-monotonous behavior of the BCD, in its turn, is due to the fact that while the size of the Fermi surface increases as ε_F increases, the Berry curvature decreases. We also note that the transport coefficient goes to zero, as expected, when ε_F approaches the bottom of the conduction band, since there are no charge carriers. However, we remark that Boltzmann transport theory is less justified as the carrier density goes to zero. In that case the Fermi wavevector also goes to zero and the wavepacket description loses its meaning.

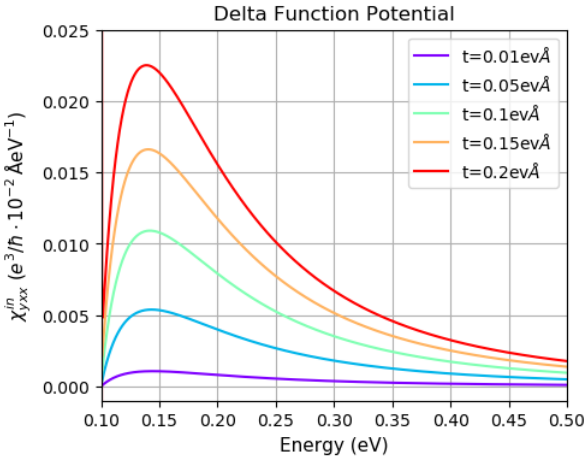

Figure 3.3: Intrinsic contribution to the conductivity tensor for scattering described by a delta function potential in the tilted massive 2D Dirac model, for values of the tilt parameter, t, from 0.01eVÅ to 0.2eVÅ. Parameters are choosen as $n_{imp}u_0^2 = 100\text{eV}^2\text{Å}^2$, $\hbar v = 1\text{eVÅ}$, $m = 0.1\text{eV}$ and $\omega = 200\text{Hz}$.

Partial Side-Jump contribution

As seen in section 2.3, the side-jump velocity is given by Equation 2.31, which we rewrite here for convenience of the reader:

$$v_a^{sj} = \sum_{\mathbf{k}'} w^{in}_{\mathbf{k}\mathbf{k}'} \delta \mathbf{r}^a_{\mathbf{k}\mathbf{k}'}.$$

Since we already computed the transition probability rate, $w^{in}_{\mathbf{k}\mathbf{k}'}$, for a delta function potential (Equation 3.22), and the coordinate shift, both in the context of the tilted Dirac model, we can easily extract the side-jump velocity (see Appendix C.3.2) obtaining:

$$
\begin{aligned}
v_y^{sj} &= -\frac{u_0^2 n_{imp}}{8\hbar\nu}\frac{\cos\phi}{\hbar^2 v^2}\left[4v\hbar\sin\phi\cos\theta + t\Big(3+\cos^2\phi - 2\sin^2\phi\cos^2\theta\Big)\right] \\
v_x^{sj} &= \frac{u_0^2 n_{imp}}{4\hbar\nu}\frac{\cos\phi\sin\theta}{\hbar^2 v^2}\left[2v\hbar\sin\phi - t\sin^2\phi\cos\theta\right].
\end{aligned}
\tag{3.27}
$$

Having an expression for the side-jump velocity allow us to compute the term of the non-linear conductivity tensor in Equation 2.41, related to this quantity (more details on Appendix C.3.2):

$$
\begin{aligned}
\tilde{\chi}_{yxx}^{sj,1} &= \frac{e^3}{\hbar^2}\frac{\tau}{1+i\omega\tau}\frac{\tau}{1+i2\omega\tau}\int_k \partial_{\mathbf{k}}^x f_{\mathbf{k}}^0 \partial_x v_y^{sj} \\
&= \frac{e^3}{\hbar^2}\frac{\tau}{1+i\omega\tau}\frac{\tau}{1+i2\omega\tau}\frac{u_0^2\, n_{imp}}{8\pi\hbar^3 v^2} t\left(\frac{5}{8}\frac{m}{\varepsilon_F} - \frac{38}{8}\frac{m^3}{{\varepsilon_F}^3} + \frac{33}{8}\frac{m^5}{{\varepsilon_F}^5}\right).
\end{aligned}
\tag{3.28}
$$

The remaining terms of the side-jump contribution, as well as the skew-scattering contribution to the conductivity tensor, can be calculated using the same procedure. However, these calculations are lengthy and have not been fully completed.

3.3.2 Screened Coulomb Potential

Representing long-range interactions between electrons and impurities, consider a screened coulomb potential described by

$$
U_C = \sum_{j=1}^{N_{imp}} \frac{eQ}{4\pi\epsilon_0\epsilon|\mathbf{r}-\mathbf{R}_j|} e^{-|\mathbf{r}-\mathbf{R}_j|/L_D},
\tag{3.29}
$$

where eQ is the charge of the impurity, ϵ_0 is the vacuum permittivity, ϵ is the dielectric constant of the material, L_D is the Debye screening length, and $\mathbf{R}_j$ represents the positions of the impurities.

As a first step, let us compute the Boltzmann relaxation time in Equation 3.19, as it is present in all components of the conductivity tensor. The matrix element for the intrinsic transition probability rate given by Fermi's golden rule in Equation 3.20, when applying the screened Coulomb potential, is the following:

$$
\begin{aligned}
\langle \mathbf{k}'|\hat{U}_C|\mathbf{k}\rangle &= \int d\vec{r}\ \Psi_{\mathbf{k}'}^{\dagger}(\vec{r})\ U_C(\vec{r})\ \Psi_{\mathbf{k}}(\vec{r}) \\
&= \frac{eQ}{4\pi\epsilon_0\epsilon\nu}\sum_{j=1}^{N_{imp}}\int d\vec{r'} e^{-i\mathbf{K}\cdot(\mathbf{r}'+\mathbf{R}_j)}\ \frac{e^{-r'/L_D}}{r'}\left(\cos\frac{\phi'}{2}\cos\frac{\phi}{2} + \sin\frac{\phi'}{2}\sin\frac{\phi}{2}e^{-i\tilde{\theta}'}\right),
\end{aligned}
\tag{3.30}
$$

where $\mathbf{K} = \mathbf{k}' - \mathbf{k}$. One way of solving the angular part of the integral is by using the Modified Bessel Function,

$$
I_\alpha(x) = \frac{1}{\pi}\int_0^\pi e^{x\cos\theta}\cos(\alpha\theta)d\theta - \frac{\sin(\alpha\pi)}{\pi}\int_0^\infty e^{-x\cosh t-\alpha t}dt = i^{-\alpha}J_\alpha(ix),
\tag{3.31}
$$

for $\alpha = 0$ and $x = -iKr'$, where $J_\alpha(ix)$ is the Bessel Function. The radial integral then reduces to a standard form, with a known solution available in mathematical tables or

reference books, such as Gradshteyn and Ryzhik's *Table of Integrals, Series, and Products* [34],

$$\int_0^\infty e^{-\nu x} J_\alpha(\beta x)\, dx = \frac{\beta^{-\alpha}\left[\sqrt{\nu^2+\beta^2}-\nu\right]^\alpha}{\sqrt{\nu^2+\beta^2}} \qquad \left[\mathrm{Re}\ \alpha > -1,\ \mathrm{Re}(\nu \pm i\beta) > 0\right], \tag{3.32}$$

for $\beta = K$ and $\nu = 1/L_D$. The matrix element is, therefore:

$$\langle \mathbf{k}'|\hat{U}_C|\mathbf{k}\rangle = \frac{eQ}{2\epsilon_0\epsilon\nu}\frac{L_D}{\sqrt{1+K^2L_D^2}}\left(\cos\frac{\phi'}{2}\cos\frac{\phi}{2}+\sin\frac{\phi'}{2}\sin\frac{\phi}{2}e^{-i\tilde{\theta}'}\right)\left[\sum_{j=1}^{N_{imp}} e^{-i\mathbf{K}\cdot\mathbf{R}_j}\right]. \tag{3.33}$$

Now we can compute the transition probability rate, $w^{in}_{\mathbf{k}\mathbf{k}'}$, by simplifying the modulus squared terms, as done in Equation 3.22 for the delta function potential, obtaining

$$w^{in}_{\mathbf{k}\mathbf{k}'} = \frac{\pi}{\hbar}\frac{n_{imp}}{\nu}\left(\frac{eQ}{2\epsilon_0\epsilon}\right)^2\frac{L_D^2}{1+K^2L_D^2}\left[1+\cos\phi'\cos\phi+\sin\phi'\sin\phi\cos\tilde{\theta}'\right]\delta(\varepsilon_{\mathbf{k}'}-\varepsilon_{\mathbf{k}}), \tag{3.34}$$

to finally substituting it in the Boltzmann relaxation time,

$$\frac{1}{\tau_{\mathbf{k}}} = \sum_{k'}\frac{\pi n_{imp}}{\hbar\nu}\left(\frac{eQ}{2\epsilon_0\epsilon}\right)^2\frac{L_D^2}{1+K^2L_D^2}\left[1+\cos\phi'\cos\phi+\sin\phi'\sin\phi\cos\tilde{\theta}'\right]\left[1-\cos\tilde{\theta}'\right]\delta(\varepsilon_{\mathbf{k}'}-\varepsilon_{\mathbf{k}}). \tag{3.35}$$

We can solve the relaxation time by once again transforming the sum into an integral in polar coordinates, $\frac{\nu}{(2\pi)^2}\int k'dk'd\theta'$, and expanding the Dirac delta as $\delta(\varepsilon_{\mathbf{k}'}-\varepsilon_{\mathbf{k}}) \approx \delta\left(\varepsilon^0_{\mathbf{k}'}-\varepsilon^0_{\mathbf{k}}\right) + t(k'\cos\theta'-k\cos\theta)\partial_{\varepsilon^0_{\mathbf{k}'}}\delta\left(\varepsilon^0_{\mathbf{k}'}-\varepsilon^0_{\mathbf{k}}\right)$ with $\varepsilon^0_{\mathbf{k}}$ indicating the energy of the untilted massive Dirac cone and remembering that $\cos\phi = \frac{m}{\varepsilon^0_{\mathbf{k}}}$. To simplify the angular part, we wrote $\tilde{\theta}'$ in terms of K using the relation $K = 2k\sin\left(\frac{\tilde{\theta}'}{2}\right)$. Note that the integral limits for K are from 0 to $2k$ to cover the entire range, and we must multiply the integral by 2 to account for the full circular surface, as illustrated in Figure 3.4.

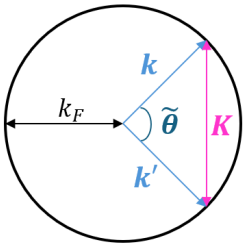

Figure 3.4: Schematic representation of scattering in k-space, illustrating the parameters used to derive the scattering kinematics. Assuming elastic scattering, the k-vectors, $\mathbf{k}$ and $\mathbf{k}'$, have the same magnitude k_F, as indicated by the Fermi surface. The angle between the scatterers is $\tilde{\theta}'$, which is related to the magnitude of $\mathbf{K} = \mathbf{k}' - \mathbf{k}$.

Thus, we obtain the Boltzmann relaxation time for a screened coulomb potential,

$$\tau_{\mathbf{k}}^{-1} = \frac{n_{imp}}{4\hbar^3v^2}\left(\frac{eQ}{2\epsilon_0\epsilon}\right)^2\frac{\varepsilon^0_{\mathbf{k}}}{a^2k^2}\left[a^2\left(2-\frac{2}{\sqrt{a^2+1}}\right)+\frac{\hbar^2v^2k^2}{\varepsilon^{0\,2}_{\mathbf{k}}}\left(2-\frac{2}{\sqrt{a^2+1}}-a^2\right)\right]$$
$$+\frac{n_{imp}}{4\hbar^3v^2}\left(\frac{eQ}{2\epsilon_0\epsilon}\right)^2\frac{8t\cos\theta}{k}\left[\frac{1}{a^2}\left(\frac{a^2+2}{\sqrt{1+a^2}}-2\right)\frac{\varepsilon^{0\,2}_{\mathbf{k}}}{\varepsilon^{0\,2}_{\mathbf{k}}-m^2}+\frac{1}{a^4}\left(\frac{3a^2+4}{\sqrt{1+a^2}}-a^2-4\right)\right],$$

(3.36)

with $a = 2kL_D$. By incorporating the Boltzmann relaxation time in the limit $t \ll \hbar v$ into the intrinsic conductivity tensor from Equation 3.7 for scattering described by a screened Coulomb potential, we observe in Figure 3.5 how it varies with different values of the tilt parameter. In panel 3.5(a), we show the result for the case when the screening length is small, $L_D = 1$Å. Clearly, the result is very similar to the one obtained for the Delta-potential. We see in panel 3.5(b), where we used $L_D = 10$Å, that Coulomb scattering becomes less relevant as the range of the potential increases.

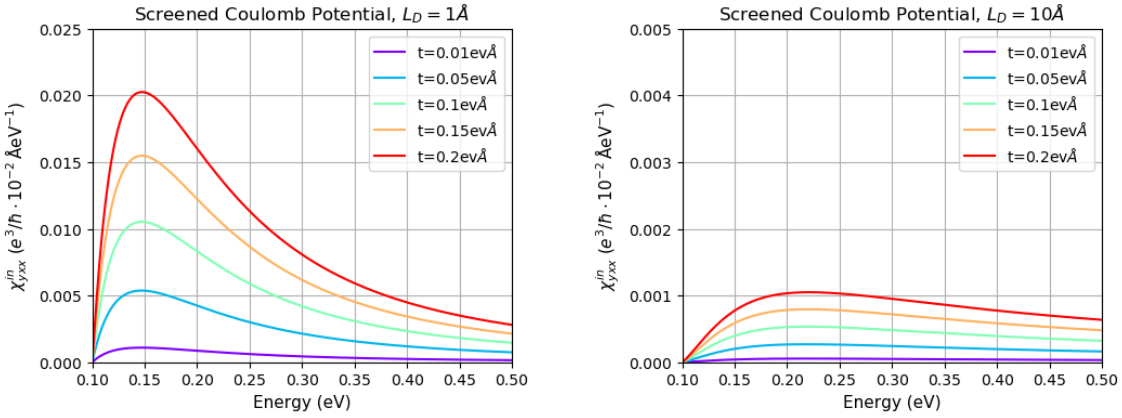

(a) (b)

Figure 3.5: Intrinsic contribution to the conductivity tensor for scattering described by a screened Coulomb potential in the tilted massive 2D Dirac model, for values of the tilt parameter, t, from 0.01eVÅ to 0.2eVÅ. Parameters are chosen as $n_{imp}(\frac{eQ}{2\epsilon_0\epsilon})^2 = 100\text{eV}^2\text{Å}^2$, $\hbar v = 1$eVÅ, $m = 0.1$eV, and $\omega = 200$Hz. a) $L_D = 1$Å. b) $L_D = 10$Å.

3.3.3 Electron-Phonon Interaction

When disorder is caused by lattice scattering, the perturbation can be represented by the Hamiltonian of the electron-phonon interaction expressed in second quantization:

$$\begin{aligned}\mathcal{H}_{ep} &= \sum_{c=a,b} \sum_{\mathbf{k_1},\mathbf{k_2},\tilde{\mathbf{q}}} V_{\tilde{\mathbf{q}}} c^\dagger_{\mathbf{k_1}} c_{\mathbf{k_2}} \left[\alpha_{\tilde{\mathbf{q}}} + \alpha^\dagger_{-\tilde{\mathbf{q}}}\right] \delta_{\mathbf{k_2},\mathbf{k_1}-\tilde{\mathbf{q}}} \\ &= \sum_{\mathbf{k_1},\mathbf{k_2},\tilde{\mathbf{q}}} V_{\tilde{\mathbf{q}}} \left[a^\dagger_{\mathbf{k_1}} a_{\mathbf{k_2}} + b^\dagger_{\mathbf{k_1}} b_{\mathbf{k_2}}\right] \left[\alpha_{\tilde{\mathbf{q}}} + \alpha^\dagger_{-\tilde{\mathbf{q}}}\right] \delta_{\mathbf{k_2},\mathbf{k_1}-\tilde{\mathbf{q}}}\end{aligned} \tag{3.37}$$

where $(\alpha_{\mathbf{q}}, \alpha^\dagger_{\mathbf{q}})$ are the destruction and creation operators for phonons with wavenumber $\mathbf{q}$, and $(c_{\mathbf{k}}, c^\dagger_{\mathbf{k}})$ denotes the destruction and creation operators of an electron in a given sublattice a or b and with wavevector $\mathbf{k}$. The deformation potential induced by the phonons for an electron-phonon coupling parameter g_0, is given by

$$V_{\tilde{\mathbf{q}}} = \frac{g_0}{\varepsilon(\tilde{q})} i\tilde{q} \sqrt{\frac{\hbar}{2\nu\rho\omega_{\tilde{\mathbf{q}}}}}, \tag{3.38}$$

where we take into account screening effects through the dielectric function $\varepsilon(\tilde{\mathbf{q}})$ (details are given in Appendix D).

The scattering occurs only through the emission or absorption of a phonon, thus the initial and final states are, respectively, tensorial products of the form $|i\rangle \equiv |\mathbf{k}\rangle \otimes |n_{\mathbf{q}}\rangle$

and $|f\rangle \equiv |\mathbf{k}'\rangle \otimes |n_{\mathbf{q}} \pm 1\rangle$, where $|n_{\mathbf{q}}\rangle$ is the phonon state in the occupation number representation.

We can write the matrix element as the following:

$$\langle f|\mathcal{H}_{ep}|i\rangle = \langle \mathbf{k}'; n_{\mathbf{q}} \pm 1| \sum_{\mathbf{k_1},\mathbf{k_2},\tilde{\mathbf{q}}} V_{\tilde{\mathbf{q}}} \left[a^{\dagger}_{\mathbf{k_1}} a_{\mathbf{k_2}} + b^{\dagger}_{\mathbf{k_1}} b_{\mathbf{k_2}}\right] \left[\alpha_{\tilde{\mathbf{q}}} + \alpha^{\dagger}_{-\tilde{\mathbf{q}}}\right] \delta_{\mathbf{k_2},\mathbf{k_1}-\tilde{\mathbf{q}}} \, |\mathbf{k}; n_{\mathbf{q}}\rangle \, . \quad (3.39)$$

The destruction and creation operators of an electron can be expressed in terms of the eigenmodes of the free Hamiltonian, where $e_{\mathbf{k}}$ stands for electron-like (positive energy) excitations and $h_{\mathbf{k}}$ for hole-like (negative energy) excitations,

$$\begin{aligned} a_{\mathbf{k}} &= \cos\frac{\phi_{\mathbf{k}}}{2} e_{\mathbf{k}} + \sin\frac{\phi_{\mathbf{k}}}{2} h_{\mathbf{k}} \\ b_{\mathbf{k}} &= \sin\frac{\phi_{\mathbf{k}}}{2} e^{-i\theta_{\mathbf{k}}} e_{\mathbf{k}} - \cos\frac{\phi_{\mathbf{k}}}{2} e^{-i\theta_{\mathbf{k}}} h_{\mathbf{k}}. \end{aligned} \quad (3.40)$$

Since the Fermi level is in the conduction band, the matrix element becomes:

$$\langle \mathbf{k}'; n_{\mathbf{q}} \pm 1| \sum_{\mathbf{k_1},\mathbf{k_2},\tilde{\mathbf{q}}} V_{\tilde{\mathbf{q}}} \left[\cos\frac{\phi_{\mathbf{k_1}}}{2}\cos\frac{\phi_{\mathbf{k_2}}}{2} + \sin\frac{\phi_{\mathbf{k_1}}}{2}\sin\frac{\phi_{\mathbf{k_2}}}{2} e^{i(\theta_{\mathbf{k_1}}-\theta_{\mathbf{k_2}})}\right] e^{\dagger}_{\mathbf{k_1}} e_{\mathbf{k_2}} \left[\alpha_{\tilde{\mathbf{q}}} + \alpha^{\dagger}_{-\tilde{\mathbf{q}}}\right] \delta_{\mathbf{k_2},\mathbf{k_1}-\tilde{\mathbf{q}}} \, |\mathbf{k}; n_{\mathbf{q}}\rangle \, . \quad (3.41)$$

For scattering occurring by absorption of a phonon, $|f\rangle \equiv |\mathbf{k}'; n_{\mathbf{q}} - 1\rangle$, and by emission of a phonon, $|f\rangle \equiv |\mathbf{k}'; n_{\mathbf{q}} + 1\rangle$, the matrix element for each event are, respectively:

$$\langle f|\mathcal{H}_{ep}|i\rangle_{abs} = \left[\cos\frac{\phi'}{2}\cos\frac{\phi}{2} + \sin\frac{\phi'}{2}\sin\frac{\phi}{2} e^{i\tilde{\theta}'}\right] V_{\mathbf{q}}\sqrt{n_{\mathbf{q}}} \; \delta_{\mathbf{k},\mathbf{k}'-\mathbf{q}}, \quad (3.42)$$

$$\langle f|\mathcal{H}_{ep}|i\rangle_{emi} = \left[\cos\frac{\phi'}{2}\cos\frac{\phi}{2} + \sin\frac{\phi'}{2}\sin\frac{\phi}{2} e^{i\tilde{\theta}'}\right] V_{-\mathbf{q}}\sqrt{n_{\mathbf{q}}+1} \; \delta_{\mathbf{k},\mathbf{k}'+\mathbf{q}}. \quad (3.43)$$

The transition probability rate is the sum of all possible mechanisms,

$$W^{\mathbf{k}'}_{\mathbf{k}} = \left[W^{\mathbf{k}'}_{\mathbf{k}}\right]_{abs} + \left[W^{\mathbf{k}'}_{\mathbf{k}}\right]_{emi}. \quad (3.44)$$

The Boltzmann relaxation time can be obtained by calculating the transition probability rate using Fermi's golden rule,

$$w^{in}_{\mathbf{k}\mathbf{k}'} = \frac{2\pi}{\hbar} \left|\langle f|\mathcal{H}_{ep}|i\rangle\right|^2 \delta(\varepsilon_f - \varepsilon_i). \quad (3.45)$$

The initial energy corresponds to $\varepsilon_{\mathbf{k}}$ and the final energy is $\varepsilon_{\mathbf{k}'} \equiv \varepsilon_{\mathbf{k}} \pm \hbar\omega_{\mathbf{q}}$ depending on whether the phonon is absorbed or emitted, with $\hbar\omega_{\mathbf{q}}$ representing the phonon energy.

$$\left[w^{in}_{\mathbf{k}\mathbf{k}'}\right]_{abs} = \frac{2\pi}{\hbar} \left|\cos\frac{\phi'}{2}\cos\frac{\phi}{2} + \sin\frac{\phi'}{2}\sin\frac{\phi}{2} e^{i\tilde{\theta}'}\right|^2 \left|V_{\mathbf{q}}\sqrt{n_{\mathbf{q}}}\delta_{\mathbf{k},\mathbf{k}'-\mathbf{q}}\right|^2 \delta(\varepsilon_{\mathbf{k}'} - \varepsilon_{\mathbf{k}} - \hbar\omega_{\mathbf{q}}), \quad (3.46)$$

$$\left[w^{in}_{\mathbf{k}\mathbf{k}'}\right]_{emi} = \frac{2\pi}{\hbar} \left|\cos\frac{\phi'}{2}\cos\frac{\phi}{2} + \sin\frac{\phi'}{2}\sin\frac{\phi}{2} e^{i\tilde{\theta}'}\right|^2 \left|V_{-\mathbf{q}}\sqrt{n_{\mathbf{q}}+1}\delta_{\mathbf{k},\mathbf{k}'+\mathbf{q}}\right|^2 \delta(\varepsilon_{\mathbf{k}'} - \varepsilon_{\mathbf{k}} + \hbar\omega_{\mathbf{q}}). \quad (3.47)$$

By employing the conventional quasielastic approximation of neglecting the phononic contribution to the energy conservation, as the typical phonon energies are small compared to ε_F, and by simplifying the modulus squared,

$$w^{in}_{\mathbf{k}\mathbf{k}'} = \frac{\pi}{\hbar}\Big[1 + \cos\phi'\cos\phi + \sin\phi'\sin\phi\cos\tilde{\theta}'\Big]|V_{\mathbf{q}}|^2\Big[n_{\mathbf{q}}\ \delta_{\mathbf{k},\mathbf{k}'-\mathbf{q}} + \Big(n_{\mathbf{q}}+1\Big)\delta_{\mathbf{k},\mathbf{k}'+\mathbf{q}}\Big]\delta(\varepsilon_{\mathbf{k}'} - \varepsilon_{\mathbf{k}})$$
$$= \frac{\pi}{\hbar}f(\phi,\phi',\tilde{\theta}')|V_{\mathbf{q}}|^2\Big[n_{\mathbf{q}}\ \delta_{\mathbf{k},\mathbf{k}'-\mathbf{q}} + \Big(n_{\mathbf{q}}+1\Big)\delta_{\mathbf{k},\mathbf{k}'+\mathbf{q}}\Big]\delta(\varepsilon_{\mathbf{k}'} - \varepsilon_{\mathbf{k}}), \tag{3.48}$$

where we used that $|V_{\mathbf{q}}| = |V_{-\mathbf{q}}|$ since the deformation potential is a pure imaginary quantity.

By inserting the transition probability rate into the Boltzmann relaxation time Equation 3.19, we obtain

$$\frac{1}{\tau_{\mathbf{k}}} = \frac{\pi}{\hbar}\sum_{k'} f(\phi,\phi',\tilde{\theta}')\Big[1-\cos\tilde{\theta}'\Big]|V_{\mathbf{k}'-\mathbf{k}}|^2\Big[2n_{\mathbf{k}'-\mathbf{k}}+1\Big]\delta(\varepsilon_{\mathbf{k}'}-\varepsilon_{\mathbf{k}}). \tag{3.49}$$

After introducing the variable substitution, $\mathbf{K} = \mathbf{k}'-\mathbf{k}$, let the phonon occupation number, $n_{\mathbf{K}}$, be described by the Bose-Einstein distribution function, $n_{\mathbf{K}} = [\exp(\hbar\omega_{\mathbf{K}}/k_BT)-1]^{-1}$. At high temperatures, where this scattering mechanism dominates over the temperature-independent ones, all phonons contribute significantly to the scattering, meaning that $n_{\mathbf{K}} \gg 1$. This condition implies $\hbar\omega_{\mathbf{K}} \ll k_BT$, enabling us to approximate $2n_{\mathbf{K}}+1 \approx 2k_BT/\hbar\omega_{\mathbf{K}}$, with $\omega_{\mathbf{K}} = v_PK$. The relaxation time thus becomes,

$$\frac{1}{\tau_{\mathbf{k}}} = \frac{2\pi k_BT}{\hbar^2 v_P}\sum_{k'} f(\phi,\phi',\tilde{\theta}')\Big[1-\cos\tilde{\theta}'\Big]\frac{|V_{\mathbf{K}}|^2}{K}\delta(\varepsilon_{\mathbf{k}'}-\varepsilon_{\mathbf{k}}), \tag{3.50}$$

and we can solve it by transforming the sum into an integral in polar coordinates, $\frac{\nu}{(2\pi)^2}\int k'dk'd\theta'$, and expanding the Dirac delta as $\delta(\varepsilon_{\mathbf{k}'}-\varepsilon_{\mathbf{k}}) \approx \delta\left(\varepsilon^0_{\mathbf{k}'}-\varepsilon^0_{\mathbf{k}}\right)+t(k'\cos\theta'-k\cos\theta)\partial_{\varepsilon^0_{\mathbf{k}'}}\delta\left(\varepsilon^0_{\mathbf{k}'}-\varepsilon^0_{\mathbf{k}}\right)$ with $\varepsilon^0_{\mathbf{k}}$ indicating the energy of the untilted massive Dirac cone and remembering that $\cos\phi = \frac{m}{\varepsilon^0_{\mathbf{k}}}$. To simplify the angular part, we wrote $\tilde{\theta}'$ in terms of K using the relation $K = 2k\sin\left(\frac{\tilde{\theta}'}{2}\right)$. Note that the integral limits for K are from 0 to $2k$ to cover the entire range, and we must multiply the integral by 2 to account for the full circular surface, as illustrated in Figure 3.4.

Thus, we obtain the Boltzmann relaxation time for lattice scattering represented by the electron-phonon interaction,

$$\tau_{\mathbf{k}} = \frac{2\rho}{g^2}\frac{\hbar v_P^2}{k_BT}\hbar^2v^2\left[\frac{2{\varepsilon^0_{\mathbf{k}}}^2+10m^2}{\varepsilon^0_{\mathbf{k}}} + tk\cos\theta\ \frac{5{\varepsilon^0_{\mathbf{k}}}^2+7m^2}{{\varepsilon^0_{\mathbf{k}}}^2-m^2}\right]^{-1}. \tag{3.51}$$

By incorporating the Boltzmann relaxation time in the limit $t \ll \hbar v$ into the intrinsic conductivity tensor from Equation 3.7 for scattering described by electron-phonon interaction, we observe in Figure 3.6 how it varies with different values of the tilt parameter.

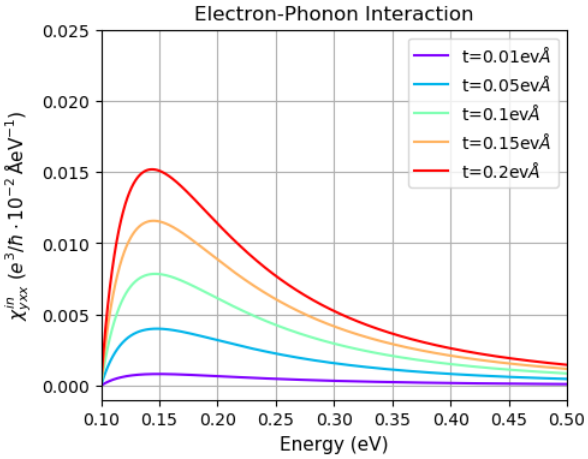

Figure 3.6: Intrinsic contribution to the conductivity tensor for scattering described by electron-phonon interaction in the tilted massive 2D Dirac model, for values of the tilt parameter, t, from 0.01eVÅ to 0.2eVÅ. Parameters are choosen as $\frac{g^2}{2\rho v_P^2} = 500\text{eVÅ}^2$, $T = 270\text{K}$, $\hbar v = 1\text{eVÅ}$, $m = 0.1\text{eV}$ and $\omega = 200\text{Hz}$.

By choosing a fixed tilt parameter, we can see how the conductivity tensor changes with temperature when the scattering is dominated by lattice scattering instead of impurity scattering. In the limit $\omega\tau \ll 1$, which is the experimentally relevant case, we find $\chi^{in}_{yxx} \propto T^{-1}$.

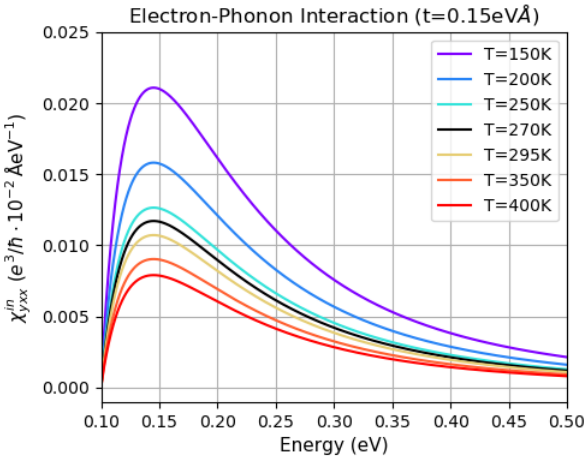

Figure 3.7: Intrinsic contribution to the conductivity tensor for scattering described by electron-phonon interaction in the tilted massive 2D Dirac model, for temperatures from 150K to 400K. Parameters are chosen as $t = 0.15\text{eVÅ}$, $\frac{g^2}{2\rho v_P^2} = 500\text{eVÅ}^2$, $\hbar v = 1\text{eVÅ}$, $m = 0.1\text{eV}$ and $\omega = 200\text{Hz}$.

Chapter 4

Future Work

The work presented in this thesis has advanced our understanding of the non-linear Hall effect, but it also opens the door to numerous avenues for further investigation. Several aspects remain to be explored in greater depth, such as the extrinsic contributions to the non-linear conductivity tensor for the different scattering mechanisms (Delta function potential, Screened Coulomb potential and Electron-Phonon interaction), and a scaling law that will allow us to distinguish between the three contributions of the non-linear conductivity tensor (intrinsic, side-jump and skew-scattering).

To complement the theoretical study, although no measurement results were obtained during this study, an experimental setup was successfully implemented as part of this thesis. This setup lays the foundation for future advancements in exploring non-linear electric transport phenomena and provides a robust starting point for experimental validation.

4.1 Experimental Setup for Non-Linear Hall Measurements

Experimentally, exploring non-linear electric transport often involves detecting second harmonic generation Hall voltages under sinusoidal excitation. This measurement is typically conducted using a lock-in amplifier in conjunction with a Keithley 6221 DC/AC current source [7]. However, due to specific experimental requirements, a custom AC current source was developed.

The sinusoidal excitation was generated using the reference signal from an SR830 Lock-In Amplifier, which provides a maximum output of 5V, and single frequency sine waves that can be generated from 1mHz to 102kHz, corresponding to the low-frequency regime. The custom AC current source was designed with a high-value series resistor, chosen to be 100 times greater than the expected resistance of the sample. For samples with resistances ranging from 100 $k\Omega$ to 1 $M\Omega$, a 100 $M\Omega$ series resistor was selected. This configuration ensures that the current through the sample deviates by no more than 1%, a critical requirement for maintaining measurement accuracy. A schematic representation of the circuit is shown in Figure 4.1.

The series resistor plays a pivotal role in converting the input voltage into a stable sinusoidal current. This design eliminates potential issues related to saturation, thereby preserving the integrity of the Hall voltage measurements. By employing this resistor-based approach, precise control over the excitation current is achieved, enabling accurate studies of the non-linear Hall effect and reliable measurement of second harmonic Hall voltages.

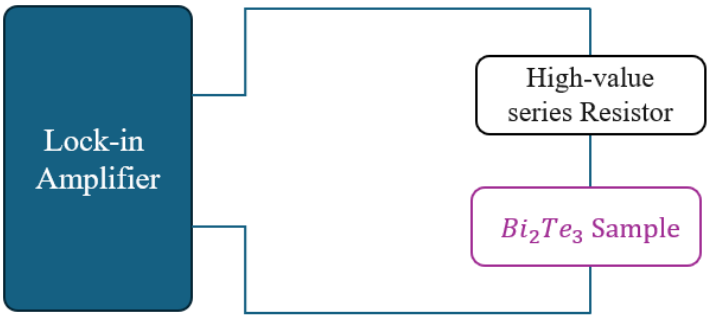

Figure 4.1: Schematic representation of the non-linear Hall effect circuit adapted with a lock-in amplifier and a high-value series resistor.

Another important step in investigating the non-linear Hall effect, experimentally, is the careful preparation of the samples. In this study, we used Bi_2Te_3 thin films, a well-known topological insulator, as our material platform. The choice of Bi_2Te_3 was motivated by its strong spin-orbit coupling and the presence of topological surface states, from which we expect a significant contribution to the non-linear Hall response.

The thin films were deposited using a CY Scientific Instrument Sputtering device under carefully controlled deposition conditions: an applied current of 20 mA, an argon (Ar) flux of 50 sccm, and a table rotation speed of 60 rpm. Prior to the sputtering process, the substrates underwent chemical treatment to ensure a clean surface, free from contaminants, which is critical for ensuring proper film adhesion and high-quality deposition.

Once the films were prepared, the samples were patterned into Hall bar geometries using optical lithography. The Hall bars were created using a flexible polyester mask, which allowed for precision in defining the geometry of the sample. To further illustrate the quality and structure of the prepared samples, Figure 4.2 shows a microscopic image of the fabricated Hall bar, showing the well-defined edges and reasonably uniform surface.

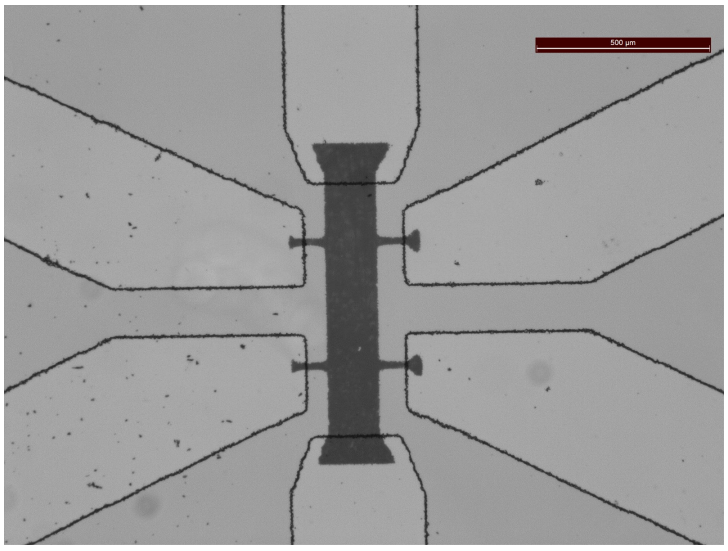

Figure 4.2: Microscopic image of the fabricated Bi_2Te_3 Hall bar, showing the well-defined geometry achieved through optical lithography. The scale bar represents 500 μm.

To perform the measurements at low temperatures, the sample will be placed inside a vacuum chamber. This setup will ensure thermal isolation and enable precise control over the temperature, which is critical for studying electric transport phenomena under cryogenic conditions.

Chapter 5

Conclusions

This thesis has provided an in-depth exploration of the Non-Linear Hall Effect through the development of a theoretical framework within the semiclassical Boltzmann transport theory. By deriving and analyzing the Boltzmann equation, we identified the three primary disorder contributions – intrinsic, side-jump, and skew-scattering mechanisms. These mechanisms, arising from distinct physical origins, were systematically separated and addressed through their corresponding distribution functions under appropriate approximations. This approach clarified the structure of the non-linear conductivity tensor and its dependence on various scattering processes.

Furthermore, we established the importance of incorporating specific scattering mechanisms, such as impurity or lattice scattering, to determine the $\mathcal{T}$-matrix elements and the relaxation time parameter. These quantities are crucial for quantifying the contributions of different scattering processes to the NLHE. The formalism laid out in this work not only provides a comprehensive understanding of the NLHE but also sets the stage for its application to specific physical models, enabling deeper insights into the interplay between topology, symmetry, and transport phenomena in condensed matter systems.

By aiming to use the topological insulator Bi_2Te_3 as the material sample in the experimental study, we applied the Tilted 2D Massive Dirac model to the transport theory. We investigated three primary types of scattering mechanisms: impurity scattering characterized by a delta function and screened Coulomb potentials, and temperature-driven lattice scattering described by the electron-phonon interaction. The exploration of electron-phonon scattering provided insights into how temperature affects the NLHE, enhancing our understanding of its temperature dependence.

To complement the theoretical study, although no measurement results were obtained during this study, an experimental setup was successfully implemented as part of this thesis. Our experimental approach involved adapting a conventional Hall setup with an AC current and lock-in amplifiers for the study of Bi_2Te_3 samples.

Ultimately, the theoretical and experimental groundwork laid in this thesis presents a strong basis for future research.

Appendix A

Relaxation time

In the presence of an electric field, $\mathbf{E}$, the Boltzmann equation for a spatially uniform system is:

$$\left[\frac{\partial}{\partial t} - \frac{e}{\hbar}\mathbf{E}\cdot\frac{\partial}{\partial \mathbf{k}}\right] f_{\mathbf{k}} = \sum_{\mathbf{k}'} W_{\mathbf{k}\mathbf{k}'}\left[f_{\mathbf{k}'} - f_{\mathbf{k}}\right] \tag{A.1}$$

where $W_{\mathbf{k}\mathbf{k}'}$ is given by Fermi's golden rule and is assumed to have only symmetric contributions. In the weak field regime, the steady-state distribution should not depart very far from equilibrium, $f_{\mathbf{k}} = f^0_{\mathbf{k}} + \delta f_{\mathbf{k}}$ [29], such that $\delta f_{\mathbf{k}}$ can be expanded in the applied field. Therefore, the Boltzmann equation can be simplified by keeping only the first-order terms in the applied field,

$$\frac{\partial \delta^1 f_{\mathbf{k}}}{\partial t} - \frac{e}{\hbar}\mathbf{E}\cdot\frac{\partial f^0_{\mathbf{k}}}{\partial \mathbf{k}} = \sum_{\mathbf{k}'} W_{\mathbf{k}\mathbf{k}'}\left[\delta^1 f_{\mathbf{k}'} - \delta^1 f_{\mathbf{k}}\right]. \tag{A.2}$$

To solve the equation, the relaxation time approximation for the scattering term, is usually used,

$$\sum_{\mathbf{k}'} W_{\mathbf{k}\mathbf{k}'}\left[\delta^1 f_{\mathbf{k}'} - \delta^1 f_{\mathbf{k}}\right] = -\frac{\delta^1 f_{\mathbf{k}}}{\tau_{\mathbf{k}}}. \tag{A.3}$$

This suggests that we can write $\sum_{\mathbf{k}'} W_{\mathbf{k}\mathbf{k}'}\delta^1 f_{\mathbf{k}'}$ in terms of $\delta^1 f_{\mathbf{k}}$. On the other hand, the second term on the left-hand side of Eq. (A.2) is proportional to $\cos(\theta_{\mathbf{k},\mathbf{E}})$, where $\theta_{\mathbf{k},\mathbf{E}}$ is the angle between the vectors $\mathbf{k}$ and $\mathbf{E}$. If we take the term of the time derivative to the right-hand side of the equation, we see that $\delta^1 f$ appears in all terms, suggesting that it must be $\delta^1 f_{\mathbf{k}}$ that depends on $\cos(\theta_{\mathbf{k},\mathbf{E}})$. In fact, assuming isotropic energy surfaces, we have $W_{\mathbf{k}\mathbf{k}'} = W(k, \theta_{\mathbf{k}\mathbf{k}'})$, where $\theta_{\mathbf{k}\mathbf{k}'} = \theta_{\mathbf{k}',\mathbf{E}} - \theta_{\mathbf{k},\mathbf{E}}$ is the angle between $\mathbf{k}$ and $\mathbf{k}'$, which clearly does not depend on $\cos(\theta_{\mathbf{k},\mathbf{E}})$. Then we make the simplest possible ansatz, $\delta^1 f_{\mathbf{k}} = \alpha(k)\cos\theta_{\mathbf{k},\mathbf{E}}$, which turns out to be the exact solution in this case. The right-hand side of Equation A.2 then becomes

$$\begin{aligned}\sum_{\mathbf{k}'} W_{\mathbf{k}\mathbf{k}'}\left[\delta^1 f_{\mathbf{k}'} - \delta^1 f_{\mathbf{k}}\right] &= \sum_{\mathbf{k}'} W_{\mathbf{k}\mathbf{k}'}\left[\alpha(k')\cos\theta_{\mathbf{k}',\mathbf{E}} - \alpha(k)\cos\theta_{\mathbf{k},\mathbf{E}}\right] \\ &= \alpha(k)\sum_{k'} W_{\mathbf{k}\mathbf{k}'}\left[\cos\theta_{\mathbf{k}',\mathbf{E}} - \cos\theta_{\mathbf{k},\mathbf{E}}\right],\end{aligned} \tag{A.4}$$

where we used $k = k'$ for elastic (or quasi-elastic) scattering.

Let us write $\cos\theta_{\mathbf{k}',\mathbf{E}} = \hat{\mathbf{k}}'\cdot\hat{\mathbf{E}}$ and $\cos\theta_{\mathbf{k},\mathbf{E}} = \hat{\mathbf{k}}\cdot\hat{\mathbf{E}}$, where we use vectors with a hat as a notation for unit vectors. Then, Eq. (A.4) becomes

$$\sum_{\mathbf{k}'} W_{\mathbf{k}\mathbf{k}'} \left[\delta^1 f_{\mathbf{k}'} - \delta^1 f_{\mathbf{k}}\right] = \alpha(\mathbf{k}) \sum_{\mathbf{k}'} W_{\mathbf{k}\mathbf{k}'} \left[\hat{\mathbf{k}}' \cdot \hat{\mathbf{E}} - \hat{\mathbf{k}} \cdot \hat{\mathbf{E}}\right]. \tag{A.5}$$

Additionally, let us write $\mathbf{k}' = \hat{\mathbf{k}}(\hat{\mathbf{k}}\cdot\mathbf{k}')+\mathbf{k}_\perp$, where $\mathbf{k}_\perp$ is the component of $\mathbf{k}'$ perpendicular to $\mathbf{k}$. Then we have

$$\begin{aligned}
\sum_{\mathbf{k}'} W_{\mathbf{k}\mathbf{k}'} \left[\delta^1 f_{\mathbf{k}'} - \delta^1 f_{\mathbf{k}}\right] &= \alpha(k) \sum_{\mathbf{k}'} W_{\mathbf{k}\mathbf{k}'} \left[\hat{\mathbf{k}}' \cdot \hat{\mathbf{E}} - \hat{\mathbf{k}} \cdot \hat{\mathbf{E}}\right] \\
&= \alpha(k) \sum_{\mathbf{k}'} W_{\mathbf{k}\mathbf{k}'} \left[(\hat{\mathbf{k}} \cdot \hat{\mathbf{E}})(\hat{\mathbf{k}}' \cdot \hat{\mathbf{k}}) + \mathbf{k}_\perp \cdot \hat{\mathbf{E}} - \hat{\mathbf{k}} \cdot \hat{\mathbf{E}}\right] \\
&= \alpha(k) \sum_{\mathbf{k}'} W_{\mathbf{k}\mathbf{k}'} \left[\hat{\mathbf{k}} \cdot \hat{\mathbf{E}} \left((\hat{\mathbf{k}}' \cdot \hat{\mathbf{k}}) - 1\right)\right] \\
&= \delta^1 f_{\mathbf{k}} \sum_{\mathbf{k}'} W_{\mathbf{k}\mathbf{k}'} \left[(\hat{\mathbf{k}}' \cdot \hat{\mathbf{k}}) - 1\right],
\end{aligned} \tag{A.6}$$

where we used the fact that [8],

$$\sum_{\mathbf{k}'} W_{\mathbf{k}\mathbf{k}'} \mathbf{k}_\perp \cdot \hat{\mathbf{E}} = \hat{\mathbf{E}} \cdot \sum_{\mathbf{k}'} W_{\mathbf{k}\mathbf{k}'} \mathbf{k}'_\perp = \hat{\mathbf{E}} \cdot \sum_{\mathbf{k}'} W(k, \theta_{\mathbf{k}\mathbf{k}'}) \mathbf{k}_\perp = 0. \tag{A.7}$$

Going back to Eq. (A.3), and using the result

$$\sum_{\mathbf{k}'} W_{\mathbf{k}\mathbf{k}'} \left[\delta^1 f_{\mathbf{k}'} - \delta^1 f_{\mathbf{k}}\right] = \delta^1 f_{\mathbf{k}} \sum_{\mathbf{k}'} W_{\mathbf{k}\mathbf{k}'} \left[(\hat{\mathbf{k}}' \cdot \hat{\mathbf{k}}) - 1\right] = -\frac{\delta^1 f_{\mathbf{k}}}{\tau_{\mathbf{k}}}, \tag{A.8}$$

we obtain the expression for the relaxation time, $\tau_{\mathbf{k}}$,

$$\frac{1}{\tau_{\mathbf{k}}} = \sum_{\mathbf{k}'} W_{\mathbf{k}\mathbf{k}'} \left(1 - \cos\theta_{\mathbf{k}\mathbf{k}'}\right). \tag{A.9}$$

Often, when applying the Boltzmann equation within the relaxation time approximation, a k-independent relaxation time is assumed. In this scenario, the summation in Eq. (A.9) is confined to the Fermi surface, which is expected to dominate the transport contribution in the low-field and low-frequency regime where the Boltzmann equation is applicable. There are cases where the constant relaxation time approximation is an excellent approach: the linear conductivity of a metal with isotropic Fermi surface is a famous example.

All the above considerations were made assuming an isotropic Fermi surface. A generalization to the anisotropic case is possible and has been done, for example, in Ref. [35]. In this dissertation, any anisotropy of the Fermi surface is considered to be a small perturbation. In order to evaluate conductivities to first order in the anisotropy, it is enough to consider the isotropic approximation for the relaxation time.

Appendix B

Non-linear Conductivity Tensor

By expanding the distribution function up to second order, the current density can be written as

$$j_a = -e\int_k \Big(f^0_{\mathbf{k}} + \delta^1 f_{\mathbf{k}} + \delta^2 f_{\mathbf{k}}\Big)\Big(\frac{1}{\hbar}\partial^a_{\mathbf{k}}\varepsilon_{\mathbf{k}} + \epsilon_{abc}\Omega_b\frac{e}{\hbar}E_c + v^{sj}_a\Big). \tag{B.1}$$

In order to determine the non-linear conductivity tensor, let us focus on the second harmonic generation of the current density, i.e., the term quadratic in the electric field,

$$\begin{aligned} j^{2\omega}_a &= -e\int_k \delta^1 f_{\mathbf{k}}\epsilon_{abc}\Omega_b\frac{e}{\hbar}E_c + \delta^2 f_{\mathbf{k}}\Big(\frac{1}{\hbar}\partial^a_{\mathbf{k}}\varepsilon_{\mathbf{k}} + v^{sj}_a\Big) \\ &= -e\int_k\left(\frac{\delta^1\tilde{f}_{\mathbf{k}}e^{i\omega t} + \delta^1\tilde{f}_{\mathbf{k}}{}^* e^{-i\omega t}}{2}\right)\epsilon_{abc}\Omega_b\frac{e}{\hbar}\left(\frac{\mathcal{E}_c e^{i\omega t} + \mathcal{E}^*_c e^{-i\omega t}}{2}\right) + \\ &\quad + \left(\frac{\tilde{f}^0_{\mathbf{k}} + \tilde{f}^{0*}_{\mathbf{k}}}{2} + \frac{\delta^2\tilde{f}_{\mathbf{k}}e^{i2\omega t} + \delta^2\tilde{f}_{\mathbf{k}}{}^* e^{-i2\omega t}}{2}\right)\Big(\frac{1}{\hbar}\partial^a_{\mathbf{k}}\varepsilon_{\mathbf{k}} + v^{sj}_a\Big) \end{aligned} \tag{B.2}$$

where we use that $E_a(t) = \mathfrak{Re}\Big(\mathcal{E}_a e^{i\omega t}\Big)$ and similarly $\delta^n f_{\mathbf{k}} = \mathfrak{Re}\Big(\delta^n\tilde{f}_{\mathbf{k}}e^{in\omega t}\Big)$.

Let $j^{2\omega}_a = \mathfrak{Re}\Big(\tilde{j}^0_a + \tilde{j}^{2\omega}_a e^{i2\omega t}\Big) = \frac{\tilde{j}^0_a + \tilde{j}^{0*}_a}{2} + \frac{\tilde{j}^{2\omega}_a e^{i2\omega t} + \tilde{j}^{2\omega *}_a e^{-i2\omega t}}{2}$, the current density at twice the frequency can be written as

$$\tilde{j}^{2\omega}_a = -e\int_k \delta^1\tilde{f}_{\mathbf{k}}\epsilon_{abc}\Omega_b\frac{e}{2\hbar}\mathcal{E}_c + \delta^2\tilde{f}_{\mathbf{k}}\Big(\frac{1}{\hbar}\partial^a_{\mathbf{k}}\varepsilon_{\mathbf{k}} + v^{sj}_a\Big) = \tilde{\chi}_{abc}\mathcal{E}_b\mathcal{E}_c. \tag{B.3}$$

To further obtain the non-linear conductivity tensor, we only need to derive the distribution function.

B.1 Intrinsic contribution

B.1.1 Intrinsic distribution function

The Boltzmann equation for the intrinsic contribution is given by:

$$\left[\frac{\partial}{\partial t} - \frac{e}{\hbar}E_a(t)\partial^a_{\mathbf{k}}\right]f^{in}_{\mathbf{k}} = -\frac{\delta f^{in}_{\mathbf{k}}}{\tau_{\mathbf{k}}}. \tag{B.4}$$

By solving the Boltzmann equation in the first order in the electric field we obtain:

$$\begin{aligned}
&\tau\partial_t\delta^1 f^{in}_{\mathbf{k}} - \frac{e}{\hbar}\tau E_a(t)\partial^a_{\mathbf{k}} f^0_{\mathbf{k}} = -\delta^1 f^{in}_{\mathbf{k}} \\
\Leftrightarrow\ &\tau\partial_t\big(\delta^1\tilde{f}^{in}_{\mathbf{k}} e^{i\omega t}\big) + \delta^1\tilde{f}^{in}_{\mathbf{k}} e^{i\omega t} = \frac{e}{\hbar}\tau\mathcal{E}_a e^{i\omega t}\partial^a_{\mathbf{k}} f^0_{\mathbf{k}} \\
\Leftrightarrow\ &\tau\delta^1\tilde{f}^{in}_{\mathbf{k}} i\omega e^{i\omega t} + \delta^1\tilde{f}^{in}_{\mathbf{k}} e^{i\omega t} = \frac{e}{\hbar}\tau\mathcal{E}_a e^{i\omega t}\partial^a_{\mathbf{k}} f^0_{\mathbf{k}} \\
\Leftrightarrow\ &\delta^1\tilde{f}^{in}_{\mathbf{k}}(1+i\omega\tau) = \frac{e}{\hbar}\tau\mathcal{E}_a\partial^a_{\mathbf{k}} f^0_{\mathbf{k}} \\
\Longrightarrow\ &\delta^1\tilde{f}^{in}_{\mathbf{k}} = \frac{e}{\hbar}\frac{\tau}{1+i\omega\tau}\mathcal{E}_a\partial^a_{\mathbf{k}} f^0_{\mathbf{k}}.
\end{aligned} \tag{B.5}$$

Once we know $\delta^1\tilde{f}^{in}_{\mathbf{k}}$, we may solve the Boltzmann equation in the second order in the electric field:

$$\begin{aligned}
&\tau\partial_t\delta^2 f^{in}_{\mathbf{k}} - \frac{e}{\hbar}\tau E_a(t)\partial^a_{\mathbf{k}}\delta^1 f^{in}_{\mathbf{k}} = -\delta^2 f^{in}_{\mathbf{k}} \\
\Leftrightarrow\ &\tau\partial_t\big(\delta^2\tilde{f}^{in}_{\mathbf{k}} e^{i2\omega t}\big) + \delta^2\tilde{f}^{in}_{\mathbf{k}} e^{i2\omega t} = \frac{e}{\hbar}\tau\mathcal{E}_a e^{i\omega t}\partial^a_{\mathbf{k}}\big(\delta^1\tilde{f}^{in}_{\mathbf{k}} e^{i\omega t}\big) \\
\Leftrightarrow\ &\tau\delta^2\tilde{f}^{in}_{\mathbf{k}} i2\omega e^{i2\omega t} + \delta^2\tilde{f}^{in}_{\mathbf{k}} e^{i2\omega t} = \frac{e}{\hbar}\tau\mathcal{E}_a e^{i2\omega t}\partial^a_{\mathbf{k}}\delta^1\tilde{f}^{in}_{\mathbf{k}} \\
\Leftrightarrow\ &\delta^2\tilde{f}^{in}_{\mathbf{k}}(1+i2\omega\tau) = \frac{e}{\hbar}\tau\mathcal{E}_a\partial^a_{\mathbf{k}}\delta^1\tilde{f}^{in}_{\mathbf{k}} \\
\Longrightarrow\ &\delta^2\tilde{f}^{in}_{\mathbf{k}} = \frac{e^2}{\hbar^2}\frac{\tau\mathcal{E}_a\mathcal{E}_b}{1+i2\omega\tau}\partial^a_{\mathbf{k}}\left(\frac{\tau\partial^b_{\mathbf{k}} f^0_{\mathbf{k}}}{1+i\omega\tau}\right).
\end{aligned} \tag{B.6}$$

In the constant relaxation time approximation, we may write:

$$\delta^2\tilde{f}^{in}_{\mathbf{k}} = \frac{e^2}{\hbar^2}\frac{\tau^2}{(1+i\omega\tau)(1+i2\omega\tau)}\mathcal{E}_a\mathcal{E}_b\partial^a_{\mathbf{k}}\partial^b_{\mathbf{k}} f^0_{\mathbf{k}}. \tag{B.7}$$

B.1.2 Intrinsic non-linear conductivity tensor

By inserting the expressions for the distribution functions, in both first and second order, into the current density, we obtain the intrinsic non-linear conductivity tensor, for constant relaxation time:

$$\begin{aligned}
\left[j^{2\omega}_a\right]_{in} &= \tilde{\chi}^{in}_{abc}\mathcal{E}_b\mathcal{E}_c \\
&= -e\int_k \delta^1\tilde{f}^{in}_{\mathbf{k}}\epsilon_{abc}\Omega_b\frac{e}{2\hbar}\mathcal{E}_c + \delta^2\tilde{f}^{in}_{\mathbf{k}}\frac{1}{\hbar}\partial^a_{\mathbf{k}}\varepsilon_{\mathbf{k}} \\
&= -\frac{e^3}{\hbar^2}\frac{\tau}{1+i\omega\tau}\int_k\left[\frac{1}{2}\partial^b_{\mathbf{k}} f^0_{\mathbf{k}}\epsilon_{adc}\Omega_d\mathcal{E}_b\mathcal{E}_c + \frac{1}{\hbar}\frac{\tau}{1+i2\omega\tau}\partial^b_{\mathbf{k}}\partial^c_{\mathbf{k}} f^0_{\mathbf{k}}\partial^a_{\mathbf{k}}\varepsilon_{\mathbf{k}}\mathcal{E}_b\mathcal{E}_c\right]
\end{aligned} \tag{B.8}$$

$$\Longrightarrow \tilde{\chi}^{in}_{abc} = -\frac{e^3}{\hbar^2}\frac{\tau}{1+i\omega\tau}\left[\frac{1}{2}\int_k \partial^b_{\mathbf{k}} f^0_{\mathbf{k}}\epsilon_{adc}\Omega_d + \frac{1}{\hbar}\frac{\tau}{1+i2\omega\tau}\int_k \partial^b_{\mathbf{k}}\partial^c_{\mathbf{k}} f^0_{\mathbf{k}}\partial^a_{\mathbf{k}}\varepsilon_{\mathbf{k}}\right]. \tag{B.9}$$

B.2 Side-jump contribution

B.2.1 Side-jump distribution function

The Boltzmann equation for the side-jump contribution is given by:

$$\begin{aligned}\left[\partial_t - \frac{e}{\hbar}E_a\partial^a_{\mathbf{k}}\right]\delta f^{sj}_{\mathbf{k}} &= -\frac{\delta f^{sj}_{\mathbf{k}}}{\tau} + \mathcal{I}^{sj}_{ex}(f^{in}_{\mathbf{k}}) \\ &= -\frac{\delta f^{sj}_{\mathbf{k}}}{\tau} - e\tau E_a\sum_{\mathbf{k}'} S^a_{\mathbf{k}\mathbf{k}'}\left[f^{in}_{\mathbf{k}'} - f^{in}_{\mathbf{k}}\right].\end{aligned} \tag{B.10}$$

By solving the Boltzmann equation in the first order in the electric field we obtain:

$$\begin{aligned}&\tau\partial_t\delta^1 f^{sj}_{\mathbf{k}} = -\delta^1 f^{sj}_{\mathbf{k}} - e\tau E_a\sum_{\mathbf{k}'} S^a_{\mathbf{k}\mathbf{k}'}\left[f^0_{\mathbf{k}'} - f^0_{\mathbf{k}}\right] \\ \Leftrightarrow\ &\tau\partial_t\big(\delta^1\tilde{f}^{sj}_{\mathbf{k}}e^{i\omega t}\big) + \delta^1\tilde{f}^{sj}_{\mathbf{k}}e^{i\omega t} = -e\tau\mathcal{E}_a e^{i\omega t}\partial^a_{\mathbf{k}}\sum_{\mathbf{k}'} S^a_{\mathbf{k}\mathbf{k}'}\left[f^0_{\mathbf{k}'} - f^0_{\mathbf{k}}\right] \\ \Leftrightarrow\ &\delta^1\tilde{f}^{sj}_{\mathbf{k}}(1+i\omega\tau) = -e\tau\mathcal{E}_a\partial^a_{\mathbf{k}}\sum_{\mathbf{k}'} S^a_{\mathbf{k}\mathbf{k}'}\left[f^0_{\mathbf{k}'} - f^0_{\mathbf{k}}\right] \\ \Longrightarrow\ &\delta^1\tilde{f}^{sj}_{\mathbf{k}} = \frac{-e\tau\mathcal{E}_a}{1+i\omega\tau}\partial^a_{\mathbf{k}}\sum_{\mathbf{k}'} S^a_{\mathbf{k}\mathbf{k}'}\left[f^0_{\mathbf{k}'} - f^0_{\mathbf{k}}\right].\end{aligned} \tag{B.11}$$

By solving the Boltzmann equation in the second order in the electric field we obtain:

$$\begin{aligned}&\tau\partial_t\ \delta^2 f^{sj}_{\mathbf{k}} - \frac{e\tau}{\hbar}E_a\partial^a_{\mathbf{k}}\ \delta^1 f^{sj}_{\mathbf{k}} = -\delta^2 f^{sj}_{\mathbf{k}} - e\tau E_a\sum_{\mathbf{k}'} S^a_{\mathbf{k}\mathbf{k}'}\left[\delta^1 f^{in}_{\mathbf{k}'} - \delta^1 f^{in}_{\mathbf{k}}\right] \\ \Leftrightarrow\ &\tau i2\omega\delta^2\tilde{f}^{sj}_{\mathbf{k}} + \delta^2\tilde{f}^{sj}_{\mathbf{k}} = \frac{e\tau}{\hbar}\mathcal{E}_a\partial^a_{\mathbf{k}}\delta^1\tilde{f}^{sj}_{\mathbf{k}} - e\tau\mathcal{E}_a\sum_{\mathbf{k}'} S^a_{\mathbf{k}\mathbf{k}'}\left[\delta^1\tilde{f}^{in}_{\mathbf{k}'} - \delta^1\tilde{f}^{in}_{\mathbf{k}}\right] \\ \Leftrightarrow\ &\delta^2\tilde{f}^{sj}_{\mathbf{k}} = \frac{e\tau\mathcal{E}_a}{1+i2\omega\tau}\left[\frac{\partial^a_{\mathbf{k}}\delta^1\tilde{f}^{sj}_{\mathbf{k}}}{\hbar} - \sum_{\mathbf{k}'} S^a_{\mathbf{k}\mathbf{k}'}\left[\delta^1\tilde{f}^{in}_{\mathbf{k}'} - \delta^1\tilde{f}^{in}_{\mathbf{k}}\right]\right].\end{aligned} \tag{B.12}$$

In the constant relaxation time approximation, we may write:

$$\delta^2\tilde{f}^{sj}_{\mathbf{k}} = \frac{-e^2}{\hbar}\frac{\tau^2\mathcal{E}_a\mathcal{E}_b}{(1+i\omega\tau)(1+i2\omega\tau)}\left[\partial^a_{\mathbf{k}}\partial^b_{\mathbf{k}}\sum_{\mathbf{k}'} S^b_{\mathbf{k}\mathbf{k}'}\left[f^0_{\mathbf{k}'} - f^0_{\mathbf{k}}\right] - \sum_{\mathbf{k}'} S^a_{\mathbf{k}\mathbf{k}'}\left[\partial^b_{\mathbf{k}'}f^0_{\mathbf{k}'} - \partial^b_{\mathbf{k}}f^0_{\mathbf{k}}\right]\right]. \tag{B.13}$$

B.2.2 Side-jump non-linear conductivity tensor

By inserting the expressions for the distribution functions, in both first and second order, into the current density, we obtain the side-jump non-linear conductivity tensor, for constant relaxation time:

$$
\begin{aligned}
\left[j_a^{2\omega}\right]_{sj} =& \tilde{\chi}^{sj}_{abc}\mathcal{E}_b\mathcal{E}_c \\
=& -e\int_k \delta^1\tilde{f}^{sj}_{\mathbf{k}}\epsilon_{abc}\Omega_b\frac{e}{2\hbar}\mathcal{E}_c + \delta^2\tilde{f}^{sj}_{\mathbf{k}}\frac{1}{\hbar}\partial^a_{\mathbf{k}}\varepsilon_{\mathbf{k}} + \delta^2\tilde{f}^{in}_{\mathbf{k}}v^{sj}_a \\
=& \frac{e^3}{2\hbar}\frac{\tau}{1+i\omega\tau}\int_k\left[\partial^b_{\mathbf{k}}\sum_{\mathbf{k}'}S^b_{\mathbf{k}\mathbf{k}'}\left[f^0_{\mathbf{k}'}-f^0_{\mathbf{k}}\right]\right]\epsilon_{adc}\Omega_d\ \mathcal{E}_b\mathcal{E}_c + \\
&+\frac{e^3}{\hbar^2}\frac{\tau^2}{(1+i\omega\tau)(1+i2\omega\tau)}\int_k\left[\partial^b_{\mathbf{k}}\partial_c\sum_{\mathbf{k}'}S^c_{\mathbf{k}\mathbf{k}'}\left[f^0_{\mathbf{k}'}-f^0_{\mathbf{k}}\right]-\sum_{\mathbf{k}'}S^b_{\mathbf{k}\mathbf{k}'}\left[\partial^c_{\mathbf{k}'}f^0_{\mathbf{k}'}-\partial_c f^0_{\mathbf{k}}\right]\right]\partial^a_{\mathbf{k}}\varepsilon_{\mathbf{k}}\ \mathcal{E}_b\mathcal{E}_c \\
&+\frac{e^3}{\hbar^2}\frac{\tau^2}{(1+i\omega\tau)(1+i2\omega\tau)}\int_k\partial^b_{\mathbf{k}}f^0_{\mathbf{k}}\partial_c v^{sj}_a\ \mathcal{E}_b\mathcal{E}_c
\end{aligned}
\tag{B.14}
$$

$$
\begin{aligned}
\Longrightarrow \tilde{\chi}^{sj}_{abc} =& \frac{e^3}{\hbar}\frac{\tau}{1+i\omega\tau}\left[\frac{1}{2}\int_k\left[\partial^b_{\mathbf{k}}\sum_{\mathbf{k}'}S^b_{\mathbf{k}\mathbf{k}'}\left[f^0_{\mathbf{k}'}-f^0_{\mathbf{k}}\right]\right]\epsilon_{adc}\Omega_d + \right. \\
&\left.+\frac{1}{\hbar}\frac{\tau}{1+i2\omega\tau}\int_k\left[\partial^b_{\mathbf{k}}\partial_c\sum_{\mathbf{k}'}S^c_{\mathbf{k}\mathbf{k}'}\left[f^0_{\mathbf{k}'}-f^0_{\mathbf{k}}\right]-\sum_{\mathbf{k}'}S^b_{\mathbf{k}\mathbf{k}'}\left[\partial^c_{\mathbf{k}'}f^0_{\mathbf{k}'}-\partial_c f^0_{\mathbf{k}}\right]\right]\partial^a_{\mathbf{k}}\varepsilon_{\mathbf{k}}+\partial^b_{\mathbf{k}}f^0_{\mathbf{k}}\partial_c v^{sj}_a\right].
\end{aligned}
\tag{B.15}
$$

B.3 Skew-scattering contribution

B.3.1 Skew-scattering distribution function

The Boltzmann equation for the skew-scattering contribution is given by:

$$
\begin{aligned}
\left[\partial_t-\frac{e}{\hbar}E_a\partial^a_{\mathbf{k}}\right]\delta f^{sk}_{\mathbf{k}} =& -\frac{\delta f^{sk}_{\mathbf{k}}}{\tau}\ +\ \mathcal{I}^{sk}_{ex}(f^{in}_{\mathbf{k}}) \\
=& -\frac{\delta f^{sk}_{\mathbf{k}}}{\tau}\ -\ \sum_{\mathbf{k}'}w^{sk}_{\mathbf{k}\mathbf{k}'}\left[f^{in}_{\mathbf{k}'}+f^{in}_{\mathbf{k}}-2f^{in}_{\mathbf{k}'}f^{in}_{\mathbf{k}}\right].
\end{aligned}
\tag{B.16}
$$

By solving the Boltzmann equation in the first order in the electric field we obtain:

$$
\begin{aligned}
&\tau\partial_t\delta^1 f^{sk}_{\mathbf{k}} = -\delta^1 f^{sk}_{\mathbf{k}} - \tau\sum_{\mathbf{k}'}w^{sk}_{\mathbf{k}\mathbf{k}'}\left[\delta^1 f^{in}_{\mathbf{k}'}+\delta^1 f^{in}_{\mathbf{k}}\right] \\
\Leftrightarrow\ &\tau\partial_t\left(\delta^1\tilde{f}^{sk}_{\mathbf{k}}e^{i\omega t}\right)+\delta^1\tilde{f}^{sk}_{\mathbf{k}}e^{i\omega t} = -\tau\sum_{\mathbf{k}'}w^{sk}_{\mathbf{k}\mathbf{k}'}\left[\delta^1\tilde{f}^{in}_{\mathbf{k}'}e^{i\omega t}+\delta^1\tilde{f}^{in}_{\mathbf{k}}e^{i\omega t}\right] \\
\Leftrightarrow\ &\delta^1\tilde{f}^{sk}_{\mathbf{k}}(1+i\omega\tau) = -\frac{e}{\hbar}\frac{\tau^2}{1+i\omega\tau}\mathcal{E}_a\sum_{\mathbf{k}'}w^{sk}_{\mathbf{k}\mathbf{k}'}\left[\partial^a_{\mathbf{k}'}f^0_{\mathbf{k}}+\partial^a_{\mathbf{k}}f^0_{\mathbf{k}}\right] \\
\Longrightarrow\ &\delta^1\tilde{f}^{sk}_{\mathbf{k}} = -\frac{e}{\hbar}\frac{\tau^2}{(1+i\omega\tau)^2}\mathcal{E}_a\sum_{\mathbf{k}'}w^{sk}_{\mathbf{k}\mathbf{k}'}\left[\partial^a_{\mathbf{k}'}f^0_{\mathbf{k}}+\partial^a_{\mathbf{k}}f^0_{\mathbf{k}}\right].
\end{aligned}
\tag{B.17}
$$

By solving the Boltzmann equation in the second order in the electric field we obtain:

$$\begin{aligned}
&\tau\partial_t\ \delta^2 f^{sk}_{\mathbf{k}} - \frac{e\tau}{\hbar}E_a\partial^a_{\mathbf{k}}\ \delta^1 f^{sk}_{\mathbf{k}} = -\delta^2 f^{sk}_{\mathbf{k}} - \tau\sum_{\mathbf{k}'} w^{sk}_{\mathbf{k}\mathbf{k}'}\left[\delta^2 f^{in}_{\mathbf{k}'} + \delta^2 f^{in}_{\mathbf{k}} - 2\delta^1 f^{in}_{\mathbf{k}'}\delta^1 f^{in}_{\mathbf{k}}\right] \\
\Leftrightarrow\ &\tau i2\omega\delta^2\tilde{f}^{sk}_{\mathbf{k}} + \delta^2\tilde{f}^{sk}_{\mathbf{k}} = \frac{e\tau}{\hbar}\mathcal{E}_a\partial^a_{\mathbf{k}}\delta^1\tilde{f}^{sk}_{\mathbf{k}} - \tau\sum_{\mathbf{k}'} w^{sk}_{\mathbf{k}\mathbf{k}'}\left[\delta^2\tilde{f}^{in}_{\mathbf{k}'} + \delta^2\tilde{f}^{in}_{\mathbf{k}} - 2\delta^1\tilde{f}^{in}_{\mathbf{k}'}\delta^1\tilde{f}^{in}_{\mathbf{k}}\right] \\
\Leftrightarrow\ &\delta^2\tilde{f}^{sk}_{\mathbf{k}} = \frac{\tau}{1+i2\omega\tau}\left[\frac{e}{\hbar}\mathcal{E}_a\partial^a_{\mathbf{k}}\delta^1\tilde{f}^{sk}_{\mathbf{k}} - \sum_{\mathbf{k}'} w^{sk}_{\mathbf{k}\mathbf{k}'}\left[\delta^2\tilde{f}^{in}_{\mathbf{k}'} + \delta^2\tilde{f}^{in}_{\mathbf{k}} - 2\delta^1\tilde{f}^{in}_{\mathbf{k}'}\delta^1\tilde{f}^{in}_{\mathbf{k}}\right]\right].
\end{aligned} \tag{B.18}$$

In the constant relaxation time approximation, we may write:

$$\begin{aligned}
\delta^2\tilde{f}^{sk}_{\mathbf{k}} = -\frac{e^2}{\hbar^2}\frac{\tau^3\mathcal{E}_a\mathcal{E}_b}{(1+i\omega\tau)(1+i2\omega\tau)}\Bigg[&\frac{1}{1+i\omega\tau}\partial^a_{\mathbf{k}}\sum_{\mathbf{k}'} w^{sk}_{\mathbf{k}\mathbf{k}'}\left[\partial^b_{\mathbf{k}'}f^0_{\mathbf{k}'} + \partial^b_{\mathbf{k}}f^0_{\mathbf{k}}\right] + \\
&+\sum_{\mathbf{k}'} w^{sk}_{\mathbf{k}\mathbf{k}'}\left[\frac{1}{1+i2\omega\tau}\left[\partial^a_{\mathbf{k}'}\partial^b_{\mathbf{k}'}f^0_{\mathbf{k}'} + \partial^a_{\mathbf{k}}\partial^b_{\mathbf{k}}f^0_{\mathbf{k}}\right] - \frac{2}{1+i\omega\tau}\partial^a_{\mathbf{k}'}f^0_{\mathbf{k}'}\partial^a_{\mathbf{k}}f^0_{\mathbf{k}}\right]\Bigg].
\end{aligned} \tag{B.19}$$

B.3.2 Skew-scattering non-linear conductivity tensor

By inserting the expressions for the distribution functions, in both first and second order, into the current density, we obtain the side-jump non-linear conductivity tensor, for constant relaxation time:

$$\begin{aligned}
\left[j^{2\omega}_a\right]_{sk} &= \tilde{\chi}^{sk}_{abc}\mathcal{E}_b\mathcal{E}_c \\
&= -e\int_k \delta^1\tilde{f}^{sk}_{\mathbf{k}}\epsilon_{abc}\Omega_b\frac{e}{2\hbar}\mathcal{E}_c + \delta^2\tilde{f}^{sk}_{\mathbf{k}}\frac{1}{\hbar}\partial^a_{\mathbf{k}}\varepsilon_{\mathbf{k}}
\end{aligned} \tag{B.20}$$

$$\begin{aligned}
\Longrightarrow \tilde{\chi}^{sk}_{abc} = \ &\frac{e^3}{\hbar^2}\frac{\tau^2}{1+i\omega\tau}\Bigg[\frac{1}{2}\int_k \frac{1}{1+i\omega\tau}\sum_{\mathbf{k}'} w^{sk}_{\mathbf{k}\mathbf{k}'}\left[\partial^b_{\mathbf{k}'}f^0_{\mathbf{k}} + \partial^b_{\mathbf{k}}f^0_{\mathbf{k}}\right]\epsilon_{adc}\Omega_d + \\
&+\frac{1}{\hbar}\frac{\tau}{1+i2\omega\tau}\int_k \frac{1}{1+i\omega\tau}\partial^b_{\mathbf{k}}\sum_{\mathbf{k}'} w^{sk}_{\mathbf{k}\mathbf{k}'}\left[\partial^c_{\mathbf{k}'}f^0_{\mathbf{k}'} + \partial^c_{\mathbf{k}}f^0_{\mathbf{k}}\right]\partial^a_{\mathbf{k}}\varepsilon_{\mathbf{k}} + \\
&+\frac{1}{\hbar}\frac{\tau}{1+i2\omega\tau}\int_k \sum_{\mathbf{k}'} w^{sk}_{\mathbf{k}\mathbf{k}'}\left[\frac{1}{1+i2\omega\tau}\left[\partial^b_{\mathbf{k}'}\partial^c_{\mathbf{k}'}f^0_{\mathbf{k}'} + \partial^b_{\mathbf{k}}\partial^c_{\mathbf{k}}f^0_{\mathbf{k}}\right] - \frac{2}{1+i\omega\tau}\partial^b_{\mathbf{k}'}f^0_{\mathbf{k}'}\partial^b_{\mathbf{k}}f^0_{\mathbf{k}}\right]\partial^a_{\mathbf{k}}\varepsilon_{\mathbf{k}}\Bigg].
\end{aligned} \tag{B.21}$$

Appendix C

Tilted 2D Dirac Model

In this appendix we provide further details on the derivation of the analytical results presented in chapter 3.

C.1 Intrinsic non-linear conductivity tensor and Berry curvature dipole

The intrinsic non-linear conductivity tensor in the constant relaxation time approximation, derived in section B.1 is given by:

$$\begin{aligned}\tilde{\chi}^{in}_{yxx} = &- \frac{e^3}{2\hbar^2}\frac{\tau}{1+i\omega\tau}\int_k \partial^x_{\mathbf{k}} f^0_{\mathbf{k}}\Omega_z + \\ &- \frac{e^3}{\hbar^3}\frac{\tau}{1+i\omega\tau}\frac{\tau}{1+i2\omega\tau}\int_k \partial^x_{\mathbf{k}}\partial^x_{\mathbf{k}} f^0_{\mathbf{k}}\partial^y_{\mathbf{k}}\varepsilon_{\mathbf{k}}.\end{aligned} \tag{C.1}$$

For $\mu \gg k_B T$, we have $f^0_{\mathbf{k}} \approx \Theta(\varepsilon_{\mathbf{k}} - \mu)$, consequently $\partial\varepsilon_{\mathbf{k}}\Theta(\varepsilon_{\mathbf{k}} - \mu) = \delta(\varepsilon_{\mathbf{k}} - \mu)$. Using the Sommerfeld expansion in this limit, the chemical potential becomes $\mu \approx \varepsilon_F + \mathcal{O}(k_B^2 T^2)$, therefore we can rewrite $\partial^x_{\mathbf{k}} f^0_{\mathbf{k}} = \partial^x_{\mathbf{k}}\varepsilon_{\mathbf{k}}\partial_{\varepsilon_{\mathbf{k}}} f^0_{\mathbf{k}} \approx \partial^x_{\mathbf{k}}\varepsilon_{\mathbf{k}}\delta(\varepsilon_{\mathbf{k}} - \varepsilon_F)$:

$$\begin{aligned}\tilde{\chi}^{in}_{yxx} = &- \frac{e^3}{2\hbar^2}\frac{\tau}{1+i\omega\tau}\int_k \Omega_z\partial^x_{\mathbf{k}}\varepsilon_{\mathbf{k}}\delta(\varepsilon_{\mathbf{k}} - \varepsilon_F) + \\ &- \frac{e^3}{\hbar^3}\frac{\tau}{1+i\omega\tau}\frac{\tau}{1+i2\omega\tau}\int_k \partial^y_{\mathbf{k}}\varepsilon_{\mathbf{k}}\partial^x_{\mathbf{k}}\left(\partial^x_{\mathbf{k}}\varepsilon_{\mathbf{k}}\delta(\varepsilon_{\mathbf{k}} - \varepsilon_F)\right).\end{aligned} \tag{C.2}$$

C.1.1 Group velocity term

Let us start by evaluating the integral of the non-linear conductivity tensor part related to the group velocity, by performing a partial integration:

$$\begin{aligned}\int_k \partial^y_{\mathbf{k}}\varepsilon_{\mathbf{k}}\partial^x_{\mathbf{k}}\left(\partial^x_{\mathbf{k}}\varepsilon_{\mathbf{k}}\delta(\varepsilon_{\mathbf{k}} - \varepsilon_F)\right) &= -\int_k \partial^x_{\mathbf{k}}\partial^y_{\mathbf{k}}\varepsilon_{\mathbf{k}}\partial^x_{\mathbf{k}}\varepsilon_{\mathbf{k}}\delta(\varepsilon_{\mathbf{k}} - \varepsilon_F) \\ &= \int_k \frac{\hbar^4 v^4 k_x k_y}{{\varepsilon^0_{\mathbf{k}}}^3}\left[t + \frac{\hbar^2 v^2 k_x}{\varepsilon^0_{\mathbf{k}}}\right]\delta(\varepsilon_{\mathbf{k}} - \varepsilon_F)\end{aligned} \tag{C.3}$$

Assuming t small compared to the Fermi velocity, we are allowed to expand the Dirac delta as

$$\delta(tk_x + \varepsilon^0_{\mathbf{k}} - \varepsilon_F) \approx \delta\left(\varepsilon^0_{\mathbf{k}} - \varepsilon_F\right) + tk_x\partial_{\varepsilon^0_{\mathbf{k}}}\delta\left(\varepsilon^0_{\mathbf{k}} - \varepsilon_F\right). \tag{C.4}$$

By writing the integral in polar coordinates, $\frac{\nu}{(2\pi)^2}\int kdkd\theta$,

$$\frac{\nu}{(2\pi)^2}\int kdkd\theta\frac{\hbar^4v^4k^2\cos\theta\sin\theta}{{\varepsilon^0_{\mathbf{k}}}^3}\left[t+\frac{\hbar^2v^2k\cos\theta}{\varepsilon^0_{\mathbf{k}}}\right]\left[\delta\left(\varepsilon^0_{\mathbf{k}}-\varepsilon_F\right)+tk\cos\theta\partial_{\varepsilon^0_{\mathbf{k}}}\delta\left(\varepsilon^0_{\mathbf{k}}-\varepsilon_F\right)\right], \tag{C.5}$$

the angular integral vanishes. Therefore, for this model, the intrinsic part of the non-linear conductivity tensor only depends on the Berry curvature dipole term.

C.1.2 Berry Curvature Dipole term

The non-linear conductivity tensor part related to the Berry curvature dipole is given by:

$$\begin{aligned}\tilde{\chi}^{in}_{yxx} =& -\frac{e^3}{2\hbar^2}\frac{\tau}{1+i\omega\tau}\int_k\Omega_z\partial^x_{\mathbf{k}}\varepsilon_{\mathbf{k}}\delta(\varepsilon_{\mathbf{k}}-\varepsilon_F)=\\ =&\frac{e^3}{16\pi^2}\frac{\tau}{1+i\omega\tau}\int d^2k\ \frac{mv^2}{(\hbar^2v^2k^2+m^2)^{\frac{3}{2}}}\left[t+\frac{\hbar^2v^2k_x}{\varepsilon^0_{\mathbf{k}}}\right]\delta(\varepsilon_{\mathbf{k}}-\varepsilon_F)=\\ =&\frac{e^3}{16\pi^2}\frac{\tau}{1+i\omega\tau}\int kdkd\theta\ \frac{mv^2}{(\hbar^2v^2k^2+m^2)^{\frac{3}{2}}}\left[t+\frac{\hbar^2v^2k\cos\theta}{\varepsilon^0_{\mathbf{k}}}\right]\left[\delta\left(\varepsilon^0_{\mathbf{k}}-\varepsilon_F\right)+tk\cos\theta\partial_{\varepsilon^0_{\mathbf{k}}}\delta\left(\varepsilon^0_{\mathbf{k}}-\varepsilon_F\right)\right]\end{aligned}$$

Keeping only terms up to first order in t:

$$\begin{aligned}&\frac{e^3}{16\pi^2}\frac{\tau}{1+i\omega\tau}\int kdk\ \frac{mv^2}{(\hbar^2v^2k^2+m^2)^{\frac{3}{2}}}\left[\int_0^{2\pi}\left[t+\frac{\hbar^2v^2k\cos\theta}{\varepsilon^0_{\mathbf{k}}}\right]d\theta\delta\left(\varepsilon^0_{\mathbf{k}}-\varepsilon_F\right)+\right.\\ &\qquad\left.+t\frac{\hbar^2v^2k^2}{\varepsilon^0_{\mathbf{k}}}\int_0^{2\pi}\cos^2\theta d\theta\partial_{\varepsilon^0_{\mathbf{k}}}\delta\left(\varepsilon^0_{\mathbf{k}}-\varepsilon_F\right)\right]=\\ =&\frac{e^3}{16\pi^2}\frac{\tau}{1+i\omega\tau}\int kdk\ \frac{mv^2t}{(\hbar^2v^2k^2+m^2)^{\frac{3}{2}}}\left[2\pi\delta\left(\varepsilon^0_{\mathbf{k}}-\varepsilon_F\right)+\frac{\hbar^2v^2k^2}{\varepsilon^0_{\mathbf{k}}}\pi\partial_{\varepsilon^0_{\mathbf{k}}}\delta\left(\varepsilon^0_{\mathbf{k}}-\varepsilon_F\right)\right]\end{aligned}$$

Remembering that $\varepsilon^0_{\mathbf{k}}=\sqrt{\hbar^2v^2k^2+m^2}$:

$$\begin{aligned}&\frac{e^3}{16\pi}\frac{\tau}{1+i\omega\tau}\int\frac{\varepsilon^0_{\mathbf{k}}}{\hbar^2v^2}\ d\varepsilon^0_{\mathbf{k}}\ \frac{mv^2t}{{\varepsilon^0_{\mathbf{k}}}^3}\left[2\delta\left(\varepsilon^0_{\mathbf{k}}-\varepsilon_F\right)+\frac{\hbar^2v^2}{\varepsilon^0_{\mathbf{k}'}}\frac{{\varepsilon^0_{\mathbf{k}}}^2-m^2}{\hbar^2v^2}\partial_{\varepsilon^0_{\mathbf{k}}}\delta\left(\varepsilon^0_{\mathbf{k}}-\varepsilon_F\right)\right]=\\ =&\frac{e^3}{16\pi}\frac{\tau}{1+i\omega\tau}\frac{mt}{\hbar^2}\int d\varepsilon^0_{\mathbf{k}}\left[\frac{2}{{\varepsilon^0_{\mathbf{k}}}^2}\delta\left(\varepsilon^0_{\mathbf{k}}-\varepsilon_F\right)+\frac{{\varepsilon^0_{\mathbf{k}}}^2-m^2}{{\varepsilon^0_{\mathbf{k}}}^3}\partial_{\varepsilon^0_{\mathbf{k}}}\delta\left(\varepsilon^0_{\mathbf{k}}-\varepsilon_F\right)\right]=\\ =&\frac{e^3}{16\pi}\frac{\tau}{1+i\omega\tau}\frac{mt}{\hbar^2}\left[\frac{2}{{\varepsilon_F}^2}-\frac{-{\varepsilon_F}^2+3m^2}{{\varepsilon_F}^4}\right]\end{aligned}$$

$$\implies\tilde{\chi}^{(2\omega)}_{yxx}=\frac{3e^3}{16\pi}\frac{\tau}{1+i\omega\tau}\frac{mt}{\hbar^2}\left[\frac{{\varepsilon_F}^2-m^2}{{\varepsilon_F}^4}\right] \tag{C.6}$$

C.2 Coordinate Shift

For a spin-independent impurity, the coordinate shift can be expressed as [31]:

$$\delta\mathbf{r}_{\mathbf{k}\mathbf{k}'} = \langle u_{\mathbf{k}}|i\partial_{\mathbf{k}}u_{\mathbf{k}}\rangle - \langle u_{\mathbf{k}'}|i\partial_{\mathbf{k}'}u_{\mathbf{k}'}\rangle - (\partial_{\mathbf{k}} + \partial_{\mathbf{k}'})\arg\left(\langle u_{\mathbf{k}}|u_{\mathbf{k}'}\rangle\right), \tag{C.7}$$

where $\arg\left(\langle u_{\mathbf{k}}|u_{\mathbf{k}'}\rangle\right) = -i\ln\dfrac{\langle u_{\mathbf{k}}|u_{\mathbf{k}'}\rangle}{|\langle u_{\mathbf{k}}|u_{\mathbf{k}'}\rangle|}$.

Let us start by determining the y-component of the coordinate shift,

$$\delta\mathbf{r}^{y}_{\mathbf{k}\mathbf{k}'} = \langle u_{\mathbf{k}}|i\partial_{k_y}u_{\mathbf{k}}\rangle - \langle u_{\mathbf{k}'}|i\partial_{k'_y}u_{\mathbf{k}'}\rangle - \left(\partial_{k_y} + \partial_{k'_y}\right)\arg\left(\langle u_{\mathbf{k}}|u_{\mathbf{k}'}\rangle\right). \tag{C.8}$$

In polar coordinates we write $\partial_{q_y} = \sin\alpha\partial_q + \dfrac{\cos\alpha}{q}\partial_\alpha$ for $(q,\alpha) = \{(k,\theta),(k',\theta')\}$, such that:

$$\begin{aligned} i\langle u_{\mathbf{q}}|\partial_{q_y}u_{\mathbf{q}}\rangle &= i\sin\alpha\langle u_{\mathbf{q}}|\partial_q u_{\mathbf{q}}\rangle + i\frac{\cos\alpha}{q}\langle u_{\mathbf{q}}|\partial_\alpha u_{\mathbf{q}}\rangle \\ &= 0 + i\frac{\cos\alpha}{q}\begin{pmatrix}\cos\frac{\phi}{2} & \sin\frac{\phi}{2}e^{-i\alpha}\end{pmatrix}\partial_\alpha\begin{pmatrix}\cos\frac{\phi}{2}\\ \sin\frac{\phi}{2}e^{i\alpha}\end{pmatrix} = i\frac{\cos\alpha}{q}\begin{pmatrix}\cos\frac{\phi}{2} & \sin\frac{\phi}{2}e^{-i\alpha}\end{pmatrix}\begin{pmatrix}0\\ i\sin\frac{\phi}{2}e^{i\alpha}\end{pmatrix} \\ &= i\frac{\cos\alpha}{q}i\sin^2\frac{\phi}{2} = \cos\alpha\frac{\cos\phi - 1}{2q}. \end{aligned} \tag{C.9}$$

In general, the expression for a derivative in a given coordinate λ of an argument of a complex number A is:

$$\partial_\lambda\arg(A) = \frac{-i}{|A|^2}\left(A^*\partial_\lambda A - \frac{1}{2}\partial_\lambda|A|^2\right). \tag{C.10}$$

In our case, $A \equiv \langle u_{\mathbf{k}}|u_{\mathbf{k}'}\rangle$ and $\lambda = \{k, k', \theta, \theta'\}$.

For

$$\langle u_{\mathbf{k}}|u_{\mathbf{k}'}\rangle = \begin{pmatrix}\cos\frac{\phi}{2} & \sin\frac{\phi}{2}e^{-i\theta}\end{pmatrix}\begin{pmatrix}\cos\frac{\phi'}{2}\\ \sin\frac{\phi'}{2}e^{i\theta'}\end{pmatrix} = \cos\frac{\phi'}{2}\cos\frac{\phi}{2} + \sin\frac{\phi'}{2}\sin\frac{\phi}{2}e^{i\tilde{\theta}'} \equiv A \tag{C.11}$$

$$|\langle u_{\mathbf{k}}|u_{\mathbf{k}'}\rangle|^2 = \frac{1}{2}\left[1 + \cos\phi'\cos\phi + \sin\phi'\sin\phi\cos\tilde{\theta}'\right] \equiv |A|^2, \tag{C.12}$$

we have that, for $(q,\alpha) = (k,\theta)$, the radial component is:

- $\partial_k A = \partial_\phi\left(\cos\dfrac{\phi'}{2}\cos\dfrac{\phi}{2} + \sin\dfrac{\phi'}{2}\sin\dfrac{\phi}{2}e^{i\tilde{\theta}'}\right)\partial_k\phi_k = \dfrac{1}{2}\left(-\cos\dfrac{\phi'}{2}\sin\dfrac{\phi}{2} + \sin\dfrac{\phi'}{2}\cos\dfrac{\phi}{2}e^{i\tilde{\theta}'}\right)\partial_k\phi_k$

  $\implies A^*\partial_k A = \dfrac{1}{4}\left(-\sin\phi\cos\phi' + \sin\phi'\cos\phi\cos\tilde{\theta}' + i\sin\phi'\sin\tilde{\theta}'\right)\partial_k\phi_k$

- $\partial_k|A|^2 = \dfrac{1}{2}\partial_\phi\left[1 + \cos\phi'\cos\phi + \sin\phi'\sin\phi\cos\tilde{\theta}'\right]\partial_k\phi_k = \dfrac{1}{2}\left[-\cos\phi'\sin\phi + \sin\phi'\cos\phi\cos\tilde{\theta}'\right]\partial_k\phi_k$

- $\partial_k\phi = [\partial_\phi k]^{-1} = \left[\partial_\phi\left(\dfrac{m}{v\hbar}\left|\dfrac{\sin\phi}{\cos\phi}\right|\right)\right]^{-1} = \left[\dfrac{m}{v\hbar}\dfrac{1}{\cos^2\phi}\right]^{-1} = \dfrac{\sin\phi\cos\phi}{k}$

$$\implies \partial_k \arg(A) = \frac{1}{4|A|^2}\frac{\sin\phi\cos\phi}{k}\sin\phi'\sin\tilde{\theta}'. \tag{C.13}$$

And the angular component is:

- $\partial_\theta A = -i\sin\frac{\phi'}{2}\sin\frac{\phi}{2}e^{i\tilde{\theta}'}$

$$\begin{aligned}\implies A^*\partial_\theta A &= -i\left[\cos\frac{\phi'}{2}\cos\frac{\phi}{2}+\sin\frac{\phi'}{2}\sin\frac{\phi}{2}e^{-i\tilde{\theta}'}\right]\sin\frac{\phi'}{2}\sin\frac{\phi}{2}e^{i\tilde{\theta}'} = \\ &= -i\left[\frac{1}{4}\sin\phi'\sin\phi e^{i\tilde{\theta}'}+\sin^2\frac{\phi'}{2}\sin^2\frac{\phi}{2}\right] = \\ &= -i\frac{1}{4}\left[\sin\phi'\sin\phi e^{i\tilde{\theta}'}+(1-\cos\phi)(1-\cos\phi')\right]\end{aligned}$$

- $\frac{1}{2}\partial_\theta|A|^2 = \frac{1}{4}\sin\phi'\sin\phi\sin\tilde{\theta}'$

$$\implies \partial_\theta \arg(A) = \frac{-1}{4|A|^2}\left[\sin\phi'\sin\phi\cos\tilde{\theta}'+(1-\cos\phi)(1-\cos\phi')\right]. \tag{C.14}$$

By computing similarly for $(q,\alpha)=(k',\theta')$ and redo the process for the x-component of the coordinate shift, where $\partial_{q_x} = \cos\alpha\partial_q - \frac{\sin\alpha}{q}\partial_\alpha$, we obtain the final expression for each component of the coordinate shift:

$$\begin{aligned}\delta\mathbf{r}^y_{\mathbf{k}\mathbf{k}'} &= \frac{1}{4|A|^2}\left(\frac{\sin\phi}{k}+\frac{\sin\phi'}{k'}\right)\left(\cos\phi\sin\phi'\cos\theta'-\sin\phi\cos\phi'\cos\theta\right) \\ \delta\mathbf{r}^x_{\mathbf{k}\mathbf{k}'} &= \frac{1}{4|A|^2}\left(\frac{\sin\phi}{k}+\frac{\sin\phi'}{k'}\right)\left(\sin\phi\cos\phi'\sin\theta-\cos\phi\sin\phi'\sin\theta'\right)\end{aligned} \tag{C.15}$$

C.3 Delta Function Potential

In this Appendix we provide further details on the derivation of the relaxation time for the delta function potential. We also calculate quantities related to the side-jump contribution for this potential.

C.3.1 Relaxation Time

We start from the expression for the relaxation time in Equation 3.23,

$$\begin{aligned}\frac{1}{\tau(\vec{k})} &= \sum_{k'} w^{in}_{\mathbf{k}\mathbf{k}'}\left[1-\cos\tilde{\theta}'\right] = \\ &= \sum_{k'}\frac{\pi}{\hbar}\,\frac{u_0^2\,n_{imp}}{\nu}\,\left[1+\cos\phi'\cos\phi+\sin\phi'\sin\phi\cos\tilde{\theta}'\right]\delta(\varepsilon_{\mathbf{k}'}-\varepsilon_{\mathbf{k}})\left[1-\cos\tilde{\theta}'\right].\end{aligned}$$

Replacing the summation with an integral and expressing it in polar coordinates, $\sum_{k'} \to \frac{\nu}{(2\pi)^2}\int k'dk'd\theta'$, we have:

$$\frac{u_0^2 n_{imp}}{4\pi\hbar}\int k'dk'd\theta'\left[\underbrace{1+\cos\phi'\cos\phi}_{A}+\underbrace{\sin\phi'\sin\phi}_{B}\cos\tilde{\theta}'\right]\left[1-\cos\tilde{\theta}'\right]\delta(\varepsilon_{\mathbf{k}'}-\varepsilon_{\mathbf{k}})=$$

$$=\frac{u_0^2 n_{imp}}{4\pi\hbar}\int k'dk'd\theta'\left[A+(B-A)\cos\tilde{\theta}'-B\cos^2\tilde{\theta}'\right]\delta(\varepsilon_{\mathbf{k}'}-\varepsilon_{\mathbf{k}}).$$

By expanding the delta function as

$$\delta(\varepsilon_{\mathbf{k}'}-\varepsilon_{\mathbf{k}})\approx\delta\left(\varepsilon^0_{\mathbf{k}'}-\varepsilon^0_{\mathbf{k}}\right)+t(k'\cos\theta'-k\cos\theta)\partial_{\varepsilon^0_{\mathbf{k}'}}\delta\left(\varepsilon^0_{\mathbf{k}'}-\varepsilon^0_{\mathbf{k}}\right), \tag{C.16}$$

and solving the angular integral, we obtain:

$$\frac{u_0^2 n_{imp}}{4\hbar}\int k'dk'\left[(2A-B)\left[\underbrace{\delta(\varepsilon^0_{\mathbf{k}'}-\varepsilon^0_{\mathbf{k}})}_{\otimes}-\underbrace{tk\cos\theta\partial_{\varepsilon^0_{\mathbf{k}'}}\delta\left(\varepsilon^0_{\mathbf{k}'}-\varepsilon^0_{\mathbf{k}}\right)}_{\oplus}\right]+\underbrace{(B-A)tk'\cos\theta\partial_{\varepsilon^0_{\mathbf{k}'}}\delta(\varepsilon^0_{\mathbf{k}'}-\varepsilon^0_{\mathbf{k}})}_{\odot}\right].$$

We now perform a change of variables, from $\mathbf{k}'$ to $\varepsilon^0_{\mathbf{k}'}$, such that:

$$\begin{aligned}
k' &= \frac{\sqrt{{\varepsilon^0_{\mathbf{k}'}}^2-m^2}}{\hbar v} & \cos\phi' &= \frac{m}{\varepsilon^0_{\mathbf{k}'}} & A &= 1+\frac{m^2}{\varepsilon^0_{\mathbf{k}'}\varepsilon^0_{\mathbf{k}}}\\
dk' &= \frac{\varepsilon^0_{\mathbf{k}'}}{\hbar v}\frac{d\varepsilon^0_{\mathbf{k}'}}{\sqrt{{\varepsilon^0_{\mathbf{k}'}}^2-m^2}} & \sin\phi' &= \frac{\sqrt{{\varepsilon^0_{\mathbf{k}'}}^2-m^2}}{\varepsilon^0_{\mathbf{k}'}} & B &= \frac{\sqrt{{\varepsilon^0_{\mathbf{k}'}}^2-m^2}}{\varepsilon^0_{\mathbf{k}'}}\frac{\sqrt{{\varepsilon^0_{\mathbf{k}}}^2-m^2}}{\varepsilon^0_{\mathbf{k}}}
\end{aligned} \tag{C.17}$$

For simplicity, we separate the integral in its three parts,

$$\otimes\int k'dk'(2A-B)\delta(\varepsilon^0_{\mathbf{k}'}-\varepsilon^0_{\mathbf{k}})=\int\frac{\varepsilon^0_{\mathbf{k}'}}{\hbar^2v^2}\,d\varepsilon^0_{\mathbf{k}'}\,(2A-B)\delta(\varepsilon^0_{\mathbf{k}'}-\varepsilon^0_{\mathbf{k}})=$$

$$=\frac{\varepsilon^0_{\mathbf{k}}}{\hbar^2v^2}\left[2\left(1+\frac{m^2}{{\varepsilon^0_{\mathbf{k}}}^2}\right)-\frac{{\varepsilon^0_{\mathbf{k}}}^2-m^2}{{\varepsilon^0_{\mathbf{k}}}^2}\right]=\frac{\varepsilon^0_{\mathbf{k}}}{\hbar^2v^2}\frac{2{\varepsilon^0_{\mathbf{k}}}^2+2m^2-{\varepsilon^0_{\mathbf{k}}}^2+m^2}{{\varepsilon^0_{\mathbf{k}}}^2}=\frac{{\varepsilon^0_{\mathbf{k}}}^2+3m^2}{\hbar^2v^2\varepsilon^0_{\mathbf{k}}}$$

$$\oplus\int k'dk'(2A-B)(-tk\cos\theta)\partial_{\varepsilon^0_{\mathbf{k}'}}\delta\left(\varepsilon^0_{\mathbf{k}'}-\varepsilon^0_{\mathbf{k}}\right)=$$

$$=\int\frac{\varepsilon^0_{\mathbf{k}'}}{\hbar^2v^2}\,d\varepsilon^0_{\mathbf{k}'}\,(2A-B)(-tk\cos\theta)\partial_{\varepsilon^0_{\mathbf{k}'}}\delta(\varepsilon^0_{\mathbf{k}'}-\varepsilon^0_{\mathbf{k}})=$$

$$=tk\cos\theta\int\partial_{\varepsilon^0_{\mathbf{k}'}}\left[\frac{\varepsilon^0_{\mathbf{k}'}}{\hbar^2v^2}(2A-B)\right]d\varepsilon^0_{\mathbf{k}'}\delta(\varepsilon^0_{\mathbf{k}'}-\varepsilon^0_{\mathbf{k}})=\frac{tk\cos\theta}{\hbar^2v^2}\int d\varepsilon^0_{\mathbf{k}'}\delta(\varepsilon^0_{\mathbf{k}'}-\varepsilon^0_{\mathbf{k}})=\frac{tk\cos\theta}{\hbar^2v^2}$$

$$\odot\int k'^2dk'(B-A)t\cos\theta\partial_{\varepsilon^0_{\mathbf{k}'}}\delta\left(\varepsilon^0_{\mathbf{k}'}-\varepsilon^0_{\mathbf{k}}\right)=\int\frac{\varepsilon^0_{\mathbf{k}'}\sqrt{{\varepsilon^0_{\mathbf{k}'}}^2-m^2}}{\hbar^3v^3}d\varepsilon^0_{\mathbf{k}'}\,(B-A)t\cos\theta\partial_{\varepsilon^0_{\mathbf{k}'}}\delta(\varepsilon^0_{\mathbf{k}'}-\varepsilon^0_{\mathbf{k}})=$$

$$=\frac{t\cos\theta}{\hbar^3v^3}\int\partial_{\varepsilon^0_{\mathbf{k}'}}\left[\varepsilon^0_{\mathbf{k}'}\sqrt{{\varepsilon^0_{\mathbf{k}'}}^2-m^2}(B-A)\right]d\varepsilon^0_{\mathbf{k}'}\delta(\varepsilon^0_{\mathbf{k}'}-\varepsilon^0_{\mathbf{k}})=\frac{t\cos\theta}{\hbar^3v^3}\frac{-2m^2}{\sqrt{{\varepsilon^0_{\mathbf{k}}}^2-m^2}}$$

By summing all the different parts again, we finally obtain the expression for the relaxation time under a Delta function potential:

$$\begin{aligned}\frac{1}{\tau(\vec{k})} &= \frac{u_0^2 n_{imp}}{4\hbar}\left[\frac{{\varepsilon_{\mathbf{k}}^0}^2+3m^2}{\hbar^2v^2\varepsilon_{\mathbf{k}}^0}+\frac{tk\cos\theta}{\hbar^2v^2}+\frac{t\cos\theta}{\hbar^3v^3}\frac{-2m^2}{\sqrt{{\varepsilon_{\mathbf{k}}^0}^2-m^2}}\right]= \\ &= \frac{u_0^2 n_{imp}}{4\hbar^3v^2}\left[\frac{{\varepsilon_{\mathbf{k}}^0}^2+3m^2}{\varepsilon_{\mathbf{k}}^0}+\frac{t\cos\theta}{\hbar v}\frac{{\varepsilon_{\mathbf{k}}^0}^2-3m^2}{\sqrt{{\varepsilon_{\mathbf{k}}^0}^2-m^2}}\right].\end{aligned} \tag{C.18}$$

C.3.2 Side-Jump related quantities

Let us start by computing the side-jump velocity given by Equation 2.31:

$$v_y^{sj} = \sum_{\mathbf{k}'} w^{in}_{\mathbf{k}\mathbf{k}'}\delta\mathbf{r}^y_{\mathbf{k}\mathbf{k}'}.$$

By replacing the summation with an integral and expressing it in polar coordinates, $\sum_{k'} \rightarrow \frac{\nu}{(2\pi)^2}\int k'dk'd\theta'$, we have:

$$v_y^{sj} = \frac{1}{(2\pi)^2}\int k'dk'd\theta' w^{in}_{\mathbf{k}\mathbf{k}'}\delta\mathbf{r}^y_{\mathbf{k}\mathbf{k}'} =$$

$$= \frac{u_0^2 n_{imp}}{8\pi\hbar\nu}\int k'dk'd\theta'\left(\frac{\sin\phi}{k}+\frac{\sin\phi'}{k'}\right)\Big(\cos\phi\sin\phi'\cos\theta'-\sin\phi\cos\phi'\cos\theta\Big)\delta(\varepsilon_{\mathbf{k}'}-\varepsilon_{\mathbf{k}})$$

Expanding the delta function (Eq. C.16) and solving the angular integral:

$$\frac{u_0^2 n_{imp}}{8\hbar\nu}\int k'dk'\left(\frac{\sin\phi}{k}+\frac{\sin\phi'}{k'}\right)\Bigg[-2\sin\phi\cos\phi'\cos\theta\delta\left(\varepsilon^0_{\mathbf{k}'}-\varepsilon^0_{\mathbf{k}}\right)+$$

$$+t\Big(k'\cos\phi\sin\phi'+2k\sin\phi\cos\phi'\cos^2\theta\Big)\partial_{\varepsilon^0_{\mathbf{k}'}}\delta\left(\varepsilon^0_{\mathbf{k}'}-\varepsilon^0_{\mathbf{k}}\right)\Bigg]$$

We now perform a change of variables, from $\mathbf{k}'$ to $\varepsilon^0_{\mathbf{k}'}$ (see C.17), such that:

$$\frac{u_0^2 n_{imp}}{8\hbar\nu}\int\frac{d\varepsilon^0_{\mathbf{k}'}}{\hbar v}\Bigg[-\left(\sin(2\phi)+\frac{2m}{\varepsilon^0_{\mathbf{k}'}}\sin\phi\right)\cos\theta\delta\left(\varepsilon^0_{\mathbf{k}'}-\varepsilon^0_{\mathbf{k}}\right)+$$

$$+\frac{m}{v\hbar}t\left(\frac{{\varepsilon^0_{\mathbf{k}'}}^2-m^2}{m^2}\cos^2\phi+\frac{{\varepsilon^0_{\mathbf{k}'}}^2-m^2}{m\varepsilon^0_{\mathbf{k}'}}\cos\phi+2\sin^2\phi\cos^2\theta+\frac{2m}{\varepsilon^0_{\mathbf{k}'}}\frac{\sin^2\phi}{\cos\phi}\cos^2\theta\right)\partial_{\varepsilon^0_{\mathbf{k}'}}\delta\left(\varepsilon^0_{\mathbf{k}'}-\varepsilon^0_{\mathbf{k}}\right)\Bigg]=$$

$$=\frac{u_0^2 n_{imp}}{8\hbar^2\nu v}\int d\varepsilon^0_{\mathbf{k}'}\Bigg[-\left(\sin(2\phi)+\frac{2m}{\varepsilon^0_{\mathbf{k}'}}\sin\phi\right)\cos\theta\delta\left(\varepsilon^0_{\mathbf{k}'}-\varepsilon^0_{\mathbf{k}}\right)+$$

$$-\frac{m}{v\hbar}t\left(\frac{2\varepsilon^0_{\mathbf{k}'}}{m^2}\cos^2\phi+\frac{{\varepsilon^0_{\mathbf{k}'}}^2+m^2}{m{\varepsilon^0_{\mathbf{k}'}}^2}\cos\phi-\frac{2m}{{\varepsilon^0_{\mathbf{k}'}}^2}\frac{\sin^2\phi}{\cos\phi}\cos^2\theta\right)\delta\left(\varepsilon^0_{\mathbf{k}'}-\varepsilon^0_{\mathbf{k}}\right)\Bigg]=$$

$$=-\frac{u_0^2 n_{imp}}{8\hbar^2\nu v}\left[\left(\sin(2\phi)+\frac{2m}{\varepsilon^0_{\mathbf{k}}}\sin\phi\right)\cos\theta+\frac{m}{v\hbar}t\left(\frac{2\varepsilon^0_{\mathbf{k}}}{m^2}\cos^2\phi+\frac{{\varepsilon^0_{\mathbf{k}}}^2+m^2}{m{\varepsilon^0_{\mathbf{k}}}^2}\cos\phi-\frac{2m}{{\varepsilon^0_{\mathbf{k}}}^2}\frac{\sin^2\phi}{\cos\phi}\cos^2\theta\right)\right].$$

Finally, by redoing the process for the x-component of the side-jump velocity, we obtain the final expressions:

$$\begin{aligned} v_y^{sj} &= -\frac{u_0^2 n_{imp}}{8\hbar\nu}\frac{\cos\phi}{\hbar^2 v^2}\left[4v\hbar\sin\phi\cos\theta + t\Big(3+\cos^2\phi - 2\sin^2\phi\cos^2\theta\Big)\right] \\ v_x^{sj} &= \frac{u_0^2 n_{imp}}{4\hbar\nu}\frac{\cos\phi\sin\theta}{\hbar^2 v^2}\left[2v\hbar\sin\phi - t\sin^2\phi\cos\theta\right]. \end{aligned} \tag{C.19}$$

With the x-component of the coordinate shift derived in section C.2, and the $\mathcal{T}$-matrix element given in Equation 3.21, we can easily obtain the side-jump transition probability rate, $w^{sj}_{\mathbf{k}\mathbf{k}'} = -eE_x S^x_{\mathbf{k}\mathbf{k}'}$, such that:

$$\begin{aligned} S^x_{\mathbf{k}\mathbf{k}'} &= \frac{2\pi}{\hbar}\left|\mathcal{T}^{sy}_{\mathbf{k}\mathbf{k}'}\right|^2 \delta\mathbf{r}^x_{\mathbf{k}\mathbf{k}'}\partial_{\varepsilon_{\mathbf{k}'}}\delta\left(\varepsilon_{\mathbf{k}'}-\varepsilon_{\mathbf{k}}\right) \\ &= \frac{\pi}{\hbar}\,\frac{u_0^2\;n_{imp}}{2\nu}\left(\frac{\sin\phi}{k}+\frac{\sin\phi'}{k'}\right)\Big(\sin\phi\cos\phi'\sin\theta - \cos\phi\sin\phi'\sin\theta'\Big)\partial_{\varepsilon_{\mathbf{k}'}}\delta\left(\varepsilon_{\mathbf{k}'}-\varepsilon_{\mathbf{k}}\right) \end{aligned} \tag{C.20}$$

Now, determining the integral of the side-jump conductivity tensor term of the side-jump velocity, in Equation 2.41:

$$\begin{aligned} \int_k \partial_x v_y^{sj}\partial_x f^0_{\mathbf{k}} &= \frac{\nu}{(2\pi)^2}\int kdkd\theta\;\partial_x v_y^{sj}\;\frac{\partial\varepsilon_{\mathbf{k}}}{\partial k_x}\frac{\partial f_0}{\partial\varepsilon_{\mathbf{k}}} = \\ &= \frac{\nu}{(2\pi)^2}\int kdkd\theta\;\partial_x v_y^{sj}\;\left[t+\frac{\hbar^2v^2k\cos\theta}{\varepsilon^0_{\mathbf{k}}}\right]\delta(\varepsilon_{\mathbf{k}'}-\varepsilon_F) = \\ &= \frac{u_0^2\;n_{imp}}{8\pi\hbar^3v^2}t\left(\frac{5}{8}\frac{m}{\varepsilon_F}-\frac{38}{8}\frac{m^3}{{\varepsilon_F}^3}+\frac{33}{8}\frac{m^5}{{\varepsilon_F}^5}\right). \end{aligned} \tag{C.21}$$

Appendix D

Deformation potential

Long wave length acoustic phonons induce an effective local potential called the deformation potential and proportional to the local contraction or dilation of the lattice,

$$V_1(\mathbf{r}) = g_0 u_{ii}(\mathbf{r}),$$

where g_0 is the bare deformation potential.

The respective interaction Hamiltonian is diagonal in sublattice indices and reads

$$\mathcal{H}_1 = \int d\mathbf{r}\psi^\dagger(\mathbf{r}) \left[V_1(\mathbf{r})\mathbf{1}\right] \psi(\mathbf{r}),$$

where $\mathbf{1}$ is the 2×2 identity matrix. We can rewrite it in momentum space as

$$\mathcal{H}_1 = \sum_{\mathbf{k},\mathbf{k}'} \psi^\dagger_{\mathbf{k}} \left[V_1(\mathbf{k},\mathbf{k}')\mathbf{1}\right] \psi_{\mathbf{k}'},$$

with

$$V_1(\mathbf{k},\mathbf{k}') = \mathcal{V}^{-1} \int d\mathbf{r} e^{i(\mathbf{k}'-\mathbf{k})\cdot\mathbf{r}} V_1(\mathbf{r}) \equiv V_1(|\mathbf{k}-\mathbf{k}'|) \equiv V_1(K). \tag{D.1}$$

Taking into account screening effects, we write the interaction matrix element as

$$V_1(K) \to \frac{V_1(K)}{\varepsilon(K)},$$

where for the static dielectric function $\varepsilon(K)$ we use

$$\varepsilon(K) = 1 + \mathcal{U}(K)N(k_F),$$

with $\mathcal{U}(K) = e^2/(2\epsilon_0 K)$ for the Fourier transform of the 2D Coulomb potential and $N(k_F)$ the density of states at Fermi level. We will assume $\mathcal{U}(K)N(k_F) \gg 1$, since the Boltzmann formalism requires the system to have metallic behavior (where we expect large density of states).

The electron-phonon interaction Hamiltonian is the sum of the two terms discussed above

$$H_{ep} = \mathcal{H}_1 + \mathcal{H}_2.$$

Phonons enter through the strain tensor u_{ij} which can be written in terms of static and dynamic components; the purely static term does not contribute to electron-phonon scattering and will be disregarded.

We will consider the system 2D and take into account in-plane vibrations. Introducing the Fourier series for the deformation field $\mathbf{u}(\mathbf{r}) = \mathcal{V}^{-\frac{1}{2}} \sum_{\mathbf{q}} \mathbf{u}_{\mathbf{q}} e^{i\mathbf{q}\cdot\mathbf{r}}$ we have

$$u_{ij} = \frac{\mathcal{V}^{-\frac{1}{2}}}{2} \sum_{\mathbf{q}} [iq_i u^j_{\mathbf{q}} e^{i\mathbf{q}\cdot\mathbf{r}} + iq_j u^i_{\mathbf{q}} e^{i\mathbf{q}\cdot\mathbf{r}}]. \tag{D.2}$$

For in-plane vibrations we can decouple the two components as usual by changing to longitudinal and transverse displacement fields

$$\mathbf{u}_{\mathbf{q}} = u^L_{\mathbf{q}} \frac{\mathbf{q}}{q} + u^T_{\mathbf{q}} \hat{e}_z \times \frac{\mathbf{q}}{q}, \tag{D.3}$$

where $\hat{e}_z \times \mathbf{q} = (-q_y, q_x, 0)$. The purely dynamic term of the strain tensor may then be written as,

$$\begin{aligned}
u_{xx,dyn} &= \mathcal{V}^{-\frac{1}{2}} \sum_{\mathbf{q}} iq\cos\phi[u^L_{\mathbf{q}}\cos\phi - u^T_{\mathbf{q}}\sin\phi]e^{i\mathbf{q}\cdot\mathbf{r}} && \text{(D.4)}\\
u_{yy,dyn} &= \mathcal{V}^{-\frac{1}{2}} \sum_{\mathbf{q}} iq\sin\phi[u^L_{\mathbf{q}}\sin\phi + u^T_{\mathbf{q}}\cos\phi]e^{i\mathbf{q}\cdot\mathbf{r}} && \text{(D.5)}\\
u_{xy,dyn} &= \frac{1}{2}\mathcal{V}^{-\frac{1}{2}} \sum_{\mathbf{q}} iq[\cos\phi(u^L_{\mathbf{q}}\sin\phi + u^T_{\mathbf{q}}\cos\phi) + \sin\phi(u^L_{\mathbf{q}}\cos\phi - u^T_{\mathbf{q}}\sin\phi)]e^{i\mathbf{q}\cdot\mathbf{r}}\\
&= \frac{1}{2}\mathcal{V}^{-\frac{1}{2}} \sum_{\mathbf{q}} iq[u^L_{\mathbf{q}}\sin(2\phi) + u^T_{\mathbf{q}}\cos(2\phi)]e^{i\mathbf{q}\cdot\mathbf{r}}, && \text{(D.6)}
\end{aligned}$$

where ϕ and ϕ' is the angle with respect to the x axis for $\mathbf{q}$ and $\mathbf{q}'$, respectively.

Inserting the above results into the matrix element in Eq. (D.1) we obtain

$$V_1(\mathbf{k}, \mathbf{k}') = \frac{g_0}{\varepsilon(|\mathbf{k} - \mathbf{k}'|)} \mathcal{V}^{-\frac{1}{2}} \sum_{\mathbf{q}} iq u^L_{\mathbf{q}} \delta_{\mathbf{k}'-\mathbf{k},\mathbf{q}}. \tag{D.7}$$

Note that transverse phonons do not contribute to electron-phonon scattering through the deformation potential.

Quantizing the displacement fields [9] and introducing usual destruction and creation operators $a^{(\nu)}_{\mathbf{q}}$ and $a^{(\nu)\dagger}_{\mathbf{q}}$ for phonons $\nu = L, T$ (longitudinal and transverse) with momentum $\mathbf{q}$, such that

$$u^{(\nu)}_{\mathbf{q}} = \sqrt{\frac{\hbar}{2\rho\omega^{(\nu)}_{\mathbf{q}}}} \left(a^{(\nu)}_{\mathbf{q}} + a^{(\nu)\dagger}_{-\mathbf{q}}\right),$$

we arrive at the following electron-phonon interaction Hamiltonian

$$H_{ep} = \sum_{c=a,b} \sum_{\mathbf{k},\mathbf{k}'} \sum_{\mathbf{q}} V^{(L)}_{1,\mathbf{q}} c^\dagger_{\mathbf{k}} c_{\mathbf{k}'} (a^{(L)}_{\mathbf{q}} + a^{(L)\dagger}_{-\mathbf{q}}) \delta_{\mathbf{k}',\mathbf{k}-\mathbf{q}}, \tag{D.8}$$

with matrix element

$$V^{(L)}_{1,\mathbf{q}} = \frac{g_0}{\varepsilon(q)} iq \sqrt{\frac{\hbar}{2\mathcal{V}\rho\omega^{(L)}_{\mathbf{q}}}}. \tag{D.9}$$

Bibliography

[1] K I Bolotin et al. "Ultrahigh Electron Mobility in Suspended Graphene". In: Solid State Commun. (2008).

[2] K. v. Klitzing, G. Dorda, and M. Pepper. "New Method for High-Accuracy Determination of the Fine-Structure Constant Based on Quantized Hall Resistance". In: Phys. Rev. Lett. (1980). DOI: 10.1103/PhysRevLett.45.494.

[3] K S Novoselov et al. "Two-Dimensional Gas of Massless Dirac Fermions in Graphene". In: Nature (2005).

[4] Nobel Foundation. Scientific Background on the Nobel Prize in Physics 2016. 2016. URL: https://www.nobelprize.org/uploads/2018/06/advanced-physicsprize2016.pdf.

[5] Inti Sodemann and Liang Fu. "Quantum Nonlinear Hall Effect Induced by Berry Curvature Dipole in Time-Reversal Invariant Materials". In: Physical Review Letters (2015). DOI: 10.1103/PhysRevLett.115.216806.

[6] Z. Z. Du, Hai-Zhou Lu, and X. C. Xie. "Nonlinear Hall effects". In: Nature Reviews Physics (Aug. 2021). DOI: 10.1038/s42254-021-00359-6.

[7] Pan He et al. "Quantum frequency doubling in the topological insulator Bi_2Se_3". In: Nature Communications (2021). DOI: 10.1038/s41467-021-20983-1.

[8] Steven M. Girvin and Kun Yang. Modern Condensed Matter Physics. Cambridge University Press, Feb. 2019. ISBN: 9781107137394. DOI: 10.1017/9781316480649.

[9] N. W. Ashcroft and N. D. Mermin. Solid State Physics. Holt-Saunders, 1976.

[10] N A Sinitsyn. "Semiclassical theories of the anomalous Hall effect". In: Journal of Physics: Condensed M (2007). DOI: 10.1088/0953-8984/20/02/023201.

[11] F. D. M. Haldane. "Berry Curvature on the Fermi Surface: Anomalous Hall Effect as a Topological Fermi-Liquid Property". In: Physical Review Letters (2004). DOI: 10.1103/PhysRevLett.93.206602.

[12] Di Xiao, Ming Che Chang, and Qian Niu. "Berry phase effects on electronic properties". In: Reviews of Modern Physics (2010). DOI: 10.1103/RevModPhys.82.1959.

[13] Qiong Ma et al. "Observation of the nonlinear Hall effect under time-reversal-symmetric conditions". In: Nature (2019). DOI: 10.1038/s41586-018-0807-6.

[14] Z Z Du et al. "Disorder-induced nonlinear Hall effect with time-reversal symmetry". In: Nature Communications (2019). DOI: 10.1038/s41467-019-10941-3.

[15] Zi-Shan Liao, Hong-Hao Zhang, and Zhongbo Yan. "Nonlinear Hall effect in two-dimensional class-AI metals". In: Physical Review B (June 2021). DOI: 10.1103/physrevb.103.235151.

[16] Carmine Ortix. "Nonlinear Hall Effect with Time-Reversal Symmetry: Theory and Material Realizations". In: Advanced Quantum Technologies (July 2021). DOI: 10.1002/qute.202100056.

[17] S. Nandy and Inti Sodemann. "Symmetry and quantum kinetics of the nonlinear Hall effect". In: Physical Review B (Nov. 2019). DOI: 10.1103/physrevb.100.195117.

[18] Z Z Du et al. "Quantum theory of the nonlinear Hall effect". In: Nature Communications (2021). DOI: 10.1038/s41467-021-25273-4.

[19] Kaifei Kang et al. "Observation of the nonlinear anomalous Hall effect in 2D WTe2". In: (2018).

[20] Mao-Sen Qin et al. "Strain Tunable Berry Curvature Dipole, Orbital Magnetization and Nonlinear Hall Effect in WSe 2 Monolayer*". In: Chinese Physics Letters (2021). DOI: 10.1088/0256-307X/38/1/017301.

[21] Meizhen Huang et al. "Giant nonlinear Hall effect in twisted bilayer WSe2". In: National Science Review (Oct. 2022). DOI: 10.1093/nsr/nwac232.

[22] Sheng Chin Ho et al. "Hall effects in artificially corrugated bilayer graphene without breaking time-reversal symmetry". In: Nature Electronics (Feb. 2021). DOI: 10.1038/s41928-021-00537-5.

[23] O. O. Shvetsov et al. "Nonlinear Hall Effect in Three-Dimensional Weyl and Dirac Semimetals". In: JETP Letters (June 2019). DOI: 10.1134/s0021364019110018.

[24] Sami Dzsaber et al. "Giant spontaneous Hall effect in a nonmagnetic Weyl–Kondo semimetal". In: Proceedings of the National Academy of Sciences (Feb. 2021). DOI: 10.1073/pnas.2013386118.

[25] Dushyant Kumar et al. "Room-temperature nonlinear Hall effect and wireless radiofrequency rectification in Weyl semimetal TaIrTe4". In: Nature Nanotechnology (2021). DOI: 10.1038/s41565-020-00839-3.

[26] Archana Tiwari et al. "Giant c-axis nonlinear anomalous Hall effect in Td-MoTe2 and WTe2". In: Nature Communications (Apr. 2021). DOI: 10.1038/s41467-021-22343-5.

[27] Andhika Kiswandhi and Toshihito Osada. "Observation of possible nonlinear anomalous Hall effect in organic two-dimensional Dirac fermion system". In: Journal of Physics: Condensed M (Dec. 2021). DOI: 10.1088/1361-648x/ac3fd5.

[28] Jenö Sólyom. Fundamentals of the Physics of Solids. Volume II: Electronic Properties. Springer Berlin Heidelberg, Nov. 2008. ISBN: 9783540853152. DOI: 10.1007/978-3-540-85316-9.

[29] J. M. Ziman. Principles of the Theory of Solids. Ed. by Cambridge University Press. 2nd Edition. Nov. 1979. ISBN: 9780521297332.

[30] J. J. Sakurai and Jim Napolitano. Modern Quantum Mechanics. 3rd ed. Cambridge University Press, 2020.

[31] N. A. Sinitsyn, Q. Niu, and A. H. MacDonald. "Coordinate shift in the semiclassical Boltzmann equation and the anomalous Hall effect". In: Physical Review B 73 (Feb. 2006). DOI: 10.1103/physrevb.73.075318.

[32] Di Xiao, Ming-Che Chang, and Qian Niu. "Berry phase effects on electronic properties". In: Reviews of Modern Physics 82.3 (July 2010), 1959–2007. ISSN: 1539-0756. DOI: 10.1103/revmodphys.82.1959. URL: http://dx.doi.org/10.1103/RevModPhys.82.1959.

[33] Pan He et al. "Nonlinear Planar Hall Effect". In: Physical Review Letters (2019). DOI: 10.1103/PhysRevLett.123.016801.

[34] I. S. Gradshteyn and I. M. Ryzhik. Table of integrals, series, and products. Seventh. Elsevier/Academic Press, Amsterdam, 2007.

[35] John Schliemann and Daniel Loss. “Anisotropic transport in a two-dimensional electron gas in the presence of spin-orbit coupling”. In: Phys. Rev. B 68 (16 2003), p. 165311. DOI: 10.1103/PhysRevB.68.165311. URL: https://link.aps.org/doi/10.1103/PhysRevB.68.165311.